ON FATIGUE LIFE ESTIMATIONS OF RIVETED DETAILS UNDER VARIABLE AMPLITUDE LOADING

A Dissertation

by

JACKELINE KAFIE MARTINEZ

Submitted to the Office of Graduate and Professional Studies of
Texas A&M University
in partial fulfillment of the requirements for the degree of

DOCTOR OF PHILOSOPHY

Chair of Committee,	Peter B. Keating
Committee Members,	Gary Fry
	Stefan Hurlebaus
	Vikram Kinra
Head of Department,	Robin Autenrieth

December 2017

Major Subject: Civil Engineering

ABSTRACT

Old riveted railroad bridges currently in service in North America are being subjected to much higher live loads that they were originally designed for. Current fatigue provisions have been proven to provide robust estimations for riveted details. The purpose of this study is to determine how an increase of axle loads ultimately affect the fatigue life of riveted bridges.

A linear elastic fracture mechanics approach along with a cycle-by-cycle integration method, is used to estimate fatigue life of riveted connections in railroad bridges under variable amplitude loading. Only the stress ranges with stress intensity factors larger than the fatigue threshold are assumed to produce crack growth.

The analysis is developed using the variable amplitude stresses generated due to a traversing heavy axle train on a simply supported riveted girder. Stress intensity factors for quarter elliptical corner crack emanating from a through- thickness (rivet) hole under remote tension were used. Effect of the initial crack size assumption on the fatigue life estimation was studied. Moreover, the effect of overloads on the fatigue behavior of the component was also studied.

Special care has been taken to analyze the effect on fatigue life of thermal residual stresses due to original rivet installation. Thermal residual stresses, generated during the installation process, were quantified through a finite element simulation. Superposition principle was utilized to account for localized residual stresses present on the base material.

Fatigue life estimations calculated using S-N curves (current AREMA provisions) and linear elastic fracture mechanics with and without considering clamping stress are compared. Plate thickness plays a role in the fatigue life of the components; thin plates count with a larger local compressive stress that hinders crack propagation in this direction. Crack growth proved to be different under localized residual stresses when compared to the base material. Finally, the ratio of crack depth to plate thickness also was found to play a role in the fatigue life.

DEDICATION

To my parents, for all their years of sacrifice.

ACKNOWLEDGEMENTS

This study was conducted at the Department of Civil Engineering at Texas A&M University, College Station, Texas. Great thanks are due to the department and the University for providing the opportunity and assistantship throughout the years for conducting this research toward the Ph.D.

The author is indebted to her committee chairman, Dr. Peter B. Keating, for introducing the author into research. Without his time and patience this work would have not been possible. His sense of practicality, charisma, and empathy has truly left a mark on the author. Finally, many thanks for taking a leap of faith in allowing me to teach CVEN 363.

The author is also grateful to the committee members, Dr. Gary Fry, for his continuous guidance and fatherly advices during the years of study, and Dr. Stefan Hurlebaus, for always being so approachable.

Special thanks are due to Dr. Vikram Kinra, alias “The Guru”, for guiding and mentoring the author into the world of Fracture Mechanics. His passion for teaching, and willingness to serve and help his students will always be remembered. Now that you are up, you have sent the elevator down. Thanks for showing me the kind of professor I aspire to be.

The author is also grateful to Dr. Duane Otter, from Transportation Technology Center Inc., for providing valuable information and recommendations toward this investigation.

Many thanks to Ms. Theresa Taeger, Ms. Laura Byrd and Ms. Maria Medrano for assisting with all the administrative tasks.

Sincere thanks and gratifications are extended to my colleagues, Dr. Maysam Kiani and Dr. Lorena Garcia Cucalón, for mentoring and advising the author throughout these years. Last, but not least, many thanks to my high-school physics teacher and colleague, Mrs. Gloria de Retes, for boosting my confidence at the very young age of 16.

You can if you think you can.

Jackeline Kafie Martinez

August 18th, 2017

CONTRIBUTORS AND FUNDING SOURCES

Contributors

This work was supervised by a dissertation committee consisting of Dr. Peter B. Keating, Dr. Gary Fry and Dr. Stefan Hurlebaus from the Civil Engineering Department and Dr. Vikram Kinra from the Aerospace Engineering Department.

Special mention to the Texas A&M High Performance Research Computing for providing invaluable resources to this study.

All the work conducted for the dissertation was completed by the student independently.

Funding Sources

This investigation was funded by the Association of American Railroads (AAR). Its contents are solely the responsibility of the author and do not necessarily represent the official views of AAR.

NOMENCLATURE

GREEK

α_i	=	frequency of the stress range in Palmgren-Miner Linear accumulation damage
β	=	volumetric thermal expansion
Δa	=	crack growth under one stress cycle
ΔK	=	range of stress intensity factor, calculated using Sr (Mode I)
ΔK_{eff}	=	effective range of stress intensity factor
ΔK_{th}	=	threshold value of the range of stress intensity factor (Mode I)
ΔT	=	temperature differential
ΔV	=	volume differential
ε	=	linear thermal expansion
λ	=	function defined in text
λ_a	=	thermal conductivity
ρ	=	mass density
σ_y	=	yield stress
σ_{ut}	=	ultimate stress
ν	=	Poisson's ratio

LATIN

A	=	fatigue constant in the S-N curve
a	=	crack length in a through thickness crack or crack depth in a quarter elliptical corner crack
a_f	=	final crack depth
a_o	=	initial crack depth
a_{TH}	=	crack size threshold
b	=	half of plate width
C	=	material constant in Paris' rule
c	=	half-length of crack
c_f	=	final crack length

c_o	=	initial crack length
c_p	=	specific heat
da/dN	=	crack growth rate
E	=	Young's modulus
F	=	correction factor in the stress intensity factor equation
F_{ch}	=	boundary correction factor for a corner crack at a hole under tension
f_φ	=	angular function derived from embedded elliptical crack solution
f_w	=	finite-width correction factor
g_i	=	curve fitting functions defined in text (i = 1,2 or 3)
K	=	stress intensity factor (Mode I)
K_{max}	=	maximum stress intensity factor (Mode I)
K_{min}	=	minimum stress intensity factor (Mode I)
K_{tm}	=	stress concentration factor
L	=	span length, center to center
M_i	=	curved fitting function defined in text (i = 1,2 or 3)
m	=	material constant I Paris' rule and S-N curve, or mass density
N	=	nominal cycle life determined by the full spectrum
N'	=	number of load cycles which would cause fatigue damage
n	=	total number of stress cycles in the variable amplitude stress spectrum
Q	=	shape factor for an elliptical crack
R	=	stress ratio, minimum stress over maximum stress
R_{eff}	=	effective stress ratio
r	=	plate hole radius
S_r	=	stress range, the algebraic difference between the maximum stress and the minimum stress for a stress cycle.
S_{re}	=	effective root-mean cube stress range
$S_{R\,fat}$	=	Allowable fatigue stress range given by AREMA
$S_{residual}$	=	residual stress range
S_{ri}	=	individual stress range

t	=	plate thickness
V_o	=	initial volume

TABLE OF CONTENTS

Page

LIST OF FIGURES

Page

LIST OF TABLES

1. INTRODUCTION

Freight railroads have been an important part of the U.S. transportation network for over 150 years. Forty percent of the ton-miles of the freight transported in the United States is done by train. The nation's railroad infrastructure consists of over 76,000 railroad bridges. Much of the current U.S. freight railroad network was originally built in the late 1800s and early 1900s and many of these bridges are still in used, long after their original predicted design life [1].

In the past decades, heavy axle railway loads (freight equipment greater than 200,000 lbs. capacity and gross vehicle weights exceeding 263,000 lbs.) have been used extensively on America Class 1 freight railroads. The gross weight of railway loads has increased considerably in the past four decades. Freight car weights have increased from 170,000 lbs., typically used before 1960, to 286,000 lbs., or even 315,000 lbs., sporadically used today. Specifically, since the early 1990's, freight car weights have increased from a standard 263,000 lbs. to 286,000 lbs. [2]. As of today, some railroad lines carry 315,000 lbs. cars, however, the effect of heavy axle loads on the fatigue life of structural members is still not completely understood.

With the increase of railroad traffic and further aging of the railroad bridges, proper maintenance must be provided or expensive components might need replacement. Although many existing railway bridges are structurally adequate for the increase of heavy axle loads, the cyclical application generate a significant number of cycles of stress ranges

that contribute to the accumulation of fatigue damage. An accurate estimate of the remaining fatigue life of railroad steel bridges is needed in order to provide adequate maintenance of the bridges and to keep the railroad infrastructure in optimum condition.

Even though fatigue effects have been considered in the design of steel bridges in the last 50 years, they were designed for a much lower axle load. An evaluation of the effects of heavy axle load (HAL) on the fatigue life of railway steel bridges is imperative to maintain safe, effective, and reliable transportation services on North American Class 1 railroads.

2. PROBLEM STATEMENT

Many older railroad bridges currently in service are riveted structures that were built near the beginning of the 20th century. These bridges are being subjected to much higher loads that were originally designed for [2]. Engineers do not know for certain how much remaining life a certain riveted structure has, since a proper, accurate estimation of fatigue strength in riveted details has not been developed. Most of the fatigue and fracture knowledge of these days is based upon modern welded construction and/or high strength bolts. Therefore, the demand for an accurate estimation of the fatigue life of riveted steel structural joints has increased on the last decades.

Failure by accumulated fatigue damage (initiation and propagation of small cracks) caused by repeated cycles of tensile stress is of primary concern in steel railway superstructure members and connections subjected to heavy-axle-loads (HAL). The fatigue life, or number of cycles to failure (generally taken as through-thickness fracture of a component), depends on the frequency and number of load cycles, load magnitude (stress range), member size and member details [3]. There are two possible ways to estimate the fatigue life of a component: through a fracture mechanics approach, or the stress-life approach, more commonly known as S-N curves. The former is not generally used for ordinary steel bridge design; the latter is recommended for the design of steel bridges by the American Railway Engineering and Maintenance-of-Way Association AREMA (2015).

The current fatigue strength (S–N) curve of the AREMA (2015) for riveted connection details is a combination of fatigue strength Categories C and D of welded details. For riveted spans with no stress range cycles above 9 ksi, Category C may be used for rating. However, the S-N curve of Category D must be used for stress ranges greater than 9 ksi. Broadly speaking, any mechanical detail has a better fatigue life than does its equivalent welded detail [4]. It has been realized that under the practical ranges of live load this curve underestimates the fatigue resistance of riveted bridge members and hence estimations are generally too conservative.

Consequently, a more refined fatigue assessment is desired for riveted bridge members. In order to do so, a linear elastic fracture mechanics approach will be used, since one has more control over which cycles out of the stress spectrum can induce crack propagation, contrast to the S-N approach that assumes all stress cycles of the spectrum contribute, leading to an unrealistic and conservative fatigue life estimation. Moreover, to provide an even more realistic fatigue life assessment, the residual stress field developed during the hot-riveting installation process will be accounted for in the estimation.

3. LITERATURE REVIEW

3.1 Fracture Mechanics and riveted connections

Reemsnyder [5] studied the effectiveness of rehabilitating a riveted detail by the replacement of rivets in critical locations with high strength bolts rather than replacing the entire member. Constant amplitude and service simulation of 16 full-scale model structural joints was performed. According to the experimental data, replacement of rivets with bolts at locations of anticipated cracking increased the fatigue life two to six times by significantly retarding crack propagation. Moreover, fastener replacements proved to prevent crack initiation. Finally, the research stated that the percentage of life remaining until fracture of a detail subjected to variable amplitude loading may be conservatively estimated by total crack growth measurements from the constant amplitude tests.

Out et al. [6] reported the fatigue and fracture resistance of corroded and deteriorated riveted members on the high cycle. The report stated that the major variables observed to affect the fatigue resistance of riveted joints are the rivet clamping force and the rivet bearing ratio. From the experimental data, it was concluded that weathered and deteriorated riveted members have an extreme fatigue life close to the Category D fatigue limit. An analytical study on the behavior of a cracked riveted detail through a finite element analysis was also performed. As a result, it was demonstrated that the frictional bond between plates was transferring load to the uncracked components, increasing the fatigue life of the entire component.

Baker and Kulak [7] provided a summary of the existing data on the fatigue strength evaluation of riveted connections. It also provided the results of fatigue tests performed on several highway bridge members taken from service. Fatigue tests on plates with open holes were also carried out as a reference for riveted connections. The investigation confirmed the beneficial effects of replacing rivets with high strength bolts.

Fisher et al. [8] discovered that, although the bearing ratio along with the clamping force are the two main variables in the fatigue life of small riveted shear splices, most of the cracked details in the riveted beams and girders that were tested were in a constant moment region, near or at midspan.

Zhao et al. [9] studied the probability of failure in terms of the reliability index for fatigue life of steel bridge components. The AASHTO S-N curve method was considered and compared with the linear elastic fracture mechanics method, and both methods yield almost identical reliability indexes for a full-penetration butt weld in the tension flange of a steel-box girder.

DiBattista and Kulak [10] studied the experimental and theoretical knowledge of fatigue strength of various steel details. Experimental tests were conducted on full tension diagonals taken from a railway bridge. The investigation also consisted in using various methods for the calculation of remaining fatigue life. It was concluded that connections in which rivets are subjected to bearing have reduced fatigue strength, and that the effect of staggered rivet patterns is significant. It was proposed that a simple truss model can be used to provide a reasonable description of the behavior of the diagonals for use in the

calculation of the remaining fatigue life. Finally, a technique for the repair of fatigue cracks was established.

Fisher et al. [4] on “A Fatigue Primer for Structural Engineers” provides the engineer with the background required to understand and use the design rules for fatigue strength that were current provisions by the American Association of State Highway and Transportation Officials (AASHTO) in 1998. It also establishes the basis for the fatigue problem in terms of fracture mechanics.

Unsworth [2] describes the effects of the usage of heavy axle loads (HAL) on the fatigue life of steel bridges. The investigation also outlines some of the life extension and rehabilitation techniques typically used to maintain the safety and reliability of existing steel railway bridges.

Aragón et al. [11] executed a study of a punched plate, with a simple clamping nut bolt, subjected to axial loading. The most important parameters in question were the clamping force and the coefficient of friction between the joint parts. These parameters had a great influence on the fatigue life of the joint, since they originate friction stresses that modify the stress field on the hole edge. Aragón et al. [11] performed an excellent parametric study on nut bolts, analytical and experimental, investigating the effect of initial crack size (or flaw) in a plate punched with a hole, the effect of different clamping forces and the effect of coefficient of friction in the S-N curves of bolted plates. Although this is not directly concerned to riveted members, his analytical method was found extremely valuable due to the similarities of rivets and high strength bolts, where the major

difference resides on the magnitude of the clamping force. It was established that, as the clamping force increases, the number of cycles to failure for all stress levels of the bolted plate increase.

Zhou [12] proposed a new S–N curve that reflects better the actual fatigue strength of existing riveted bridge members. Fatigue testing of full scale riveted girders was performed which provided the basis for the development of a series of S–N curves for riveted bridge members of different conditions. Zhou [12] conducted a study to measure the magnitude of clamping residual stress in riveted members from demolished bridges approximately 60 years of age. The measured clamping stress varied from 5 to 24 ksi, with an average of about 12 ksi and a standard deviation of about 6 ksi. Zhou [12] also performed a two-dimensional finite element model to examine the distribution of normal and frictional stresses on the contact surfaces. The presence of a crack was not considered in the model. It was reported that a temperature change of 400 °F during the cooling process in the rivet caused a clamping stress of about 38 ksi. Finally, fatigue crack propagation was studied by relating the crack growth rate with the stress intensity factor and later compared to the results of the full scale riveted members.

De Jesus and Correia [13] assessed the stress intensity factor for a riveted component using a finite element model. The stress intensity factors were computed from the strain energy release rate and using the virtual crack closure technique (VCCT). The effects of both tensile and bending loads were analyzed, and it accounts for the clamping force effects as well as the friction. It was found that load transfer is more effective for

higher clamping stresses on rivets, since it increases the load transfer by friction. Thus, the stress intensity factor is lower for higher clamping stresses on rivets.

3.2 Current experimental studies done in riveted bridge members

Transportation Technology Center, Inc. in conjunction with the Association of American Railroads' Strategic Research Initiatives and the Facility for Accelerated Service Testing (FAST) Bridge Research Programs are currently investigating the performance of steel bridge spans to extend their safe service life under heavy axle load (HAL) service. The steel bridge at FAST is made up of two spans: a 55.5-ft. riveted girder span and a 65-ft. welded girder. Both girders were in revenue service before their current location at FAST. The steel bridge at FAST is subjected to heavy axle loads to identify some of the issues that might arise if axle loads are increased. The HAL train consists of 110 freight cars each weighing 315,000 lbs., pulled by three SD70 six-axle locomotives. Normal train operations are at 40 mph. Both spans are being monitored for performance, including deterioration and maintenance requirements for bridge components and will ultimately provide good insight on where are when these bridges will require maintenance. Some of the life extension techniques include: stress state reduction, inspections, repairs, monitoring systems (strain/stress and deflections), etc. [14-17]

Otter et al. [18, 19] in association with the Transportation Technology Center, Inc. is currently investigating two short steel deck plate girder bridge spans at FAST. The primary goal of this research is to provide a better estimate of steel bridge life to facilitate planning for bridge capital and maintenance. The investigation consists of comparing

estimates on fatigue life based on strain gage measurements with estimates based on theoretical calculations. The investigation demonstrates the gap between theoretical estimations and reality, proving that there is much more that can be done to reduce the current overly conservative fatigue estimates.

3.3 On the finite element model

Al-Bahkali [20] developed a three-dimensional finite element model for lap riveted and rivet-bonded joints. A heat transfer analysis was performed to simulate the thermal stresses induced when the hot rivet transfers heat to the environment by convection. The analysis was proceeded by an elastic analysis where one of the plates is subjected to a constant velocity to simulate a lap shear tensile test up to failure. It was concluded that introducing an adhesive layer between the connecting plates vastly reduces the stresses developed in the joints, decreases stress concentrations, and increases fatigue life.

De Jesus et al. [21] performed a finite element model of riveted and bolted joints made of puddle iron to study the crack initiation and propagation phases in these kinds of connections. A finite element model using solid and contact elements was performed; clamping stresses as well as friction were considered. Finally, a through thickness crack depth was modeled, and the stress intensity factor was obtained for several crack lengths using the Virtual Crack Closure Technique (VCCT). A fracture mechanics approach was utilized to track and account for the crack initiation and propagation phases.

Rans and Straznicky [22] developed a three-dimensional finite element model to study the installation process of aluminum rivets in monolithic aluminum sheets. Only a

single sheet thickness and rivet diameter were considered. The following parameters were studied: 1) rivet clamping force, 2) universal vs countersunk rivets, and 3) rivet flushness before installation.

3.4 On residual stress

Glinka [23] utilizes the Paris Power Rule and Forman equation to calculate fatigue crack growth in medium strength steel weldments. Moreover, the superposition principle was introduced to combine the residual stress intensity factor with the applied stress intensity factor allied with Foreman's crack growth law. In this study, it was assumed that residual stresses do not diminish under fatigue loading. Glinka states that this assumption overestimates the residual stress effect, but it is reasonable from the practical point of view. The concept of effective range of stress intensity factor and effective stress ratio was also introduced. The study concludes that the effect of residual stresses on fatigue crack growth rate depends on the magnitude of the applied load. The lower the applied load, the higher the residual stress effect. In sum, the inclusion of residual stresses in the theoretical analysis permits more realistic predictions and makes it possible to predict fatigue life of details more accurately.

Cathey and Grandt [24] compared experimental results with theoretical calculations of fatigue crack growth life caused by coldworking fastener holes to quantify the improvements in fatigue life resistance due to coldworking. Calculations were obtained using a fracture mechanics approach and assuming a two-dimensional through-the-thickness crack and Mode I loading. Residual hoop stress distributions for unflawed

components were used to calculate stress intensity factors. Superposition was applied to add linearly the effects of remote stress field with the residual stresses introduced by coldworking. Finally, fatigue crack growth rates were computed as a function of length for the seventeen test specimens. The smallest crack length giving a predicted ΔK within the *da/dN* limits established by the Paris Power Rule was computed and found to be 0.054 in (1.37 mm).

Parker [25] expands on the concept originally proposed by Glinka [23] about the prediction of fatigue life using Linear Elastic Fracture Mechanics (LEFM) in residual stress fields. Utilizing three different configurations and types of loading, the effect of residual stress field on crack growth rate was determined. It states that the superposition principle is not violated by the 'stress fading' of residual stress fields during fatigue crack growth.

Webster and Ezeilo [26] examined the influence of residual stress on fatigue crack initiation and growth. Methods of measuring residual stress were reviewed.

Nelson [27] in the paper "Effects of Residual Stress on Fatigue Crack Propagation" compares and discusses existing approaches for predicting the influence of residual stress on fatigue crack growth. Current limitations of the methods and their relative advantages for the methods were compared. Two approaches were considered: (1) superposition of the respective stress intensity factors for the residual stress field and for the applied stresses, and (2) a simplified crack closure model. The validity of both models has been generally accepted. It is imperative to determine $K_{residual}$ using either weight function

method (WFM) or the finite element method (FEM). The WFM is generally used in simple geometries, whereas FEM is more powerful and robust when general SIF solutions cannot be found due to the complexity in either geometry or loading conditions [28]. It also discusses the possible role of residual stress re-equilibration on growth behavior as the crack extends.

4. RESEARCH OBJECTIVES

Current fatigue design procedures often result in overly conservative estimates of fatigue damages, resulting in needless replacement and repair costs. Thus, the purpose of this investigation is to improve and refine current fatigue assessment procedures to evaluate fatigue resistance of riveted details in steel bridges and allow for better use of resources.

The main objectives are:

- To determine the bending stress fluctuations generated at midspan by a train traversing a simply supported riveted girder. To determine maximum and minimum stress range using Rainflow Counting Method. To determine effective stress range using Miner's rule and root mean cube method.
- To determine the decrease in fatigue life with an increase of live load by using a Linear Elastic Fracture Mechanics (LEFM) approach of a railroad riveted girder assuming only the stress cycles larger than the fatigue threshold contribute to cracking.
- To determine the effect of overloads on the fatigue life of a riveted detail.
- To determine the initial crack size necessary to have crack growth (crack size threshold).
- To determine the clamping stress induced by a rivet fastener in the connecting plates during the riveting process and due to temperature difference.

- To determine and to be able to account for the effect of the residual stress on the ultimate fatigue life of a riveted detail, commonly found in railroad steel bridge girders.
- To compare fatigue life estimations using a LEFM approach and S-N curves (current provisions).

5. METHODOLOGY

To be able to realize a more accurate and realistic estimate of the fatigue life of a railroad riveted girder it was necessary to perform several smaller analyses. In this report, each of these small analyses will have their own separate chapter.

Two of the most important parameters in the determination of fatigue life of structural steel details is the maximum and minimum stress range obtained from live and impact loads. Consequently, a simply supported, 55.5-ft riveted girder was used to determine the stress variations at mid-span due to a traversing train. To determine the effect of increased live loads on fatigue life, it was necessary to consider three trains with different railcar weights. This analysis was performed using the structural engineering software RISA-3D and is described more in detail in Chapter 7.

A finite element model was required to quantify the clamping stresses generated during the hot-riveting process. This analysis will provide an estimate of stresses generated around the rivet hole and will later be used to incorporate the effect of clamping stress into the calculation of fatigue life. The finite element model was performed using the software ABAQUS-CAE and is described more in detail in Chapter 9.

Finally, a linear elastic fracture mechanics analysis was performed to determine the fatigue life of a riveted detail. The fatigue life of the riveted detail was obtained under variable amplitude loading, using the stress fluctuations obtained from RISA 3D, with and without overloads and for a wide range of initial crack sizes. This analysis was performed using the programming language MATLAB. The results obtained assuming no clamping

stress are shown in Chapter 9 and considering clamping stress effects are shown in Chapter 10. Comparison between fatigue life of a riveted connection utilizing a fracture mechanics approach and current fatigue provisions is also investigated and presented in Chapter 10.

6. BACKGROUND

6.1 An overview of fatigue design

Fatigue in metals is the process of initiation and growth of cracks under the action of cyclic loads. If the crack is allowed to grow long enough, the uncracked cross section of the member will be subjected to higher internal forces that might later induce fracture. Continuous inspection of structural members is highly encouraged to be able to detect possible cracks on its early stages of propagation, way before the crack length becomes long enough to cause instability and ultimately failure. Hence, the main objective of fatigue design is to prevent cracks from initiating, and if they do initiate, keep the crack growth slow enough to be able to detect it on time [12]. The typical condition that produces fatigue cracking is the application of a large number of repetitive or cyclic loads. Fatigue crack growth might occur even if the stress levels are considerably less than those associated with failure under static loading conditions. Fatigue cracking is commonly present on highway and railroad bridges, since these types of structures are subjected to moving vehicle and heavy axle loads on a daily basis.

The first approach in fatigue design is to avoid the use of fatigue prone details within the structure, and then to inspect the structure for cracks during fabrication and throughout its life. However, the usage of fatigue prone details is sometimes unavoidable. The presence of micro cracks, flaws or material discontinuities in a member subjected to repetitive loads might be enough for fatigue cracking. The fact that pre-existing micro

cracks are already present in the member, causes to skip the initiation phase of cracks and the fatigue life is reduced to the crack propagation stage only.

Cyclic loading can be of two kinds: one that is of constant amplitude and other of variable amplitude. In a control environment, such as a laboratory, it is easier to obtain a cyclic loading with constant amplitude. However, civil structures are more likely to experience variable amplitude loading stresses, and usually, they fluctuate significantly. For example, the passing of train or a heavy truck over a bridge induce stresses of variable magnitude. In the case of fatigue design, one converts the variable stress fluctuations into an equivalent constant stress to be able to compute fatigue life.

The fatigue life between the variable amplitude loading and constant amplitude loading can be correlated by means of effective root-mean-cube stress range on the Palmgren-Miner linear accumulation damage rule [29].

The effective root-mean cube (RMC) stress range S_{re} is defined as:

$$S_{re} = \left(\frac{\Sigma S_{ri}^3 \alpha_i}{n}\right)^{1/3} \qquad \text{Eq. 6.1-1}$$

where S_{ri} is the individual stress range and α_i is the corresponding frequency, and n is the total number of stress cycles in the variable amplitude stress spectrum.

This effective stress range accumulates the same damage as the variable amplitude stress cycles over the total number of stress cycles to failure [3]. Even though the sequence and interaction of load cycle effects are not accounted for, Miner's rule, which assumes a

linear function of the cycle ratio between the fatigue damage and the cycle life, provides good agreement with test results [30].

However, the usage of Miner's rule cannot be directly applied from a stress spectrum without the application of a stress counting method in order to tabulate values for the number of cycles, n_i, for different stress range levels. There are several techniques for counting the cycles of variable amplitude load or stress traces. The reservoir and rainflow methods are the ones most commonly used in civil engineering applications. Generally, rainflow counting is more suited to computer analyses of long stress histories, whereas the reservoir method is most convenient for graphical analyses of short histories [4].

The rainflow method is named for its analogy of rain drops flowing down a pagoda roof. The following algorithm is used to apply the rainflow counting:

1. Reduce the time history to a sequence of (tensile) peaks and (compressive) troughs.
2. Imagine that the time history is a pagoda.
3. Turn the sheet clockwise 90°, so the starting time is at the top.
4. Each tensile peak is imagined as a source of water that "drips" down the pagoda.
5. Count the number of half-cycles by looking for terminations in the flow occurring when either:
    a. It reaches the end of the time history
    b. It merges with a flow that started at an earlier tensile peak; or
    c. It encounters a trough of greater magnitude.

6. Repeat step 5 for compressive troughs.
7. Assign a magnitude to each half-cycle equal to the stress difference between its start and termination.
8. Pair up half-cycles of identical magnitude (but opposite sense) to count the number of complete cycles. Typically, there are some residual half-cycles.

In sum, Miner's rule correlates variable amplitude loading to constant amplitude loading by means of computing an effective stress range that will accumulate the same damage as the variable amplitude stress cycles over the total number of stress cycles to failure. Both, Miner's rule and rainflow counting method were used in this investigation. Section 6.1.1 provides information regarding the current fatigue provisions recommended by AASHTO and AREMA for highway and railroad bridges respectively.

6.1.1 Current AREMA fatigue provisions: S-N curves

Fatigue cracking is one of the primary damage mechanisms of structural components. The purpose of fatigue design is to minimize the probability of failure by preventing cracks from initiating or, if they do, keep the crack growth rate low enough to allow time for detection during an inspection to avoid compromising the integrity of the structure. Fatigue in railroad bridges due to repeated moving loads is a common and critical problem. Fatigue cracks usually initiate at details of high stress concentration located in areas of high stress range.

The current provisions of American Association of State Highway and Transportation Officials (AASHTO) and the American Railway Engineering and Maintenance-of-Way Association (AREMA) for evaluating fatigue life of highway (the former) and railroad (the latter) bridge details are based on the fatigue strength (S- N) curves of welded structural details. These S-N curves were developed from extensive tests on various types of welded structural details [31]. Due to the nature of this work, emphasize will be made in the AREMA provisions.

According to AREMA (2015), in its article 1.3.13, the major factors governing fatigue strength at a particular location of a member or connection are the number of stress cycles, the magnitude of the stress range, and the relevant Fatigue Detail Category. AREMA has classified several fatigue prone details according to their fatigue strength, and they can be A, B, B', C, C', D, E, E', or F. A category detail A has the largest fatigue strength. The live load stress range, S_r, is defined as the algebraic difference between the maximum and minimum calculated stress due to live load, mean impact load and centrifugal load. The stress range shall be computed based on the effective net section or the effective gross section. Finally, the stress range shall not exceed the allowable fatigue stress range, $S_{R\,fat}$, as shown in Table 6-1.

Table 6-1 Allowable fatigue stress range, S_{rfat} (ksi)

Detail Category	No. of Constant Stress Cycles	
	2,000,000	Over 2,000,000
A	24	24
B	18	16
B'	14.5	12
C	13	10
C'	13	12
D	10	7 Note 3
E	8	4.5
E'	5.8	2.6
F	9	8

Note 1: This table is based on bridges designed for live loading specified in Article 1.3.13e. For bridges designed for other live loadings see Part 9, Commentary, Article 9.1.3.13.

Note 2: For Fracture Critical Members, See Article 1.3.13i.

Note 3: For base metal in mebers with riveted or bolted connections with low slip resistance, use the variable amplitude stress range of 6.

According to AREMA (2015), in the article 7.3.3.2 Fatigue, “members with riveted or bolted connections with low slip resistance, subjected to repeated stress fluctuations, the requirements of Detail Category D shall be considered with a variable amplitude stress range fatigue limit of 6 ksi up to 100 million cycles”. In the event the fasteners are tight and have developed a normal level of clamping force, “Detail Category C may be used provided the Normal Rating Live Load plus Impact stress range does not exceed 9 ksi. If Detail Category C is used, the variable amplitude stress range fatigue limit is 6 ksi, up to 100 million cycles”. AREMA assigns bridges two types of ratings: Normal and Maximum. Normal rating is the load level which can be carried by the existing structure for its expected service life, and dependent on a specified speed. Maximum rating

is the load level which the structures can support at infrequent intervals, with applicable speed restrictions. In the case of variable amplitude loading, Detail Category C may be used provided the Root-Mean-Cube (RMC) stress range (S_{re}) does not and will not exceed 9 ksi.

As for the fatigue limit, for Detail Category D details and better, "If the number of cycles with stress ranges above the Constant Amplitude Fatigue Limit (CAFL) exceeds 0.1% of the spectrum considered, the CAFL is deemed not to exist and the detail line is extended below the CAFL. Stress Ranges that fall below a value of 0.5 of the CAFL should be ignored".

For riveted details, stress ranges that cause the RMC stress range to fall below the Variable Amplitude Fatigue Limit (VAFL) of 6 ksi should be ignored provided the total number of relevant cycles does not exceed 100 million.

Figure 6-1 and Table 6-2 show the current S-N curves for fatigue design following AREMA and AASHTO recommendations. The fatigue resistance above the constant amplitude fatigue threshold, in terms of cycles, is inversely proportional to the cube of the stress range. This is shown in Eq. 6.1-2. Constant amplitude fatigue thresholds for the different Fatigue Detail Categories are shown in Table 6-2.

$$S_r = \left(\frac{A}{N}\right)^{1/3} \qquad \text{Eq. 6.1-2}$$

where

S_r = stress range, the algebraic difference between the maximum stress and the minimum stress for a stress cycle.

N = number of occurrences of constant stress cycles which would cause fatigue damage

A = fatigue constant depending on fatigue category

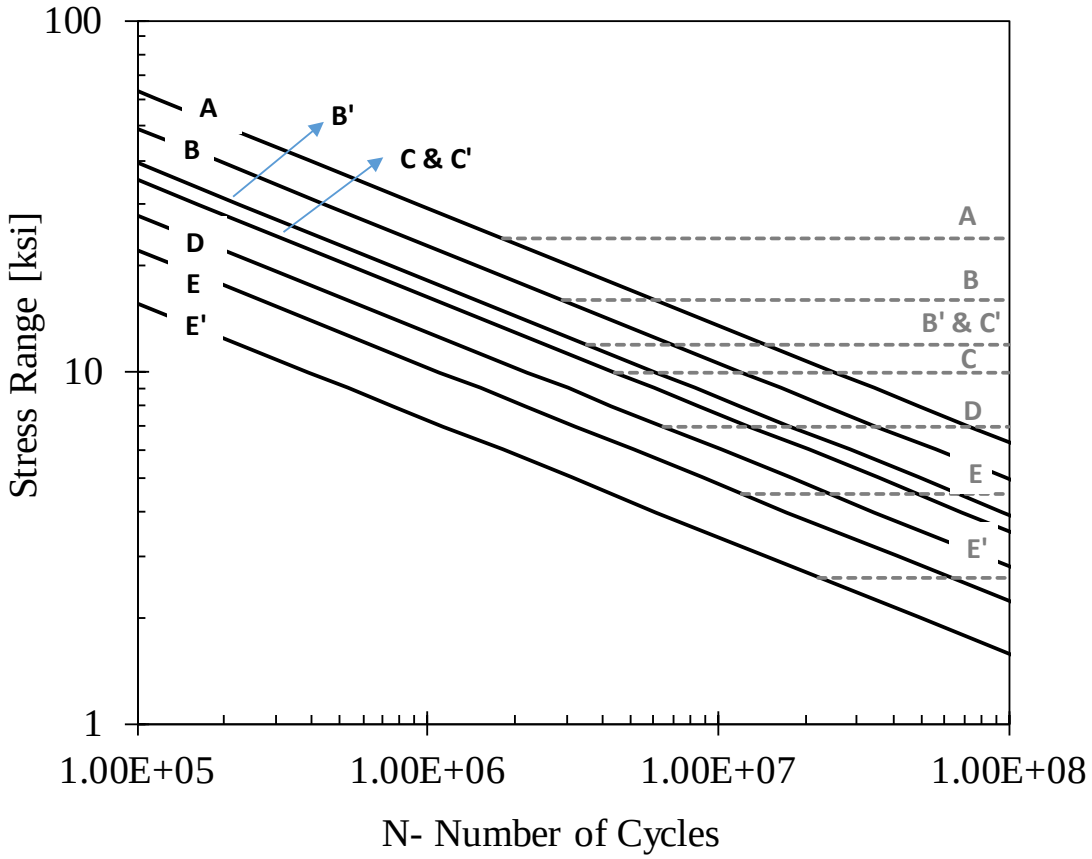

Figure 6-1 2015 AREMA fatigue strength curves.

Table 6-2 Constant *A* and thresholds for detail categories recommended by AREMA 2015.

Detail Category	Constant, *A* , Times 10^8 (ksi^3)	Threshold (CAFL) ksi
A	250.0	24
B	120.0	16
B'	61.0	12
C	44.0	10
C'	44.0	12
D	22.0	7
E	11.0	4.5
E'	3.9	2.6
F	9.0	8
A 325 Bolts in Axial Tension	17.1	31
A 490 Bolts in	31.5	38

Moreover, according to the current fatigue provisions, any structural component must be able to withstand as many as the number of stress cycles produced by assuming 315,000 lbs. railcars in 110 car trains at a frequency of 60 trains per day over an 80-year period [32].

It is important to note that riveted details have certain peculiarities that welded details does not have: the clamping force generated in the riveting process and the redundancy of the built-up section. These two characteristics typically enhance the fatigue life and since it is not accounted for, the fatigue life estimations are usually too conservative.

6.1.2 Linear Elastic Fracture Mechanics concepts

An alternate method of investigating the fatigue life of a component under cyclic loading is by describing mathematically (quantitatively) the propagation of crack(s) in the material through the use of solid mechanics. This field of mechanics, called Fracture Mechanics, has become an important method to evaluate fatigue crack growth in steel details. Crack propagation behavior can be both, fatigue crack propagation (stable growth) and rapid fracture (unstable growth). The stress intensity factor is used in fracture mechanics to describe the stress state, or stress intensity, near the tip of a crack caused by a remote load. The different load types lead to three independent cracking modes, called Mode I, II and III as shown in Figure 6-2.

Mode I is an opening tensile modem where the crack surfaces move directly apart. Mode II is a sliding, in-plane shear, where the crack surfaces slide over one another in a direction perpendicular to the leading edge of the crack. Mode III is a tearing (antiplane shear) mode, where the crack surfaces move relative to one another and parallel to the leading edge of the crack. Mode I is the most common load type encountered in engineering design.

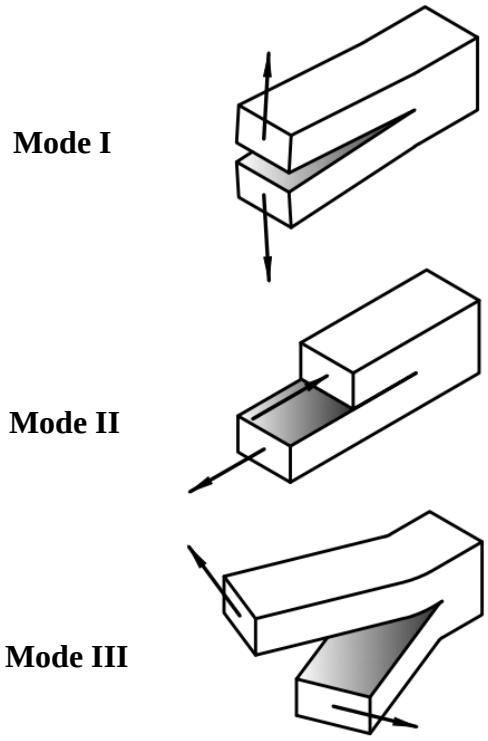

Figure 6-2 Three modes of crack front displacement under different loading conditions

The fatigue crack growth rate, $\frac{da}{dN}$, has been related to the cyclic range of stress intensity factor, ΔK, where ΔK represents the difference between the maximum and minimum stress levels [33].

The range of stress intensity factor can be approximated by the following expression:

$$\Delta K = Y\Delta\sigma\sqrt{\pi a} \qquad \text{Eq. 6.1-3}$$

where Y is an expression that corrects for plate and crack geometry, $\Delta\sigma$ is the stress range, and a is the crack length. The values of ΔK are calculated using Eq. 6.1-3 for particular magnitudes of crack length, a. At very low growth rates, the curve for crack growth in

steel becomes vertical, indicating a crack-growth threshold at ΔK_{TH}, the threshold intensity factor, see Figure 6-3. For stress ranges that produce ΔK below the ΔK_{TH}, crack growth does not occur. At higher values of ΔK, the curve straightens to a near-constant slope, and it becomes vertical again when the fracture toughness is approached at the maximum stress in the cycle. Material properties, stress level, and environment have greater influence in the end (vertical) portions of the curve than in the middle [4].

The threshold stress range intensity factor or fatigue crack propagation threshold, ΔK_{TH}, is the stress intensity associated to the amplitude of cyclic stress range that can be applied to the material without causing fatigue failure. The amplitude of the cyclic stress is also known as fatigue limit, endurance limit or even fatigue strength.

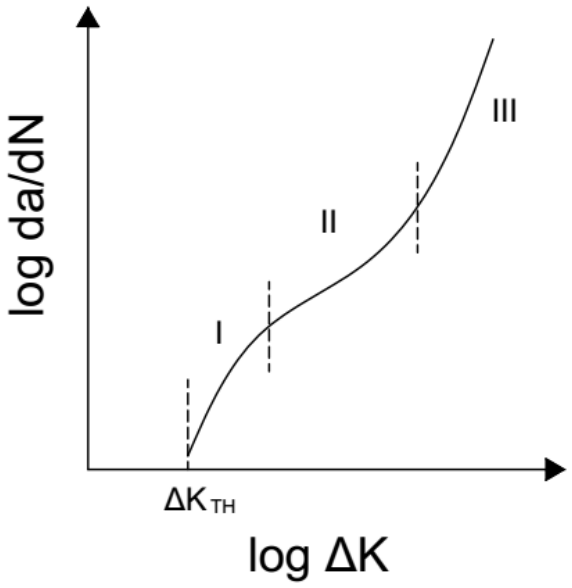

Figure 6-3 Fatigue crack propagation curve.

In region II, which is of considerable engineering interest, the Paris equation is useful. The Paris Power Rule relates the fatigue crack growth rate to the range of stress intensity factor, ΔK, and is given by,

$$\frac{da}{dN} = C\ \Delta K^m \qquad \text{Eq. 6.1-4}$$

where

a = crack length

N = number of cycles

ΔK = range of stress intensity factor

and C and m are constants, functions of material properties, environment, temperature, minimum and maximum stress levels, and frequency of loading. For common steel bridges (ferrite-pearlite steels) the above equation converts into

$$\frac{da}{dN} = 3.6\ \times\ 10^{-10}(\Delta K)^{3.0} \qquad \text{Eq. 6.1-5}$$

where a is crack length in inches and ΔK is the range stress intensity factor in $ksi\sqrt{in}$ [34]. Equation 6.1-5 will be used in the fatigue crack growth model.

A difficulty in using the Paris Power Rule relationship occurs at attempting to determine the stress intensity factor for stress range values near the threshold stress intensity factor, ΔK_{TH} , associated with the fatigue limit. For stress ranges that result in a ΔK smaller than ΔK_{TH} no crack growth occurs.

In a variable amplitude loading scenario some stress ranges result in a ΔK larger than ΔK_{TH}, for which case, the crack tip extension is obtained using the Eq. 6.1-5.

However, some stress ranges of the spectrum would not produce crack tip extension. Therefore, the need to implement a direct cycle-by-cycle integration method.

6.1.3 Direct Cycle-by-Cycle Integration Method

There are three different assumptions in calculating fatigue life of a structural component:

1. Assumes all the stress cycles contribute to crack propagation. Underestimates the fatigue life of the component.
2. Assumes only the stresses above the constant amplitude fatigue limit contribute to crack propagation. Overestimates the fatigue life of the component.
3. Assumes only the stresses above the constant amplitude fatigue limit contribute to crack propagation, *but*, as the crack length progresses the fatigue threshold decrease in magnitude, allowing smaller cycles (that initially didn't contribute to crack growth) to contribute.

Current fatigue provisions are based on the assumption that all the stress cycles of the spectrum contribute to crack propagation. As a result, the current provisions tend to give unrealistic results.

The main purpose of utilizing fracture mechanics to estimate fatigue life is to be able to determine, cycle-by-cycle, if a particular stress cycle drives the crack. Moreover, as the crack grows in length, the fatigue threshold decreases, since a smaller stress will be needed to propagate the crack even further. This cycle-by-cycle analysis is not possible with the current fatigue provisions methodology, S-N curves.

Therefore, in this investigation, crack propagation will be calculated based on a cycle-by-cycle incremental growth with the assumption that only stress ranges with stress intensity factor above the threshold value will drive the crack propagation. That is,

$$\begin{aligned} \Delta a &= C(\Delta k)^n \quad for\ \Delta k > \Delta k_{th} \\ \Delta a &= 0 \qquad\quad for\ \Delta k \le \Delta k_{th} \end{aligned} \qquad \text{Eq. 6.1-6}$$

where *Δa* denotes the crack growth under *one* stress cycle.

The stress spectrum will be repeated during the crack growth simulation model until the crack reaches the failure size (typically the thickness of the component). Information about the contribution of crack growth from each stress range will be collected during the computation. By integrating the crack growth model in increments, the number and distribution of stress cycles that contribute to crack propagation during the total life of the steel detail can be determined. The effective stress range will be calculated based upon the stress ranges that drive the crack growth. The total number of contributing cycles is referred to as the effective cycle life, *N'*. The value of the effective cycle is always less than the nominal cycle life, *N*, determined by the full spectrum.

Infinite fatigue life will be met when the stress intensity factor range, *ΔK*, due to the maximum stress range in the spectrum is less than the fatigue threshold ΔK_{th}, and hence cannot drive the crack to grow.

6.1.4 Fracture Mechanics model assumptions

The following assumptions were considered in order to obtain the fatigue life of a riveted component.

1. The crack initiation phase is negligible. It is assumed that the material has a micro crack, or flaw, that can propagate under the action of external applied cyclic loads.
2. Stress ranges with stress intensity factor above the threshold value will cause crack tip extension. Additionally, as the crack length increase, the threshold value decreases.
3. No crack acceleration or retardation due to large overloads is considered.
4. The inverse slope of the S-N curve and the slope of the crack-growth-rate curves are about equal (m = 3.0) for ferrite-pearlite steels.
5. The number of cycles to failure is set as the crack propagates through the thickness of the component, unless specified otherwise.
6. The corrosion fatigue effect of crack growth is neglected.

6.2 Characteristics of riveted members

Riveting is a method of permanently fastening structural steel components by inserting ductile metals pins, called rivets, into matching holes of the pieces to be jointed. A rivet consists of a circular steel rod, called the shank, of given length and diameter, and two heads. Initially the rivet, consisting of the shank and one head, called the *manufactured head*, is done at the shop. The material to be connected must have matching holes that are generally 1/16 in. greater than the nominal diameter of the undriven rivet. The undriven rivet is heated to the forging temperature of steel, approximately from 1000°F to 1950°F [12, 35]. Once the rivet is red hot, it is inserted into the rivet holes and a head is formed (called the *driven hea*d) at the other end with the help of a pneumatic

hammer or by continuous squeezing with the pressure riveter, as shown in Figure 6-4a. As the rivet cools, it shrinks and squeezes the connected plies together. The area of the material under the rivet head is squeezed, creating a localized compressive stress state, see Figure 6-4b.

Rivets driven in the field during the erection of a structure are known as *field rivets*. Rivets driven in the fabricating shop are known as *shop rivets*. The diameter of an unheated rivet, before driving, is known as the nominal diameter. The grip of the rivets is equal to the total thickness of plates to be joined by the rivet [35].

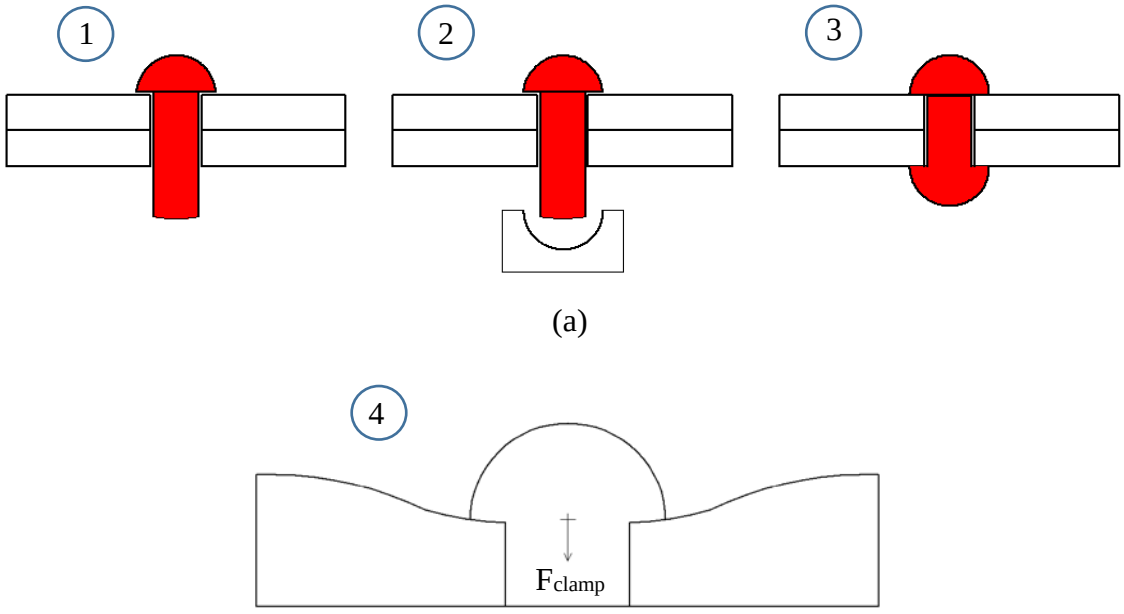

Figure 6-4 Installation process of a hot-driven rivet (b) as the rivet cools, it squeezes the material under the rivet head, creating a local compressive stress state.

6.2.1 Factors contributing to the fatigue strength of riveted members

In general, any mechanical detail (rivets and bolts) has a better fatigue life than

does its equivalent welded detail. First, welding introduces a more severe initial crack situation than does bolting and riveting. Second, inspection for defects in welded details is harder and repairing defects is also difficult. Additionally, riveted details have the beneficial effect of the clamping stress and the redundancy of the riveted built up sections makes their fatigue strength larger than its welded counterpart [4].

However, the riveting process causes residual stresses and initial defects at the connection area. Rivet holes are the major locations of stress concentration and defect in riveted members. Aside from the stress concentration due to the presence of the hole, the fabrication of the hole and rivet installation develops several defects along the edge of the hole. Punched holes give a greater reduction in the fatigue life than do drilled or sub-punched and reamed holes because of imperfections at the hole edge arising from the punching process [4, 12].

The clamping stress caused by hot-driven rivets enhances the fatigue strength in the rivet hole area. The clamping stress develops friction between the plates which restraints crack opening at the edge of rivet holes and thus decrease the crack growth rate [12].

Experiments have yielded important information regarding fatigue crack propagation in riveted members. Fatigue cracks emanating from the edge of the rivet hole are typical [12]. Additionally, the localized compressive stress around the rivet due to clamping delays the initiation of a tension crack or hinders fatigue crack growth [36].

7. ANALYSIS OF LIVE AND IMPACT LOAD STRESSES ON A SIMPLY SUPPORTED RIVETED GIRDER

7.1 Introduction

Since the early 1990's, freight railcar weights increased from 263,000 lbs. to 286,000 lbs. Presently, 286,000 lbs. is no longer the maximum weight, and the railroads have increased it to 315,000 lbs. However, the increase of weight takes a toll on the overall fatigue performance of a railroad bridge. Since one of the main purposes of this investigation is to determine the decrease of fatigue life with an increase of live and impact loads, it was necessary to determine the stresses generated at midspan by using the three heaviest freight railcars used by most railroads. The stress fluctuations were computed assuming 3 locomotives followed by 110 railcars of either 263,000 lbs., 286,000 lbs., or 315,000 lbs.

Description and specifications of the locomotive and the three different freight railcars can be found in Section 7.2.

In AREMA Chapter 15, Article 7.3.3.2, it is specified that under Normal Rating, the stress range considered for the fatigue analysis must be obtained from live load plus impact.

In order to obtain bending stress fluctuations due to a traversing span, it is necessary to count with the bending moment and the cross section geometrical properties, as shown in Eq. 7.1-1. RISA 3D was used to compute the bending moment of the tension fiber at midspan. The geometric cross section(s) and its corresponding moment(s) of inertia is described in section 7.3.

$$\sigma = \frac{Mc}{I} \qquad \text{Eq. 7.1-1}$$

where,

σ = bending stress

M = the internal bending moment about the section's neutral axis

c = the perpendicular distance from the neutral axis to a point on the section

I = the moment of inertia of the section area about the neutral axis.

7.2 Description of locomotive and railcars

To be able to determine the stress fluctuations generated at midspan generated by a passing train, the girder was subjected to the loads of 3 consecutive locomotives SD70 followed by 110 freight cars. The following section describes the specifications for the locomotive and the freight cars.

7.2.1 Locomotive

- Electro Motive Division EMD SD 70 (diesel locomotive- no hammer blow).
- Total weight of the car = 415,000 lbs.
- Overall Length of the locomotive = 72 ft 4 in.
- Number of Axles = 6
- Truck Axle Spacing, the distance between the adjacent axles of a truck = 7 ft
- Truck Center distance, the length between the center pin on the trucks = 45 ft.
- Inboard Axle Spacing, the distance between the insides axles of a railroad car = 31 ft.

- Outboard Axle Spacing, the distance between the outside axles of the railroad car = 11 ft.
- Axle Load = 69,200 lbs.
- P = 34,600 lbs.

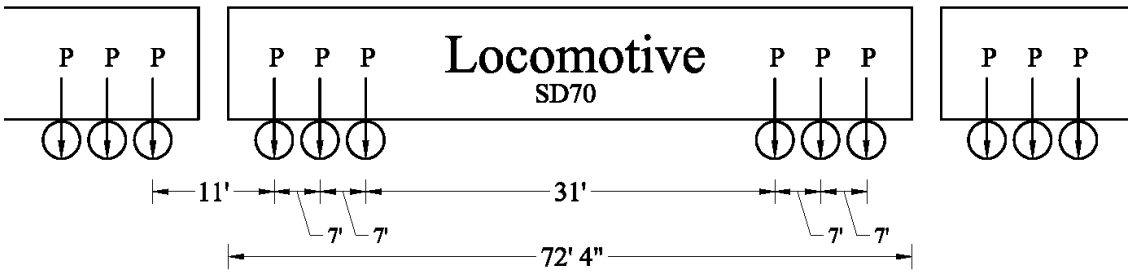

Figure 7-1 Load and spacing for a SD70 locomotive.

7.2.2 Railcars

The three SD70 locomotives pull 110 railcars. To be able to track down the effect of an increase of loading on the fatigue life of riveted details, the train was assumed to be composed of either 263,000 lbs., 286,000 lbs., or 315,000 lbs. railcars. Table 7-1 and Figure 7-2 describe the axle loads and spacing for the railcars.

- Coupler to coupler length = 53 ft.
- Number of Axles = 4
- Truck Axle Spacing, the distance between the adjacent axles of a truck = 6 ft.
- Truck Center distance, the length between the center pin on the trucks = 40.5 ft.
- Inboard Axle Spacing, the distance between the insides axles of a railroad car = 34.5 ft.

- Outboard Axle Spacing, the distance between the outside axles of the railroad car = 6.5 ft.

Table 7-1 The three axle loads for the railcar considered in the analysis.

	Railcar 1	**Railcar 2**	**Railcar 3**
Total weight of the car	263,000 lbs.	286,000 lbs.	315,000 lbs.
Axle load	65,750 lbs.	71,500 lbs.	78,750 lbs.

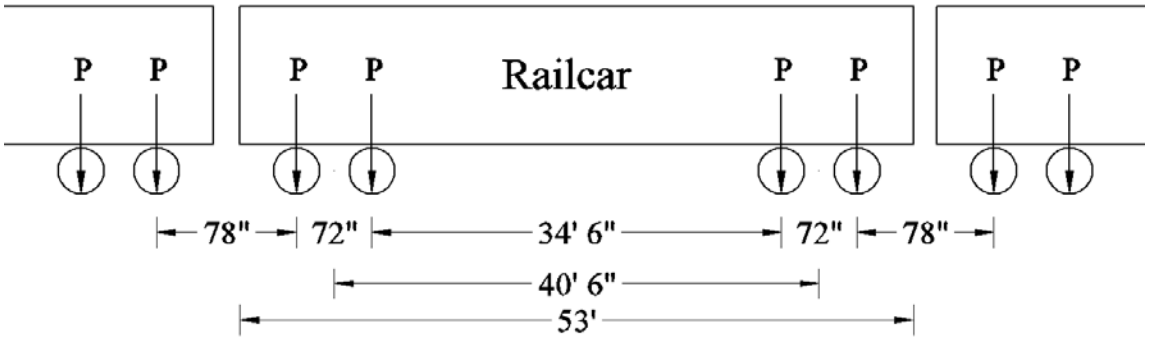

Figure 7-2 Spacing for a 53-ft railcar.

7.3 Cross section and moment of inertia

The girders cross section was obtained from Transportation Technology Center Inc. (TTCI). Norfolk Southern (NS) donated to TTCI a 1912 vintage riveted girder, originally constructed for the Wabash Railroad, and in service over Wildcat Creek in Lafayette, Indiana. The riveted girder was installed in the steel bridge at the Facility for Accelerated Service Testing (FAST) to be tested under heavy axle load (HAL) traffic.

The 55.5 ft. span is a typical example of a riveted steel deck plate girder span. TTCI provided the girder cross section details in order to utilize it in this investigation. Figure 7-3 shows the steel span in revenue service. Figure 7-4 shows the cross sectional

details, Figure 7-5 shows the cover plate terminations and finally Table 7-2 presents centroids, measured from the bottom fiber, and moment of inertias for the three different cross sections of the girder.

Figure 7-3 Vintage riveted steel girder span in revenue service. Reprinted with permission from Otter et al. [14].

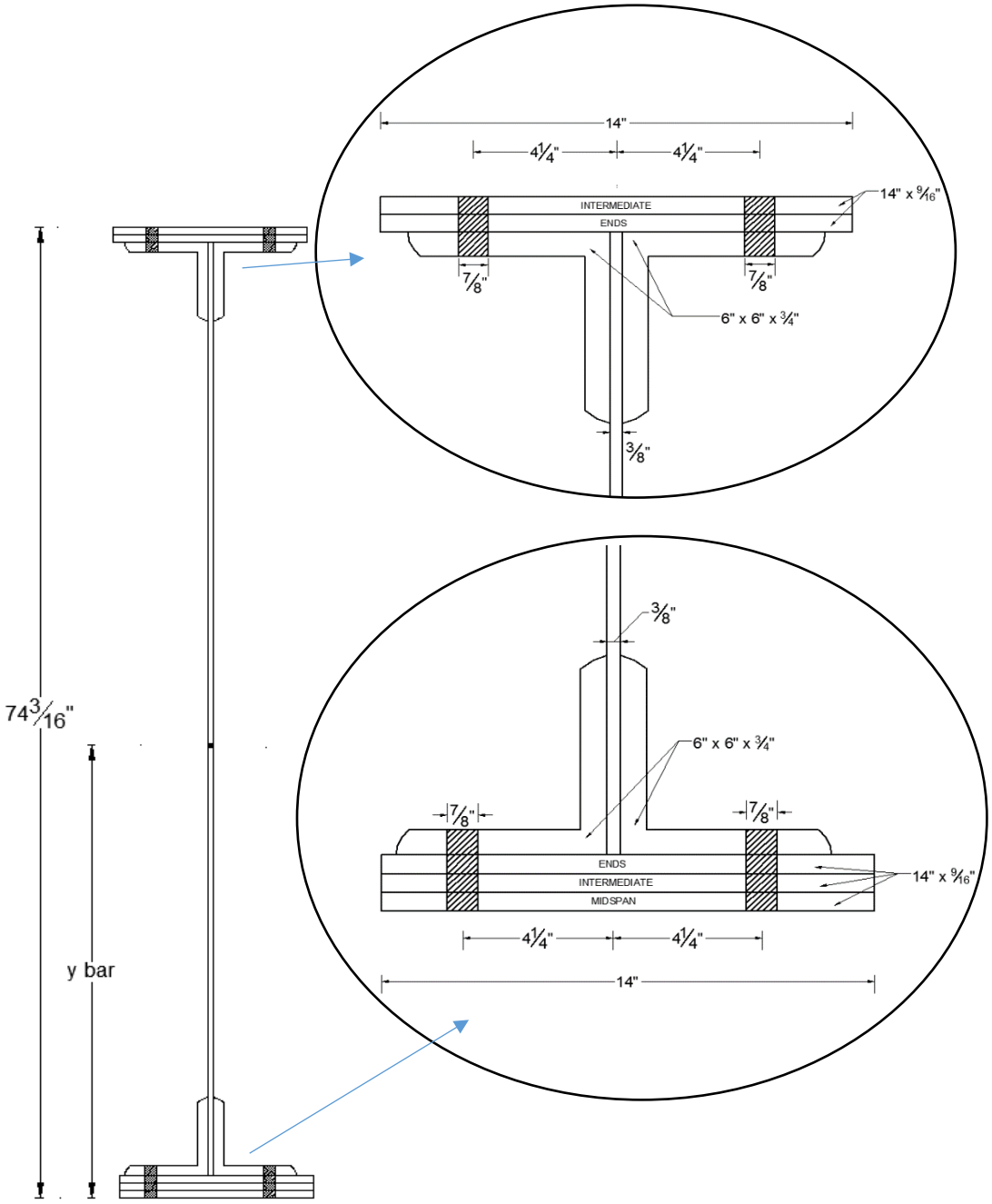

Figure 7-4 Riveted girder cross section.

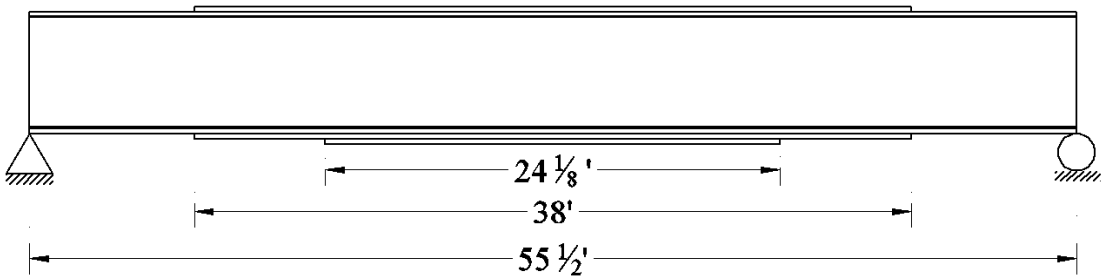

Figure 7-5 Cover plate terminations for the 55.5-foot riveted girder.

Table 7-2 Centroids and moment of inertia for the three different cross sections of the riveted girder.

Cross Section	$\bar{y}$ [in]	I [in^4]
Ends	36.3	64,460.8
Intermediate	33.6	72,793.8
Midspan	34.6	91,379.9

7.4 Number of cycles produced by a passing train

The number of stress cycles experienced by a railroad bridge girder will depend on its length and the inside axle spacing of the cars. Spans that are shorter than the inside axle spacing of the cars experience full unloading under each car, and thus full stress range cycles for each car, making them more susceptible to fatigue [32]. See Table 7-3.

Table 7-3 Number of stress cycles per train crossing for different span lengths.

Span Length, L [ft]	Stress Cycles per train crossing
$L \leq 50$	110
$50 < L \leq 75$	55
$75 < L \leq 100$	6
$L > 100$	3

On spans exceeding 100 feet, the number of cycles vary from 3 to 31 per 100-car train.

Therefore, for the 55.5-ft long span used in this study, 110 railcars will induce 55 cycles. Note that, the number of cycles presented in Table 7-3 account only for the railcars, disregarding the cycles produce by the locomotives.

7.5 Stress sequence at midspan due to live load

The bending stress variations due to a passing train consisting of 3 locomotives and 2 freight cars is shown in Figure 7-7, Figure 7-8, and Figure 7-9. The first peak is due to the locomotive's first three axles (first truck); the second and third peaks are due to 2 consecutive locomotive trucks; the fourth peak is due to the third locomotive's last truck and the first freight car truck consisting of two axles; the fifth peak is generated by 2 railcars trucks (this peak will be repeated 54 times more, since it is related to the number of railcars passing through and the span length) and the last peak is generated by the second truck of the last railcar passsing by. This makes a total of 60 peaks. Figure 7-6 shows graphically how the stress peaks are formed when the train passes through the bridge.

The following nomenclature will be adopted from here on; *Train 1* consists of 3 consecutive SD70 locomotives followed by 110 railcars each weighing 263,000 lbs.; *Train 2* consists of 3 consecutive SD70 locomotives followed by 110 railcars each weighing 286,000 lbs.; and *Train 3* consists of 3 consecutive SD70 locomotives followed by 110 railcars each weighing 315,000 lbs.

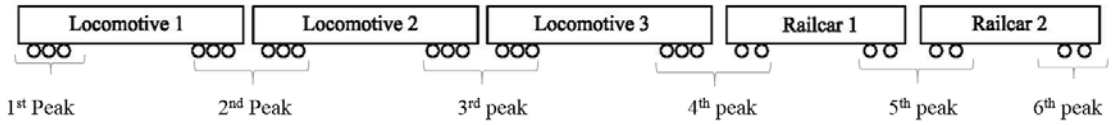

Figure 7-6 Stress peaks generated when 3 locomotive and 2 railcars pass through a 55.5-ft long girder.

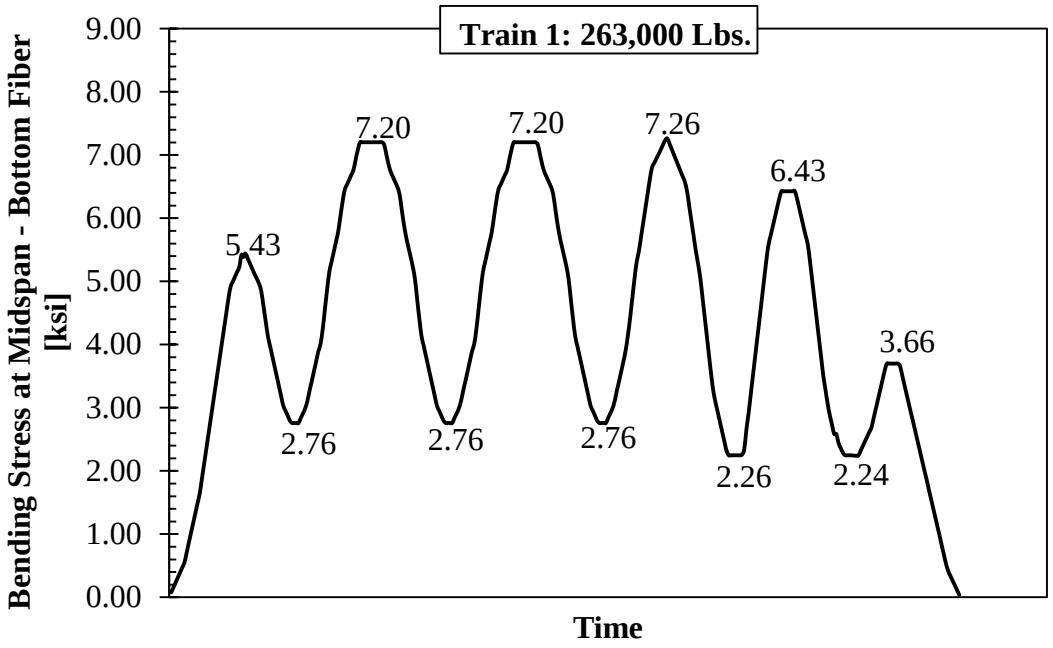

Figure 7-7 Stress fluctuations at mid-span due to Train 1 passing through a 55.5 ft-simply supported girder.

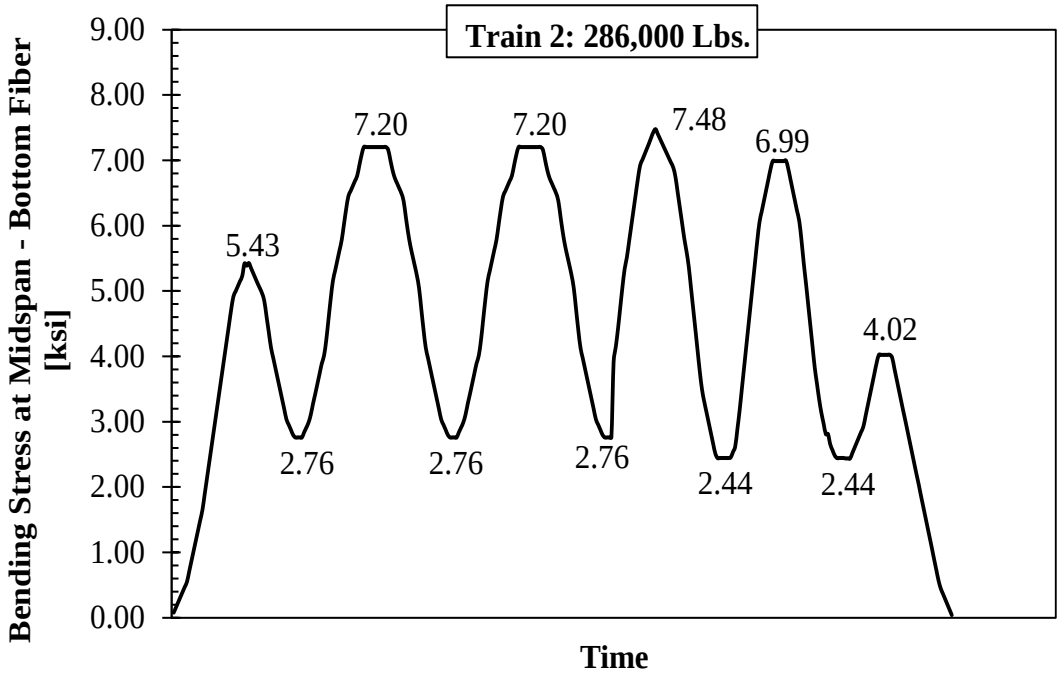

Figure 7-8 Stress fluctuations at mid-span due to Train 2 on a 55.5 ft. simply supported girder.

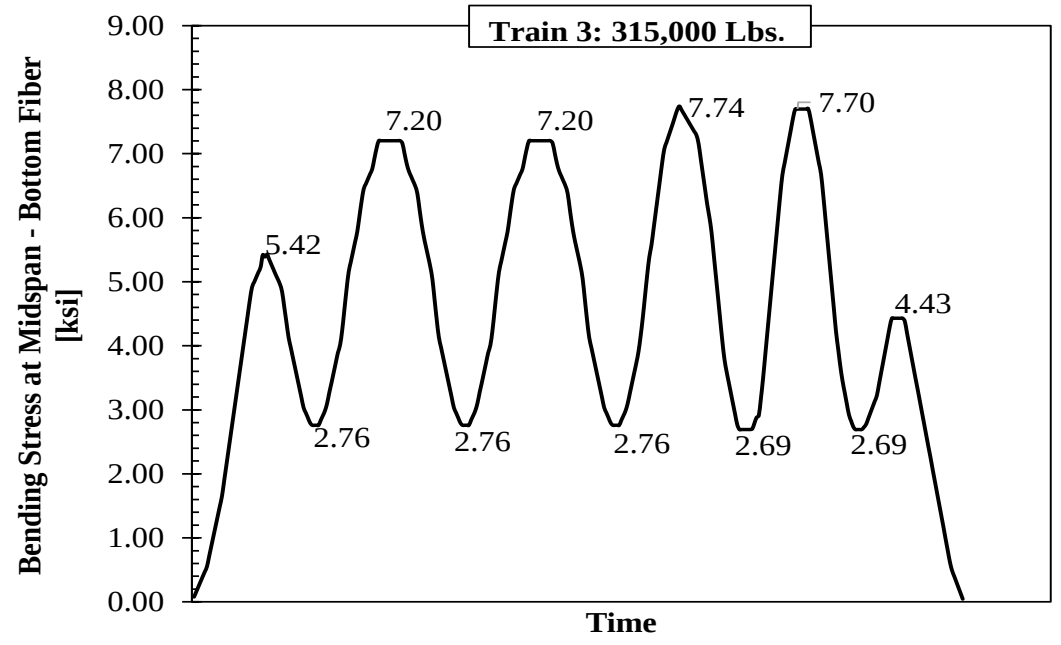

Figure 7-9 Stress fluctuations at mid-span due to Train 3 on a 55.5 ft. simply supported girder.

7.6 Effective stress range

Having obtained the stress fluctuations for Trains 1-3 in the previous section, the variable amplitude block loading is transformed into an equivalent stress range, S_{re}, using the root-mean-cube method. The effective constant amplitude stress causes the same amount of fatigue damage as the variable amplitude stress range loading.

The stress fluctuations presented in section 7.5 is utilized to identify the peaks and troughs and to identify the number of cycles generated for each passing train. Peaks and troughs for each train are shown in Table 7-4, Table 7-6, and Table 7-8 for trains 1-3. The rainflow counting method was applied on Figure 7-10, Figure 7-11 and Figure 7-12. Finally, the root mean cube method was applied for the three trains to obtain the equivalent stress range, S_{re}.

The effective stress ranges are 4.25 ksi for *Train 1*, 4.54 ksi for *Train 2*, and 5.02 ksi for *Train 3* as shown in Table 7-5, Table 7-7, and Table 7-9.

Table 7-4 Stress peaks and troughs for Train 1.

		Stress [ksi]
A	0	0
B	1	5.43
C	2	2.76
D	3	7.2
E	4	2.76
F	5	7.2
G	6	2.76
H	7	7.26
I	8	2.26
J	9	6.43
K	10	2.24
L	11	3.66
M	12	0

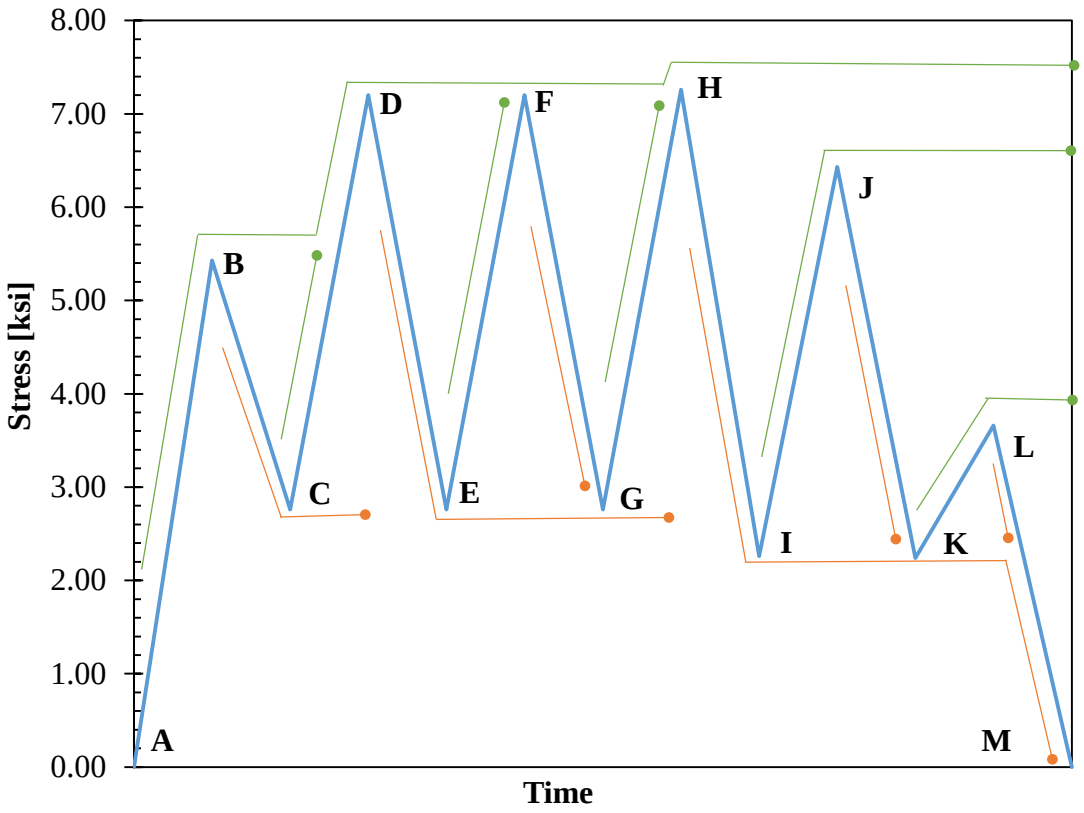

Figure 7-10 Rainflow analysis of stress history for Train 1.

Table 7-5 Rainflow counting and root-mean-cube method analysis for Train 1.

From [ksi]	To [ksi]	Cycles, ni	Stress Range, ΔS [ksi]	Frequency	Col 2 * Col 4	gi = ni/N	gi*(ΔS)^3
0	7.26	0.5	**7.26**	1	0.5	0.008	3.19
2.76	5.43	0.5	2.67	1	0.5	0.008	0.16
2.76	7.2	0.5	4.44	1	0.5	0.008	0.73
2.76	7.26	0.5	4.5	1	0.5	0.008	0.76
2.26	6.43	0.5	4.17	55	27.5	0.458	33.23
2.24	3.66	0.5	**1.42**	1	0.5	0.008	0.02
5.43	2.76	0.5	2.67	1	0.5	0.008	0.16
7.2	2.76	0.5	4.44	1	0.5	0.008	0.73
7.2	2.76	0.5	4.44	1	0.5	0.008	0.73
7.26	0	0.5	**7.26**	1	0.5	0.008	3.19
6.43	2.24	0.5	4.19	55	27.5	0.458	33.72
3.66	2.24	0.5	**1.42**	1	0.5	0.008	0.02
				N =	60	Σ =	76.64
						Sre =	**4.25** **ksi**

Table 7-6 Stress peaks and troughs for Train 2.

		Stress [ksi]
A	0	0
B	1	5.43
C	2	2.76
D	3	7.2
E	4	2.76
F	5	7.2
G	6	2.76
H	7	7.48
I	8	2.44
J	9	6.99
K	10	2.44
L	11	4.02
M	12	0

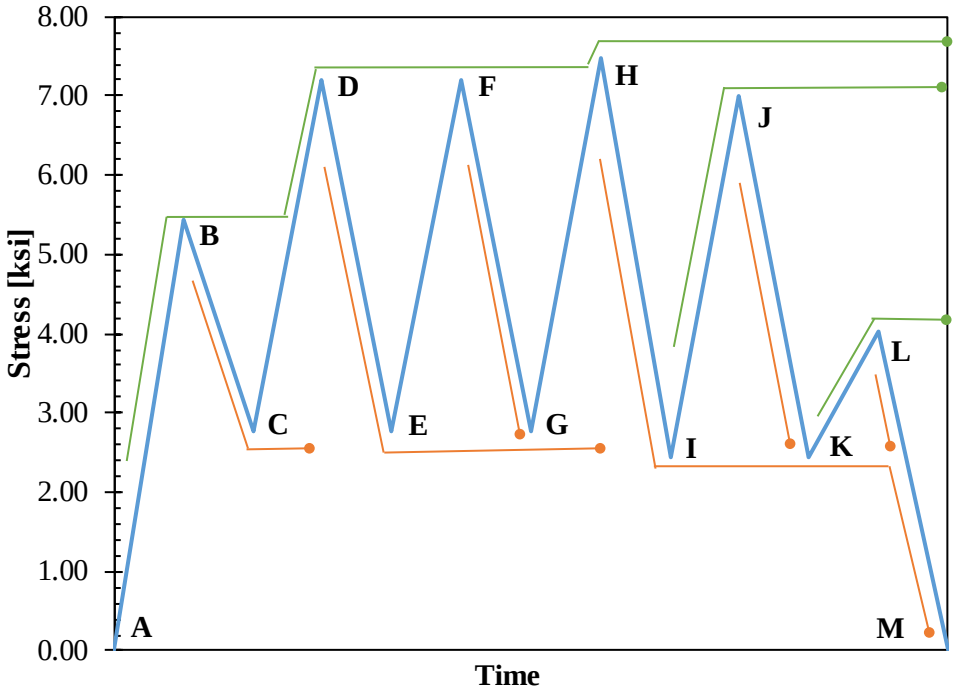

Figure 7-11 Rainflow analysis of stress history for Train 2.

Table 7-7 Rainflow counting and root-mean-cube method analysis for Train 2.

From [ksi]	To [ksi]	Stress Range, ΔS [ksi]	Cycles, ni	Frequency	Col 4 x Col 5	gi = ni/N	gi*(ΔS)^3
0	7.48	**7.48**	0.5	1	0.5	0.008	3.49
2.76	5.43	2.67	0.5	1	0.5	0.008	0.16
2.76	7.2	4.44	0.5	1	0.5	0.008	0.73
2.76	7.48	4.72	0.5	1	0.5	0.008	0.88
2.44	6.99	4.55	0.5	55	27.5	0.458	43.17
2.44	4.02	**1.58**	0.5	1	0.5	0.008	0.03
5.43	2.76	2.67	0.5	1	0.5	0.008	0.16
7.2	2.76	4.44	0.5	1	0.5	0.008	0.73
7.2	2.76	4.44	0.5	1	0.5	0.008	0.73
7.48	0	**7.48**	0.5	1	0.5	0.008	3.49
6.99	2.44	4.55	0.5	55	27.5	0.458	43.17
4.02	2.44	**1.58**	0.5	1	0.5	0.008	0.03
				N =	60	Σ =	93.28
						Sre =	**4.54** **ksi**

Table 7-8 Stress peaks and troughs for Train 3.

		Stress [ksi]
A	0	0
B	1	5.42
C	2	2.76
D	3	7.2
E	4	2.76
F	5	7.2
G	6	2.76
H	7	7.74
I	8	2.69
J	9	7.7
K	10	2.69
L	11	4.43
M	12	0

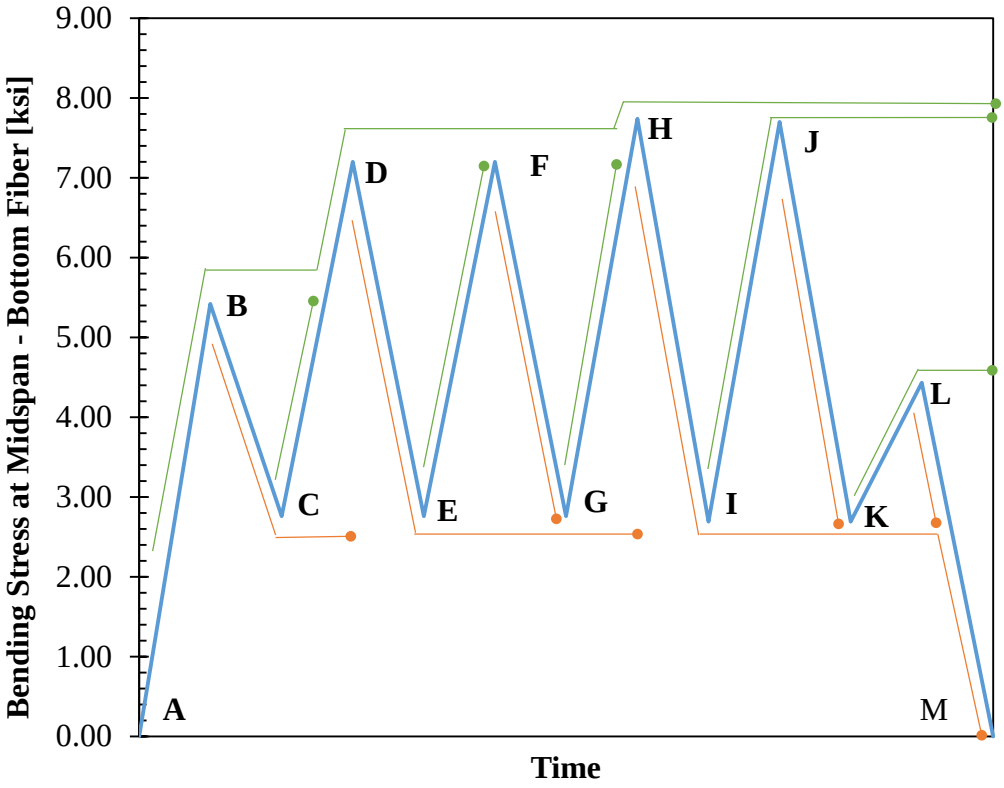

Figure 7-12 Rainflow analysis of stress history for Train 3.

Table 7-9 Rainflow counting and root-mean-cube method analysis for Train 3.

From [ksi]	To [ksi]	Stress Range [ksi]	Cycles, ni	Frequency	Col 4 x Col 5	gi = ni/N	gi*(ΔS)^3
0	7.74	**7.74**	0.5	1	0.5	0.008	3.86
2.76	5.43	2.67	0.5	1	0.5	0.008	0.16
2.76	7.2	4.44	0.5	1	0.5	0.008	0.73
2.76	7.2	4.44	0.5	1	0.5	0.008	0.73
2.69	7.7	5.01	0.5	55	27.5	0.458	57.64
2.69	4.43	**1.74**	0.5	1	0.5	0.008	0.04
5.42	2.76	2.66	0.5	1	0.5	0.008	0.16
7.2	2.76	4.44	0.5	1	0.5	0.008	0.73
7.2	2.76	4.44	0.5	1	0.5	0.008	0.73
7.74	0	**7.74**	0.5	1	0.5	0.008	3.86
7.7	2.69	5.01	0.5	55	27.5	0.458	57.64
4.43	2.69	**1.74**	0.5	1	0.5	0.008	0.04
				N =	60	Σ =	126.32
						Sre =	**5.02** **ksi**

7.7 Impact load

Since the computation of stresses for fatigue design need to include the additional stress induced by impact, it is necessary to determine the Impact load in accordance with section 1.3.5 of AREMA (2015).

The impact load due to vertical effects, expressed as a percentage of live load applied to each rail, for span lengths less than 80 feet and for freight/passenger cars and for locomotives other than steam (rolling equipment without hammer blow) was determined in the following way:

$$40 - \frac{3L^2}{1600} \qquad \text{Eq. 7.7-1}$$

where L = length in feet, center to center of supports for stringers, transverse floorbeams without stringers, longitudinal girders and trusses.

In accordance with section 1.3.13 of AREMA (2015) mean impact load for fatigue design shall be taken as a percentage of the load specified in Eq. 7.7-1. Percentage values are specified in Table 7-10.

Table 7-10 Assumed mean impact load percentages for fatigue design recommended by AREMA 2015.

Member	**Percentage**
Members with loaded Lengths ≤ 10 feet (3 m) and no load sharing	65%
Hangers	40%
Other Truss members	65%
Beams, Stringers, Girders and Floorbeams	35%
Note: Where bridges are designed for operation of trains handling a large percentage of cars with flat or out of round wheels which increase impact and/or poor track which increases impact, and the loaded length of the member is less than 80 feet (24 m), the mean impact should be 100% of the design impact.	

For the case of riveted girders, only 35% of Eq. 7.7-1 should be considered.

Moreover, AREMA allows a reduction to impact load if the speed of the train is below 60 mph. (Article 7.3.2.3). For train speeds below 60 mph, for all spans carrying equipment without hammer blow and for all spans other than truss spans carrying equipment with hammer blow, the values of the vertical effects of the impact equations shall be multiplied by the factor:

$$1 - \frac{0.8}{2500}(60 - S)^2 \geq 0.2 \text{ where } S = \text{speed in mph} \qquad \text{Eq. 7.7-2}$$

For a span length of 55.5 feet, and a train speed of 40 mph, impact load is 10.4% of the live load for the riveted girder.

Finally, the minimum and maximum stress ranges obtained in section 7.5 due to live load are presented in Table 7-11, amplified by 10.4% to account for impact.

Table 7-11 Maximum and minimum stress ranges for trains 1, 2 and 3.

	Live Load		**Live + Impact Load**	
	S_r min [ksi]	**S_r max [ksi]**	**S_r min [ksi]**	**S_r max [ksi]**
Train 1: 263,000 Lbs	1.42	7.26	1.57	8.02
Train 2: 286,000 Lbs	1.58	7.48	1.74	8.26
Train 3: 315,000 Lbs	1.74	7.74	1.92	8.55

It is important to note that most of the heavy axle load studies done so far uses 53-foot long coal cars, however, minimum-length interchange car that are typically 43-foot long can produce higher stresses on longer bridge spans. The axle spacing dimensions are critical in determination of the potential cycles that may accumulate during a train passage [37, 38]. Moreover, it has also been found that short length cars affect more severely primary members than secondary members [39]. Therefore, ratio of length of railcars to span length influence the number and magnitude of stress cycles.

8. FATIGUE CRACK PROPAGATION MODEL

8.1 Purpose and procedure

To refine the current fatigue provisions, a linear elastic fracture mechanics approach was used instead of the traditional S-N curves. It was earlier mentioned that LEFM is more convenient since it follows a certain criterion to determine if a specific stress range propagates the crack. This is not possible with the S-N curves. However, LEFM present another challenges. The stress intensity factor required in the calculation will vary significantly with the type of crack considered. In aircraft structures, where the plates being riveted are extremely thin, a through-thickness crack of length '*L*' will be wise to assume, as shown in Figure 8-1a. However, in steel bridges, where the steel plates are usually thicker than 0.25-in., a "crack emanating from a round hole" is not applicable. For thicker plates, the crack will still emanate from the edge of the rivet hole, but the crack will most likely be of a semi-elliptical shape, as given in Figure 8-1b. In the former case, fatigue life consists on the number of stress cycles that are required to take the crack from a length L_o to a critical length, L_c. In the latter case, the crack growth is different: because of its semi-elliptical shape, the crack will have a length '*c*' and a depth '*a*'. Each of these, length and depth, will grow based on the magnitude of the stress intensity factor at the crack front in these two specific directions. In other words, the crack growth rate is different along the length, $\frac{dc}{dN}$, than what it is along the depth of the crack, $\frac{da}{dN}$.

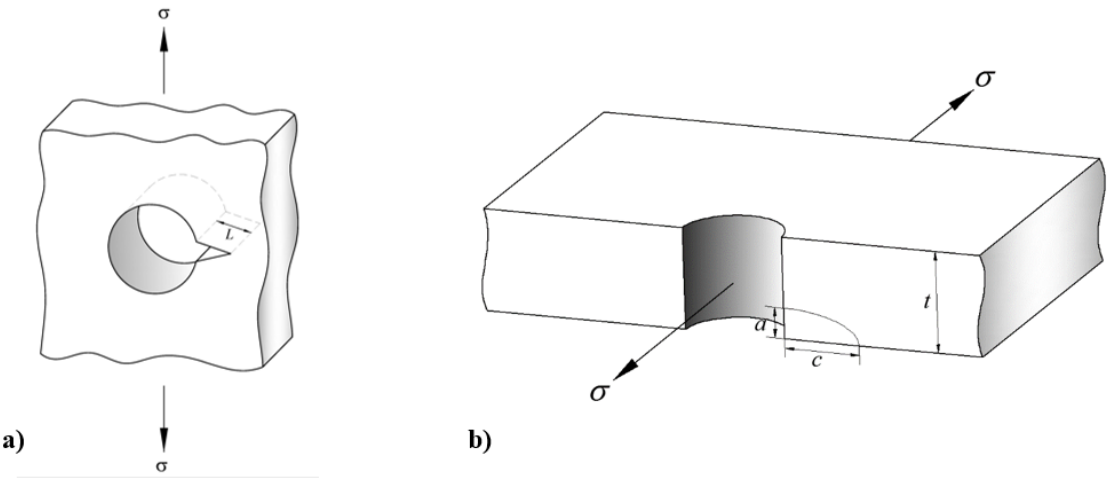

Figure 8-1 Crack configurations. (a) Crack emanating from a hole; (b) elliptical corner crack emanating from a through- thickness hole.

It is important to clarify that a riveted connection may fall into one of two situations described in Figure 8-2. Assuming a simply supported riveted girder under four-point bending, the moment diagram will be divided into three sections: at both ends, the moment will vary in a linear fashion, and between loads the moment can be consider constant. If a rivet is situated at any of the ends, where the bending moment is linear, the connection will behave as a single shear lap joint. On the other hand, if the rivet is situated in the constant moment region, there is no shear transfer between plates. Although the residual stress produced during the installation is the same (considering exact dimensions for the plates and the rivet), load endurance is different in both cases. In a shear lap joint, load is transferred from one plate to another by two means. The majority of the load transferred happens by bearing between the rivets and the plates, while the remainder is transferred through friction between the faying surfaces. While crack propagation may seem identical

for both cases, in a shear lap joint, cracks that form between faying surfaces will be relatively hindered due to the presence of friction. Additionally, shear lap joints tend to suffer fretting fatigue [40]. Predictions of a shear lap joint behavior accounting for the contribution of fretting remain in an academic interest range [41].

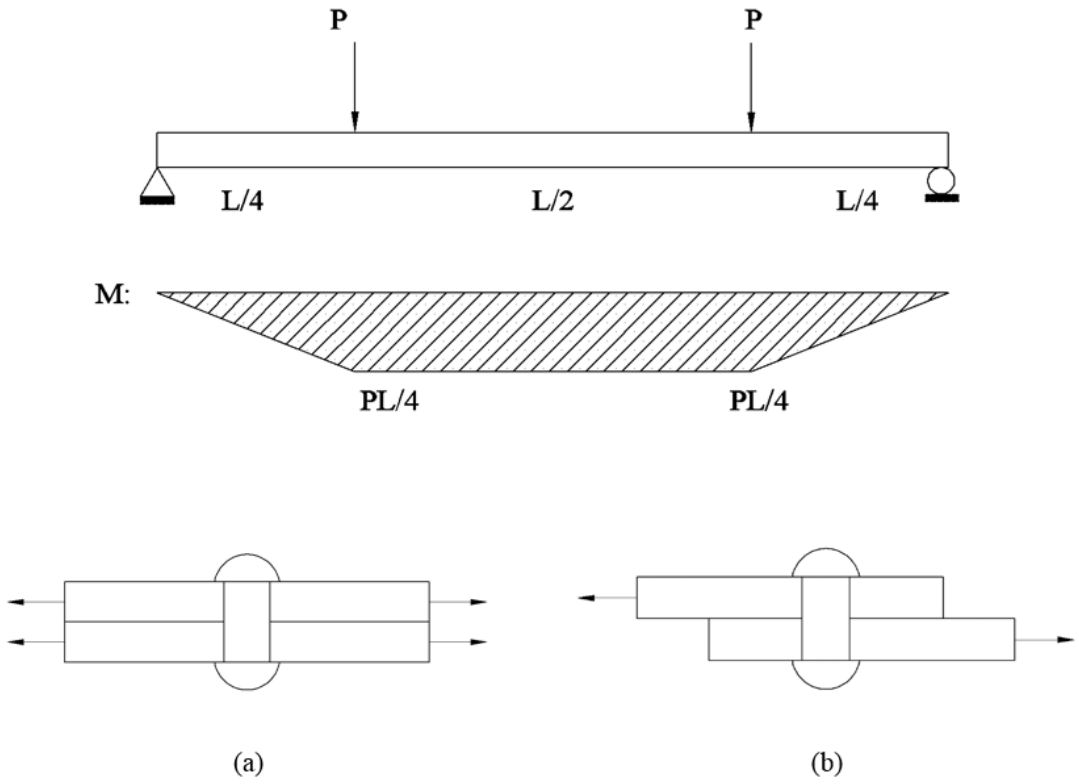

Figure 8-2 Two distinct behaviors of a riveted connection in a simply supported girder under four-point bending (a) in the constant moment region, where there is no shear (b) at both ends, where a portion of the load is transferred through shear.

In this investigation, a riveted connection located in a constant moment region will be studied. Thus, no shear transfer between plates will be assumed and therefore no

fretting will be considered. A corner crack emanating from the rivet hole under remote tension and local residual stress will be investigated.

This chapter is dedicated to the fatigue life of a riveted steel girder using a linear elastic fracture mechanics approach and assuming an elliptical corner crack will emanate from the edge of the hole. Thermal residual stresses were not included in this chapter. The stress fluctuations of Section 7.5, amplified by impact, will be utilized as the variable amplitude spectrum. Finally, a parametric study will be performed to determine the effect of overloads and the effect on the initial crack size (length and depth) have on fatigue life calculations.

8.2 Geometry and inputs

The riveted component under investigation consisted of two steel plates riveted at midspan. Figure 8-3 shows the transverse cut of the riveted detail.

Plate Dimensions: 5/8 in. thickness and width of the plate 5 in.

Rivet shank: 1.25 in. tall and a diameter of 7/8 in.

Rivet head: 11/16 in. radius.

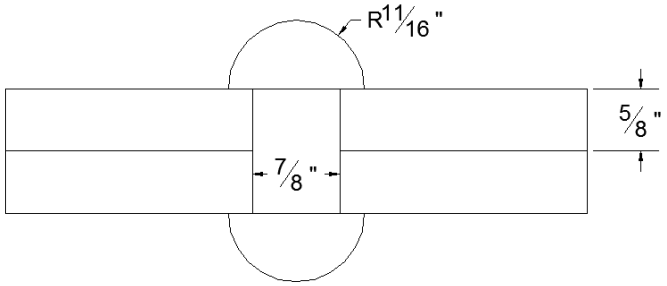

Figure 8-3 Transverse cut of the riveted detail in question.

Fatigue life will be significantly affected by the assumed initial flaw in the material. Therefore, a parametric study was performed to evaluate and quantify the impact this parameter has on the overall fatigue life of the detail. Inputs that were necessary in the analysis and remained constant throughout the investigation, are listed on Table 8-1.

Table 8-1 Values used in LEFM fatigue analysis.

Plate hole diameter, 2r	29/32 in
Plate thickness, t	5/8 in
Plate width, 2b	5 in

The plate hole diameter is equivalent to the diameter of the rivet hole plus 1/32 in, this comes out to be 29/32 in. Barsom and Rolfe [34] suggests that a good estimate of $\Delta K_{TH,}$ in ksi$\sqrt{}$in, for ferrite-pearlite steels subjected to various load ratios can be predicted from:

$$\begin{aligned} \Delta K_{TH} &= 6.4(1-0.85R) \quad R > 0.1 \\ \Delta K_{TH} &= 5.5 \quad R < 0.1 \quad ksi\sqrt{in} \end{aligned} \qquad \text{Eq. 8.2-1}$$

8.3 Stress intensity factors for two symmetrical elliptical corner cracks from an open hole

In order to predict crack-propagation life and fatigue strength, accurate stress intensity factors for the specific geometry are needed. However, due to the complexity of the problem, exact analytical solutions are not available. The use of approximate analytical methods has permitted to estimate the stress intensity factor for several configurations. Newman and Raju applied three-dimensional finite element analyses to obtain equations

for the stress-intensity factors for a wide variety of configurations subjected to either tension or bending loads [42].

In this investigation and in accordance with Zhou [12], the shape of the crack is a quarter of an ellipse, Figure 8-1b. Therefore, the stress intensity factor equations utilized will be based on the equations proposed by Newman and Raju for a quarter-elliptical corner crack at a hole. In these equations, the ratio of crack depth to plate thickness (*a/t*) ranged from 0 to 1, the ratio of crack depth to crack length (*a/c*) ranged from 0.2 to 2, the ratio of hole radius to plate thickness (*r/t*) ranged from 0.5 to 2, and the ratio $(r + c)/b < 0.5$. The effects of plate width (*b*) on stress –intensity variations along the crack front were also included, but were generally based on engineering estimates. Figure 8-4 shows an elliptical corner crack at the edge of the hole.

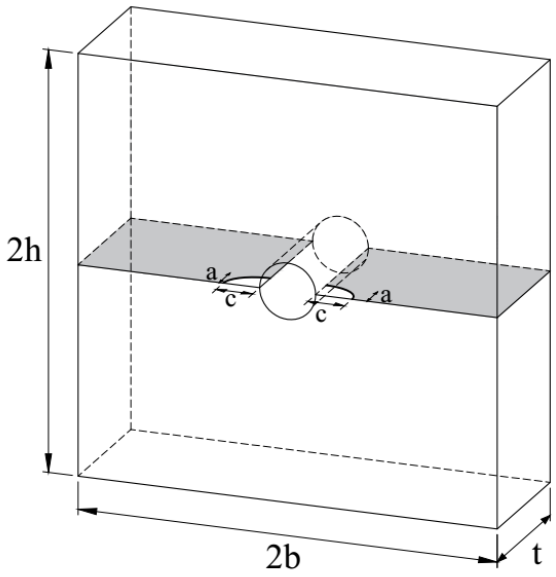

Figure 8-4 Elliptical corner crack emanating from the edge of a hole in a finite plate.

The stress intensity factor equations for *two* symmetric quarter-elliptical corner cracks at a hole in a finite plate subject to tension, *S*, is of the form:

$$K_I = S\sqrt{\pi\frac{a}{Q}}\,F_{ch}\left(\frac{a}{c},\frac{a}{t},\frac{R}{t},\frac{R}{b},\frac{c}{b},\phi\right) \qquad \text{Eq. 8.3-1}$$

where Q is the shape factor for an ellipse and F_{ch} accounts for the influence of various boundaries and geometric dimensions.

$$Q = \begin{cases} 1 + 1.464\left(\frac{c}{a}\right)^{1.65} & for\ \ \frac{a}{c} > 1 \\ 1 + 1.464\left(\frac{a}{c}\right)^{1.65} & for\ \ \frac{a}{c} \le 1 \end{cases} \qquad \text{Eq. 8.3-2}$$

$$F_{ch} = \left[M_1 + M_2\left(\frac{a}{t}\right)^2 + M_3\left(\frac{a}{t}\right)^4\right] g_1 g_2 g_3 f_\phi f_w \qquad \text{Eq. 8.3-3}$$

For $a/c \le 1$

$$M_1 = 1.13 - 0.09\left(\frac{a}{c}\right) \qquad \text{Eq. 8.3-4}$$

$$M_2 = -0.54 + \frac{0.89}{0.2 + \frac{a}{c}} \qquad \text{Eq. 8.3-5}$$

$$M_3 = 0.5 - \frac{1}{0.65 - \frac{a}{c}} + 14\left(1 - \frac{a}{c}\right)^{24} \qquad \text{Eq. 8.3-6}$$

$$g_1 = 1 + \left[0.1 + 0.35\left(\frac{a}{t}\right)^2\right](1 - sin\phi)^2 \qquad \text{Eq. 8.3-7}$$

$$g_2 = \frac{1 + 0.358\lambda + 1.425\lambda^2 - 1.578\lambda^3 + 2.156\lambda^4}{1 + 0.13\lambda^2} \quad \text{Eq. 8.3-8}$$

Where,

$$\lambda = \frac{1}{1 + \frac{c}{R}\cos(0.85\phi)} \quad \text{Eq. 8.3-9}$$

$$g_3 = \left(1 + 0.04\frac{a}{c}\right)[1 + 0.1(1 - cos\phi)^2]\left[0.85 + 0.15\left(\frac{a}{t}\right)^{1/4}\right] \quad \text{Eq. 8.3-10}$$

$$f_w = \left[sec\left(\frac{\pi R}{2b}\right) sec\left(\frac{\pi(2R + nc)}{4(b - c) + 2nc}\sqrt{\frac{a}{t}}\right)\right]^{1/2} \quad \text{Eq. 8.3-11}$$

For *a/c > 1*

$$M_1 = \sqrt{\frac{c}{a}}\left(1 + 0.04\frac{c}{a}\right) \quad \text{Eq. 8.3-12}$$

$$M_2 = 0.2\left(\frac{c}{a}\right)^4 \quad \text{Eq. 8.3-13}$$

$$M_3 = -0.11\left(\frac{c}{a}\right)^4 \quad \text{Eq. 8.3-14}$$

$$g_1 = 1 + \left[0.1 + 0.35\left(\frac{c}{a}\right)\left(\frac{a}{t}\right)^2\right](1 - sin\phi)^2 \quad \text{Eq. 8.3-15}$$

The functions g_2 and λ are given by 8.3-8 and 8.3-9.

$$g_3 = \left(1.13 - 0.09\frac{c}{a}\right)[1 + 0.1(1 - cos\phi)^2]\left[0.85 + 0.15\left(\frac{a}{t}\right)^{1/4}\right] \qquad \text{Eq. 8.3-16}$$

$$f_\phi = \left[\left(\frac{c}{a}\right)^2 sin^2\phi + cos^2\phi\right]^{1/4} \qquad \text{Eq. 8.3-17}$$

Figure 8-5 shows the coordinate system used to define the parametric angle, ϕ, for *a/c* less than and *a/c* greater than unity.

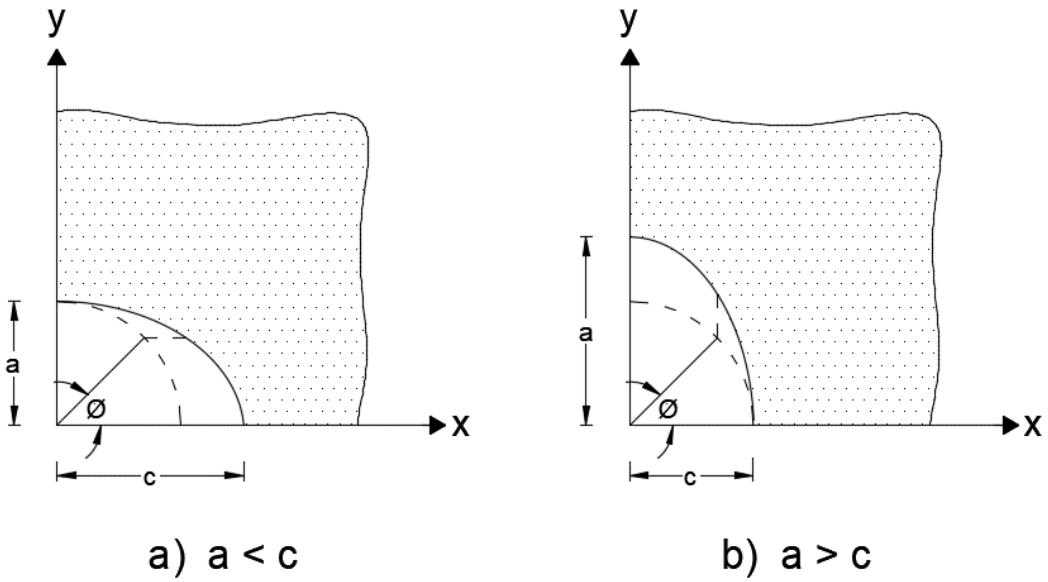

Figure 8-5 Coordinate system used to define parametric angle.

The stress intensity factor for a single crack emanating from a hole can be estimated from the results for two symmetric surface cracks by using a conversion factor developed by Shah [43]. The relationship between one and two surface cracks is given by,

$$(K_I)_{one\ crack} = \sqrt{\frac{\frac{4}{\pi} + \frac{ac}{2tR}}{\frac{4}{\pi} + \frac{ac}{tR}}}\,(K_I)_{two\ cracks} \qquad \text{Eq. 8.3-18}$$

where *K* for two cracks must be fist evaluated for an infinite plate ($f_w = 1$) and then the finite-width correction for one crack must be applied.

8.4 Algorithm

The main purpose of utilizing a linear elastic fracture mechanics approach is to be able to determine specifically the stress cycles that contribute to crack propagation. In other words, not all the stress cycles from the spectrum initially contribute to crack growth: for each stress range, the stress intensity factor (*ΔK*) at the crack tip will be determined, if, and only if, this value (*ΔK*) overcomes ΔK_{TH}, crack growth occurs. Since the calculation of stress intensity factor *ΔK* is directly proportional to the crack size, one can deduce that the longer the crack, the faster it will propagate, because more *ΔKs* will overcome the threshold value.

The algorithm used to evaluate the fatigue life of a riveted detail under variable amplitude loading using LEFM is the following:

1. Assume an initial crack size.
2. Determine ΔK_{TH} using equation 8.2-1.
3. For each stress range cycle part of the spectrum:
    a. Calculate the range of stress intensity factor.

$$\Delta K = F_{ch} S_r \sqrt{\frac{\pi a}{Q}} \qquad \text{Eq. 8.4-1}$$

b. If $\Delta K > \Delta K_{TH}$ then

   i. Calculate crack growth using Paris-Power rule for ferrite pearlite steels using Eq. 6.3-3.

   ii. Calculate the new crack length: $a + \frac{da}{dN}(1\ cycle)$

c. If $\Delta K < \Delta K_{TH}$ the crack does not grow. Move on to next stress range in the spectrum.

d. Repeat from a to c until the crack length reaches its critical size.

For an elliptical shape crack and for this investigation, crack growth will be tracked in two directions: crack depth '*a*' and crack length '*c*'. Thus, this algorithm applies for the crack depth '*a*' and for the crack length '*c*'. Initially, both values will be assumed equal, just like a quarter penny-shaped crack. Later on, the fatigue life of this geometry will be computed assuming different values for crack depth and crack length. In the event the initial crack depth and crack length are assumed equal, it will be referred simply as initial crack size. Moreover, even if the crack depth and length are assumed equal, the stress intensities will differ in magnitude when ϕ = 0° and ϕ =90°. For that reason, the crack growth rate will also differ along both directions, and hence the need to track down both crack growths.

Zhou [12] reported that the total fatigue life of a corner crack initiating from a riveted hole and propagating to failure can be approximated by the number of cycles for a

small corner crack to become a through thickness crack. In other words, the fatigue life of a quarter elliptical corner crack emanating from a hole is mostly due to the crack depth '*a*' growing along the plate's thickness. As soon as the crack depth reaches its maximum value (the plate's thickness), the crack length '*c*' starts growing at a faster pace.

In certain situations, the crack growth could be so slow, that it could require several millions of cycles for the crack to become of considerable size. Therefore, and in accordance to AREMA (2015), infinite life could be safe to assume if the structural member can endure 110- railcar train at a frequency of 60 trains per day over an 80-year period. The 110-car train refers to the heaviest railcar currently used as of today, the 315,000 lbs. car.

It is also important to note that the number of cycles that a riveted girder in a railroad bridge is subjected to for each passing train will depend on the span length. For a 55.5- foot riveted girder subjected to one passing train, consisting of 3 locomotives and 110 railcars, it will experience 60 cycles, see Figure 8-6. Therefore, 60 cycles per train, at a frequency of 60 trains per day for a period of 80 years, means that the girder needs to be safe for at least 105 million cycles. In this investigation, and for research purposes only, the fatigue life of the riveted girder will be considered to be "infinite life" if there is no crack growth after 105 million cycles.

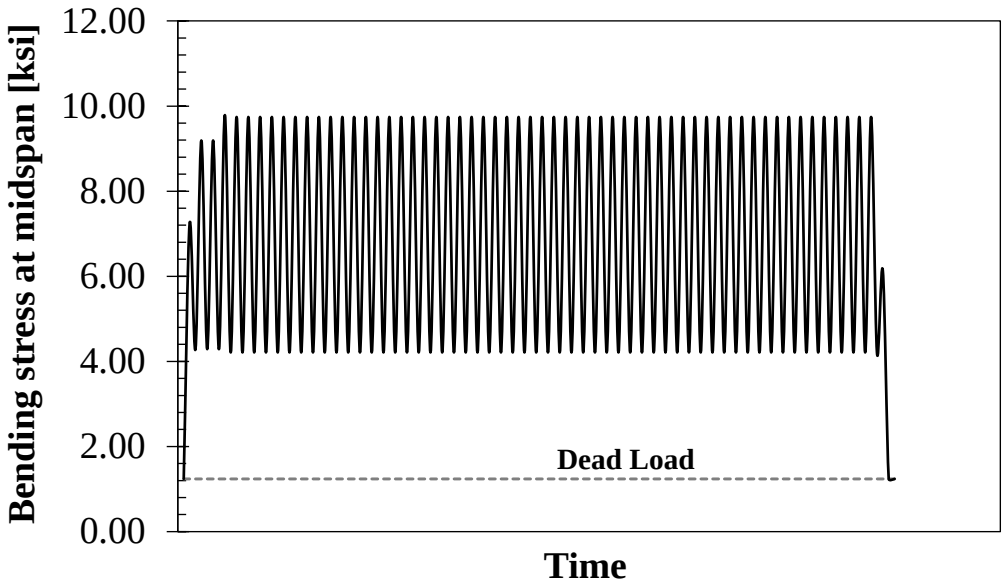

Figure 8-6 Bending stress at midspan due to dead and live load. One train consisting of 3 locomotives and 110 railcars, passing through a 55.5-ft girder, generates 60 cycles.

To perform a realistic fatigue analysis of the girder, it was necessary to analyze it under variable amplitude loading. Hence, the stress fluctuation obtained from the three different trains from chapter 8 were slightly modified in the following way:

1. Figure 7-7, Figure 7-8 and Figure 7-9 obtained for Train 1, Train 2 and Train 3 respectively were obtained assuming 3 locomotives were followed by two railcars. The second to last peak from right to left (due to two railcar trucks crossing over the bridge) will repeat itself according to the number of railcars passing through the bridge. For the 55.5-ft girder it means, this peak will repeat itself 55 times.

2. According to AREMA, fatigue design considers 60 trains per day. Thus, to create the bending stress spectrum for the fatigue analysis, the 60 cycles generated per train were repeated 60 times.

8.5 On the assumption of initial crack size

One of the major drawbacks of using fracture mechanics to estimate fatigue life is the assumption of the initial crack size (depth and length). As mentioned earlier, the procedure is extremely sensitive to this assumed value(s). The author had serious debates on what value of crack size will be realistic and not small enough that the flaw is in still in “crack initiation phase”.

It is relevant to mention that the larger the initial crack size the smaller the fatigue life of the component. Thus, if a designer needs to be conservative, a large initial flaw will produce a large stress intensity factor that will most likely be above the fatigue threshold, and, consequently crack propagation is more probable. On the other extreme, if the designer chooses an extremely small initial flaw, the crack might still be in its initiation phase, the crack will most likely will not propagate and the Paris Power Rule might not yet be applicable.

De Jesus et al. [21] states that a crack must be between 0.0098 – 0.039 in. (0.25-1 mm) long to be considered in the propagation phase. Aragón et al. [11] states that initial crack sizes in propagation phase are approximately 0.0098 – 0.02 in. (0.25- 0.5 mm) long. Zhou [12], on the other hand, states that realistic flaws in the material are somewhere

between 0.002-0.005 in. (0.05 mm – 0.13 mm). Keating [33] in his study of fatigue life of welded details, utilized 0.005, 0.01, 0.03 and even 0.05 in. (0.13 mm, 0.25 mm, 0.76 mm and 1.27 mm).

High-tech non-destructive methods are the most appropriate to help characterize the value of the initial fatigue crack size. Due to the nature of the crack, hidden by the rivet head or between plates, it is impossible to detect the crack visually, and magnetic particle inspection (MT) detects only surface cracks. Therefore, the only method available to detect sub-surface kind of cracks is ultrasonic testing (UT). UT is the only method to detect crack depth and length necessary in a fracture mechanics fatigue estimation, every other crack detection method is more suited for welded details. The UT generally has the capacity to detect cracks as small as 0.02 in. (0.5 mm). However, to achieve this accuracy, the material surface must be in optimum conditions: clean, dust and corrosion free. Clearly this is not the case for older steel bridges. Thus, the smallest detectable crack length for an uneven, corroded surface is approximately 0.08 in. (2 mm) [44]. Akesson [45], performed a fracture mechanics analysis on the Forsmo Bridge, and utilized the largest non-detectable crack at a rivet hole that would not be picked up by ultrasonic testing as the initial size defect, 0.08 in. However, the fact that smaller than 0.08 in. crack sizes in old corroded steels happen to be undetectable, does not necessarily guarantee that the material is defect free. Thus, in this study, and in accordance with [33, 46], the initial crack size (depth and length) was taken equal to 0.03 in., which is consider to be within reason.

Finally, small variations in the assumption of the final crack size, a_f, will not affect significantly the fatigue life of the component. The initial crack size assumption is far more important than the final crack size.

8.6 Fatigue life estimations of a riveted connection

For the fatigue analysis of the 55.5-ft. riveted girder, an initial crack size (depth and length) of 0.03 in. (0.8 mm) was assumed. Minimum stress is due to dead load and maximum stress is due to live load and dead load (no impact). The load ratio is simply the ratio of minimum stress to maximum stress. Delta *K* threshold was obtained using Eq. 8.2-1. Table 8-2 shows the fatigue life assessments for a riveted detail under stress ranges for the three train configurations and assuming an initial crack size of 0.03 in. Crack propagation did not occur for any of the three cases after 105 million cycles. As for the initial crack length, it is safe to state that any smaller length than the one chosen will not drive the crack. However, if the material presents a longer initial flaw than 0.03 in it is possible that the crack might propagate, for which case, it is recommended to perform the corresponding analysis.

Table 8-2 Fatigue analysis of a riveted girder with three different freight cars.

	Train 1 (263,000 lbs.)	**Train 2 (286,000 lbs.)**	**Train 3 (315,000 lbs.)**
Initial crack depth, a_O	0.03 in	0.03 in	0.03 in
Initial crack length, c_O	0.03 in	0.03 in	0.03 in
Minimum stress, S_{min}	1.24 ksi	1.24 ksi	1.24 ksi
Maximum stress, S_{max}	8.50 ksi	8.72 ksi	8.98 ksi
Load ratio, R	0.146	0.142	0.138
Fatigue threshold, ΔK_{TH}	5.61 ksi$\sqrt{}$in	5.63 ksi$\sqrt{}$in	5.65 ksi$\sqrt{}$in
Effective stress range, S_{re}	5.70 ksi	6.16 ksi	6.77 ksi
Number of cycles, N	> 105 millions	> 105 millions	> 105 millions
Final crack depth after N cycles, a_f	0.03 in	0.03 in	0.03 in
Final crack length after N cycles, c_f	0.03 in	0.03 in	0.03 in

Finally, in order to study crack propagation, it was necessary to force the crack to propagate for all the cases, and for that, there are two options: (1) Assume the girder will be subjected to random overloads during its lifetime and/or (2) Assume different initial crack sizes (length and depth). A parametric study was performed for both scenarios.

8.7 A parametric study of the fatigue life of a riveted girder under variable amplitude loading with different initial crack sizes

According to the algorithm explained in section 8.4 the stress intensity factor ΔK must be larger or equal than the stress intensity threshold value ΔK_{TH} for the crack to grow. Moreover, the maximum stress range of the stress spectrum the riveted girder will ever experience will dictate how large the crack must be to overcome the threshold value and consequently the crack to grow. Therefore, for each train, the maximum stress range

(corresponding to live and impact loads and not considering any overload) was determined. For Train 1, $S_{r\,max}$ is equivalent to 8.02 ksi; for Train 2, $S_{r\,max}$ is 8.26 ksi and finally for Train 3, $S_{r\,max}$ is 8.55 ksi. For each of the three cases, the range of stress intensity factor was determined for a wide range of initial crack sizes. The fatigue threshold for each train type will vary slightly since the load ratio in each case is not the same.

Figure 8-7, Figure 8-8, and Figure 8-9 shows the required initial crack size, or crack size threshold, for crack growth to occur. It is important to note that crack size thresholds presented in Table 8-3 were obtained assuming no overload occurred during the service life of the girder. If an overload occurs, which most likely will, the crack size threshold will decrease.

In sum, the crack size threshold is directly dependent on the maximum stress range the riveted girder experiences, as well as the load ratio that is being subjected to, since the fatigue threshold is directly proportional to the latter.

Table 8-3 Crack size threshold for train types 1, 2 and 3.

	Train 1 (263,000 lbs.)	**Train 2 (286,000 lbs.)**	**Train 3 (315,000 lbs.)**
Load ratio, R	0.146	0.142	0.138
Fatigue threshold, ΔK_{TH}	5.61 ksi$\sqrt{in}$	5.63 ksi$\sqrt{in}$	5.65 ksi$\sqrt{in}$
Maximum stress range, $S_{r\,max}$	8.02 ksi	8.26 ksi	8.55 ksi
Crack size threshold, a_{TH}	0.096 in	0.093 in	0.089 in

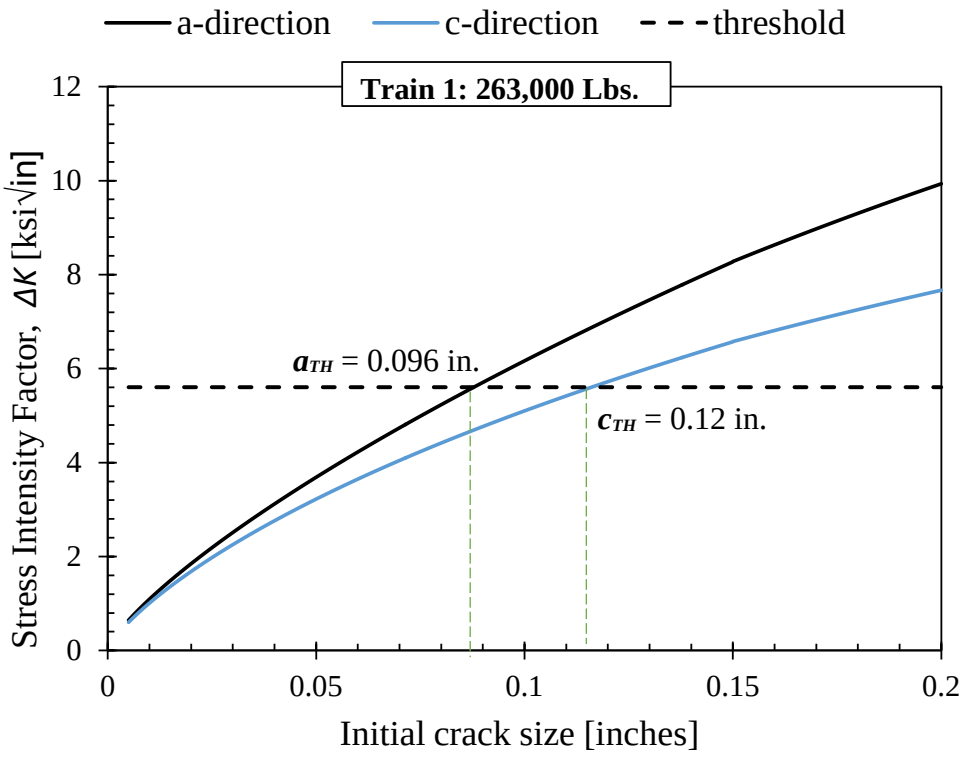

Figure 8-7 Crack size threshold for a maximum stress range of 8.02 ksi corresponding to Train 1.

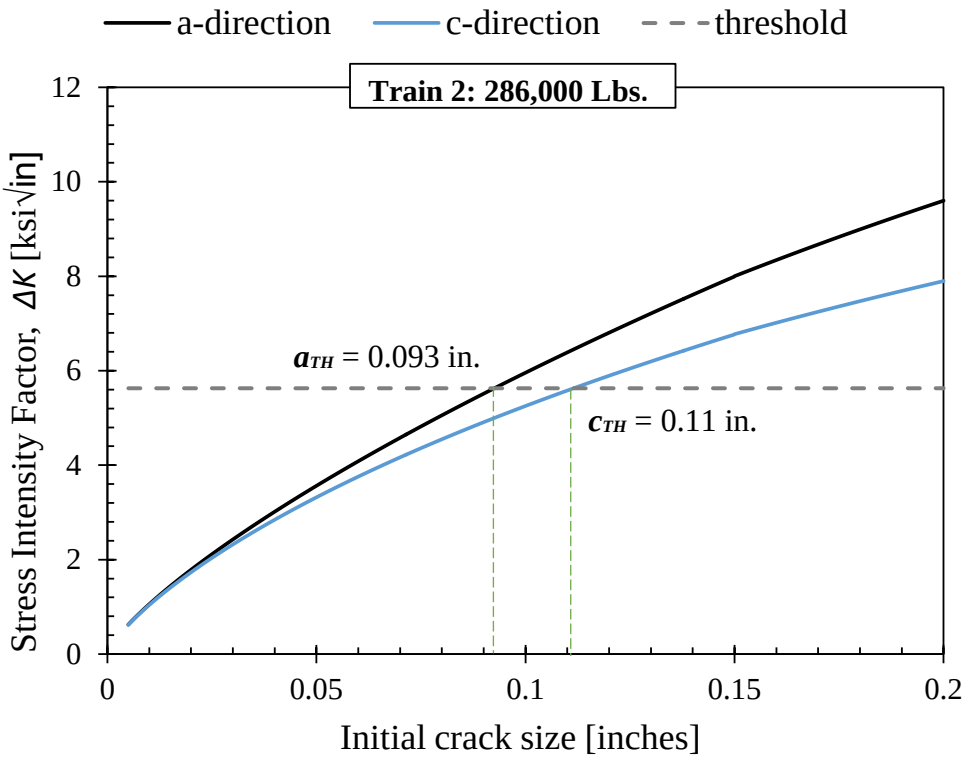

Figure 8-8 Crack size threshold for a maximum stress range of 8.26 ksi corresponding to Train 2.

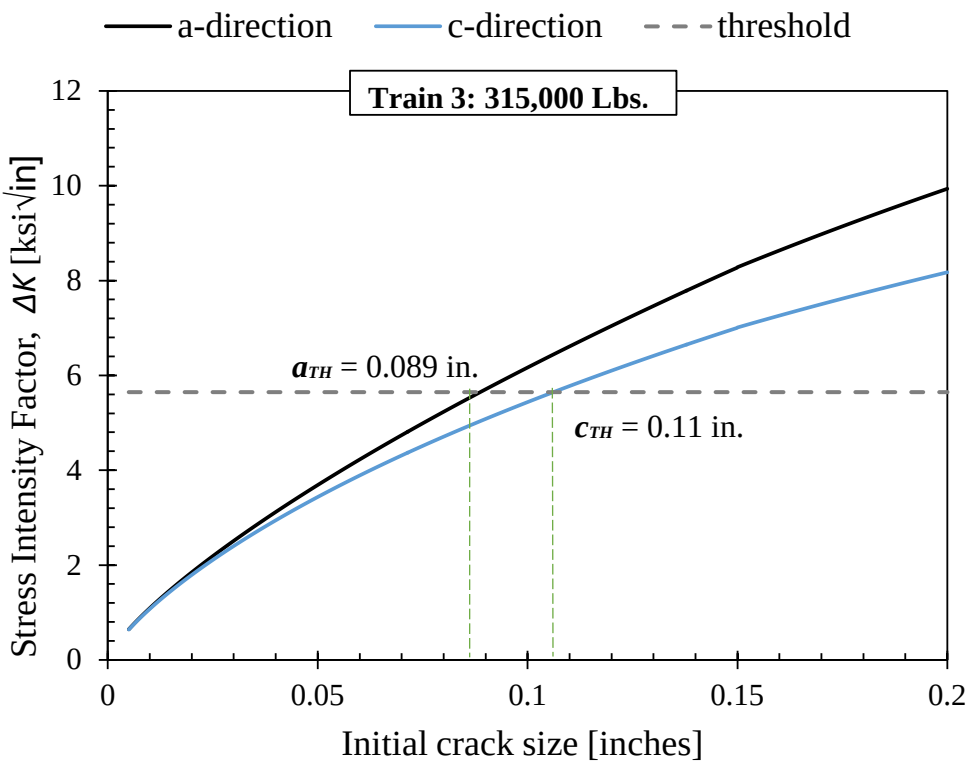

Figure 8-9 Crack size threshold for a maximum stress range of 8.55 ksi corresponding to Train 3.

8.7.1 Effect of initial crack size assumption on fatigue life estimation

As mentioned on section 8.5, the fracture mechanics methodology is extremely sensitive to the assumption of initial crack size. Different fatigue life estimations were expected for different initial crack size assumptions. However, when the analysis was performed using values smaller and larger than the threshold value, unexpected drastic fatigue estimations were seen. Table 8-4 shows the number of cycles to failure for assuming an initial crack size (depth and length) of 0.03 in, 0.085 in, 0.089 in (threshold

value for Train 3) and 0.09 in. The first two values are smaller than the threshold values, and therefore the analyses show no crack propagation after 105 million cycles. Recall that, in this study, 105 million cycles corresponds to 80 years of service. For initial crack sizes of 0.089 in and 0.090 in, the fatigue life is quite low, less than 10 million cycles in both cases. These means that once the crack size exceeds the crack size threshold value, crack propagation occurs with relatively low fatigue life. On the other hand, if the crack size is smaller than the crack size threshold value, a possibility of no crack growth or slower crack growth is almost certain. These information can lead to believe that crack initiation phase, rather than crack propagation phase is dominant in the fatigue life of riveted connections, as stated by De Jesus et al. [47] and Imam [48]. Moreover, crack initiation and growth prior to the occurrence of a visible crack consumes the major part of the fatigue life [40].

Table 8-4 Effect of initial crack size assumption on fatigue life estimation for train configuration #3.

Initial crack depth, a_O	0.03 in	0.085 in	0.089 in *	0.090 in
Initial crack length, c_O	0.03 in	0.085 in	0.089 in *	0.090 in
Minimum stress, S_{min}	1.24 ksi	1.24 ksi	1.24 ksi	1.24 ksi
Maximum stress, S_{max}	8.50 ksi	8.50 ksi	8.50 ksi	8.50 ksi
Load ratio, R	0.146	0.146	0.146	0.146
Fatigue threshold, ΔK_{TH}	5.61 ksi√in	5.61 ksi√in	5.61 ksi√in	5.61 ksi√in
Effective stress range, S_{re}	5.70 ksi	5.70 ksi	5.70 ksi	5.70 ksi
Number of cycles, N	> 105 millions	> 105 millions	5.91E+06	3.86E+06
Final crack depth after N cycles, a_f	0.03 in	0.085 in	0.50 in	0.50 in
Final crack length after N cycles, c_f	0.03 in	0.085 in	0.30 in	0.30 in

* threshold value for Train 3

8.8 A parametric study of the fatigue life of a riveted girder under variable amplitude loading with overloads

The main objective of this investigation is to determine how fatigue life of a riveted structural component is affected by increasing loads. In section 8.4, the fatigue life of a riveted component was determined using the most reasonable values possible. In this section, the same analysis with the same parameters will be used, with the exception that a larger initial crack size will be assumed (to have crack growth) and a certain number of overloads will be added to the stress spectrum.

The overload was determined as a percentage of the maximum live load and the number of overloads assumed are per day. In other words, five, ten, fifteen, thirty and sixty overloads per day with a value of 1.1 S_{max} were added to the stress spectrum. Note that the overload is ten percent of the maximum live load stress.

For an initial crack size of 0.09 in. and various overloads, crack growth occurs for the different types of trains. Cases that have less than 80 years of service life have insufficient fatigue life.

Table 8-5 shows the results obtained by assuming an initial crack length and depth of 0.09 in. and different number of overloads acting per every 60 passing trains. One can notice that the number of overloads predominates the fatigue life of the component over the effective stress range. In other words, it is more critical to have several overloads than it is to have a slightly higher effective stress range.

Table 8-5 also presents the crack depth and length after *N* cycles. One can deduce that, initially, the crack growths occurs at a much faster pace in the depth direction ('*a*'). Once '*a*' reaches its maximum value (i.e. the plate's thickness), the crack growth continues but in the length direction '*c*'. This corroborates previous research were it was stated that the total fatigue life of a corner crack initiating from a riveted hole and propagating to failure can be approximated by the number of cycles for a small corner crack to become a through thickness crack [12].

Finally, Figure 8-10 demonstrated how the fatigue life (in years of service) is affected by the number of overloads acting every 60 trains. Overloads have a far larger impact in fatigue life for smaller stress ranges. The train consisting of 263,000 lbs. railcars, produce the lowest stress range out of the three trains and therefore is severely impacted by the overloads.

Table 8-5 The effect of overloads on the fatigue life of riveted girders. Initial crack length was assumed 0.09 in.

Train 1 (263,000 Lbs.)					
Number of overloads / day (60 trains)	5	10	15	30	60
Percent of overload stresses	0.07%	0.14%	0.21%	0.41%	0.83%
Minimum stress, S_{min} [ksi]	1.24	1.24	1.24	1.24	1.24
Maximum stress, S_{max} [ksi]	8.5	8.5	8.5	8.5	8.5
Percent of overload	10%	10%	10%	10%	10%
Load ratio, R	0.146	0.146	0.146	0.146	0.146
Fatigue threshold, ΔK_{TH} [ksi√in]	5.61	5.61	5.61	5.61	5.61
Effective stress range, S_{re} [ksi]	5.71	5.71	5.72	5.72	5.75
Final crack depth after N cycles, a_f	0.63	0.63	0.63	0.63	0.63
Final crack length after N cycles, c_f	0.12	0.12	0.14	0.21	0.28
Number of cycles, N	3.99E+08	2.17E+08	1.56E+08	9.12E+07	5.32E+07
Years of Service	308.8	168.3	121.1	70.6	41.2

Train 2 (286,000 Lbs.)					
Number of overloads / day (60 trains)	5	10	15	30	60
Percent of overload stresses	0.07%	0.14%	0.21%	0.41%	0.83%
Minimum stress, S_{min} [ksi]	1.24	1.24	1.24	1.24	1.24
Maximum stress, S_{max} [ksi]	8.72	8.72	8.72	8.72	8.72
Percent of overload	10%	10%	10%	10%	26%
Load ratio, R	0.142	0.142	0.142	0.142	0.142
Fatigue threshold, ΔK_{TH} [ksi√in]	5.63	5.63	5.63	5.63	5.63
Effective stress range, S_{re} [ksi]	6.17	6.17	6.18	6.19	6.21
Final crack depth after N cycles, a_f	0.63	0.63	0.63	0.63	0.63
Final crack length after N cycles, c_f	0.10	0.10	0.10	0.28	0.33
Number of cycles, N	1.73E+08	9.83E+07	7.59E+07	4.54E+07	2.81E+07
Years of Service	134.2	76.1	58.8	35.2	21.7

Train 3 (315,000 Lbs.)					
Number of overloads / day (60 trains)	5	10	15	30	60
Percent of overload stresses	0.07%	0.14%	0.21%	0.41%	0.83%
Minimum stress, S_{min} [ksi]	1.24	1.24	1.24	1.24	1.24
Maximum stress, S_{max} [ksi]	8.98	8.98	8.98	8.98	8.98
Percent of overload	10%	10%	10%	10%	10%
Load ratio, R	0.138	0.138	0.138	0.138	0.138
Fatigue threshold, ΔK_{TH} [ksi√in]	5.65	5.65	5.65	5.65	5.65
Effective stress range, S_{re} [ksi]	6.77	6.78	6.78	6.79	6.80
Final crack depth after N cycles, a_f	0.63	0.63	0.63	0.63	0.63
Final crack length after N cycles, c_f	0.38	0.38	0.38	0.38	0.38
Number of cycles, N	4.09E+06	4.07E+06	4.05E+06	3.99E+06	3.92E+06
Years of Service	3.2	3.1	3.1	3.1	3.0

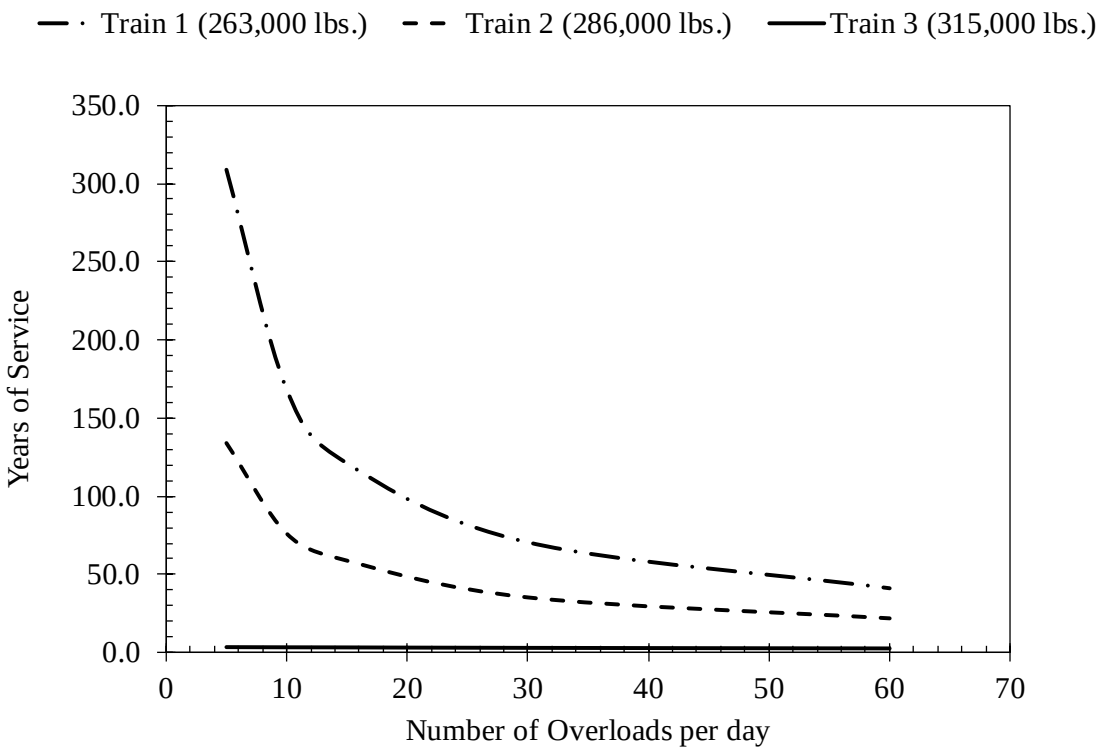

Figure 8-10 Years of service for Train 1, 2 and 3 versus the number of overloads per 60 trains.

9. DETERMINATION OF RESIDUAL STRESS*

9.1 Introduction

Part of the over conservative fatigue life estimations in riveted plates is the lack of knowledge regarding the magnitude of clamping (residual) stress generated during the rivet installation process. Thus, several previous studies neglect the effect of the clamping stress on fatigue life. A finite element simulation is necessary to estimate accurately the clamping stress around the rivet hole generated during the hot-riveting process. Thus, two identical baseline FE models are created with the exception that one is uncracked while the second will present a quarter- elliptical corner crack between faying surfaces. The uncracked model provides a general overview of the clamping stress in the critical area; the cracked model provides knowledge regarding the stress redistribution after introducing the crack.

Preliminary studies suggest that this residual stress might not only be dependent of the rivet's initial temperature, but also in the plates' thicknesses. Therefore, a parametric study was done to determine the effect of plate thickness in the thermal stress distribution. Additionally, the cracked model will be subjected to longitudinal tensile stress in order to

*Part of the data in this chapter is reprinted with permission from "Finite Element Modeling for Clamping Stresses Developed in Hot-Driven Steel Structural Riveted Connections" by Jackeline Kafie-Martinez and Peter B. Keating, 2017. *International Journal of Civil, Environmental, Structural, Construction and Architectural Engineering*, Vol: 11, No: 5, pp. 606-611, Copyright 2017 Waset.org

understand better the crack behavior and stresses near the crack tips when combined thermal and mechanical stresses act on the plates.

This chapter is to provide information regarding the residual stress induced during the hot driven installation process of rivets for both, uncracked and cracked conditions.

9.2 General description

The three-dimensional finite element analysis was performed using the commercial finite element (FE) software ABAQUS CAE. The finite element model is essentially a thermo-mechanical analysis and its main purpose is to estimate the magnitude and distribution of the residual stresses generated around the rivet hole during the hot-riveting process. This analysis was possible by specifying the initial temperature of the rivet (1868°F or 1020°C) and the plates (room temperature, 68°F or 20°C) as predefined fields. When the rivet and plates come into contact, the system seeks thermal equilibrium, and since it was assumed no clearance between the rivet and the rivet hole, the rivet shank experiences tension while inducing compressive stress field in the plates. Heat is transferred during the step analysis by specifying the final temperature (ambient temperature) as a boundary condition. This procedure simulates the hot-driven riveting process, and the specification of different initial temperatures for plates and rivet, served to generate the clamping stresses in the riveted plates.

Geometric dimensions of the riveted plate studied are described in section 9.3.

9.3 Geometry

To be in accordance with the riveted detail used in Chapter 8, the same geometry was used to determine the clamping stresses during the hot-riveting process in the finite element model, see Figure 8-3. The reader shall recall the following dimensions:

- The riveted component consists of two steel plates riveted at midspan
- Plate Dimensions: 5/8 in. thickness and width of the plate 5 in.
- Rivet shank: 1.25 in. tall and a diameter of 7/8 in.
- Rivet head: 11/16 in. radius.

The length of the plate was chosen to be large enough so that it would have a negligible effect on the analysis.

As for the cracked model, the same geometry was used as the one presented on Figure 8-3, but instead a quarter elliptical corner crack was modeled on the top plate as a crack seam with crack depth, *a*, and crack length, *c*, equivalent to 0.09 in (2.3 mm), see Figure 9-1.

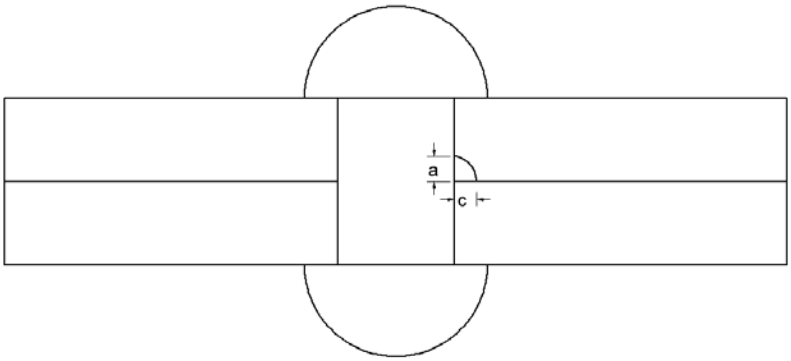

Figure 9-1 Crack location and shape.

9.4 Steel properties

In a coupled temperature-displacement step, such as the one performed, ABAQUS CAE requires the following material properties: Young's modulus, Poisson's ratio, yield stress, specific heat capacity, linear (2D) or volumetric (3D) thermal expansion, thermal conductivity and interfacial gap conductance. Section 9.4.1 describes the materials properties at ambient temperature and section 9.4.2 specifies the material's properties dependence to temperature.

9.4.1 Steel properties at ambient temperature

Steel properties commonly utilized for A36 are presented in Table 9-1. Even though is common to have steel A 502 for steel structural rivets, no distinction was made between the plates and the rivet steel in the finite element model. The difference in material properties for steel A36 and A502 is not expected to produce significant effect in the results. Moreover, the crack is expected to develop in the plates, therefore A36 is used for the entire geometry.

Table 9-1 Steel properties at room temperature.

Young's modulus, E	28,000 ksi
Poisson's ratio, υ	0.28
Yield Stress, σ_y	36 ksi
Ultimate Stress, σ_{ut}	58 ksi
Specific Heat, c_p	0.11 BTU/lb °F
Linear Thermal Expansion, α	6.7 x 10^{-6}/ °F
Thermal Conductivity, λ_a	31 BTU/ft hr °F
Mass Density, ρ	490 lb/ft^3

9.4.2 Steel properties variation with respect to temperature

When the steel elements and components are subjected to high temperatures, they progressively lose their stiffness and load carrying capacity because Young's modulus and the elasticity limit are decreasing [49]. For the thermal analysis performed in ABAQUS CAE it was deemed necessary to include the effect of temperature on the steel. Thus, it was necessary to introduce the variation of steel specific heat capacity, thermal conductivity, Poisson's ratio, yield stress, Young's modulus and thermal expansion with respect to temperature.

Specific heat is a thermal property and is defined as the amount of energy required to raise the temperature of one pound by one degree Fahrenheit [50]. It is denoted as c_p. Common units are J/Kg°C or BTU/lb °F.

Figure 9-2 shows how the specific heat capacity of steel varies with respect to temperature. As suggested by Standardization [51], the specific heat capacity $c_p \left[\frac{BTU}{lb\ °\text{F}}\right]$ can be determined by:

$$c_p = \begin{cases} 101.51x10^{-3} + 184.63x10^{-6}\left(\frac{T-32}{1.8}\right) - 403.65x10^{-9}\left(\frac{T-32}{1.8}\right)^2 + 530.24x10^{-12}\left(\frac{T-32}{1.8}\right)^3 & for\ 68°\text{F} \le T < 1112°\text{F} \\ 159.07x10^{-3} - \frac{3.10}{\frac{5}{9}T - 755.78} & for\ 1112°\text{F} \le T < 1355°\text{F} \\ 130.17x10^{-3} + \frac{4.26}{\frac{5}{9}T - 748.78} & for\ 1355°\text{F} \le T < 1652°\text{F} \\ 0.155 & for\ 1652°\text{F} \le T \le 2192°\text{F} \end{cases} \quad \text{Eq. 9.4-1}$$

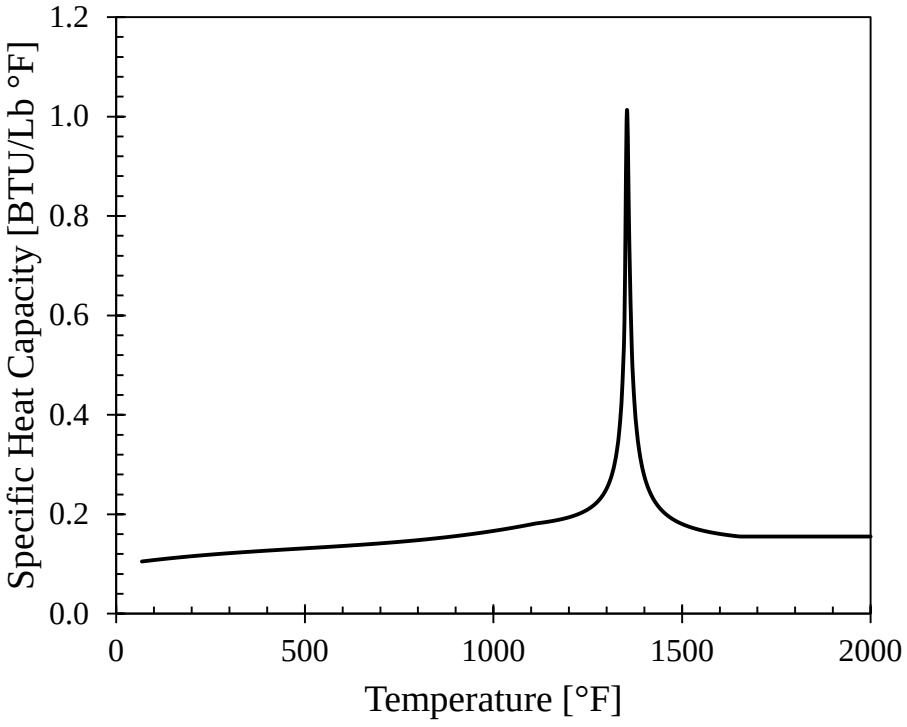

Figure 9-2 Dependence of steel specific heat capacity vs. temperature

Thermal conductivity is defined as the amount of heat that would pass a certain material depending on the temperature gradient over the material [50]. Figure 9-3 shows how the thermal conductivity of steel varies with temperature. as suggested by the Standardization [51], the variation of the thermal conductivity of steel $\lambda_a \left[\frac{BTU}{ft \cdot hr \cdot °F}\right]$ can be determined by:

$$\lambda_a = \begin{cases} 31.5427 - 0.0107T & for\ 68°F \leq T < 1472°F \\ 15.77 & for\ 1472°F \leq T \leq 2192°F \end{cases} \quad \text{Eq. 9.4-2}$$

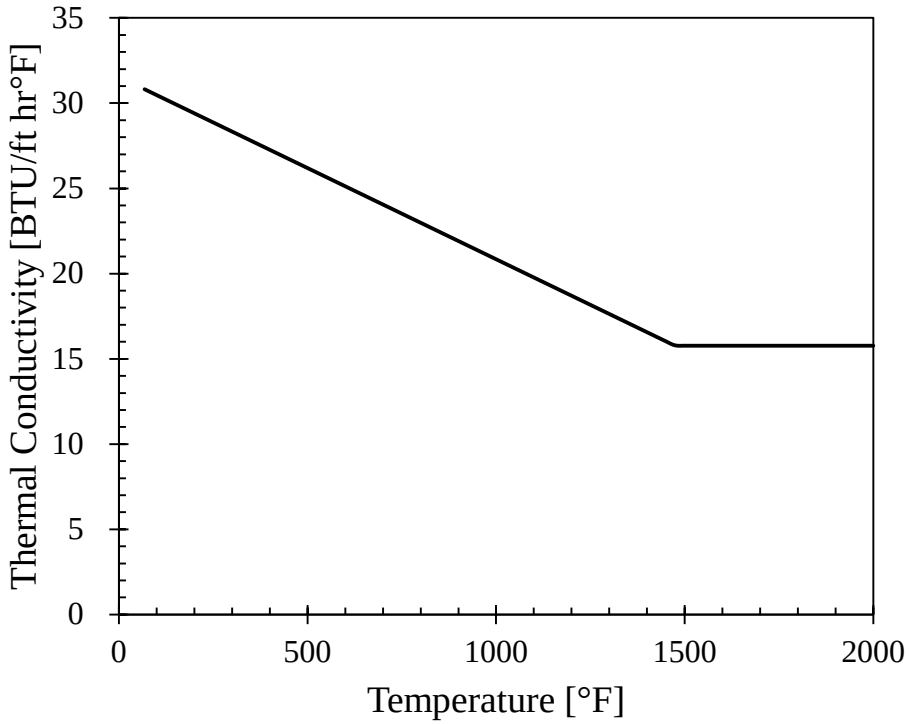

Figure 9-3 Dependence of steel thermal conductivity vs. temperature

As suggested by Ancas and Gorbanescu [49], Poisson's ratio for steel can be determined by:

$$\upsilon(T) = \begin{cases} 3.78\ x\ 10^{-5}\dfrac{(T-32)}{1.8} + 0.283 & for\ 0 \le T \le 842°\text{F} \\ 9.20\ x\ 10^{-5}\dfrac{(T-32)}{1.8} + 0.259 & for\ T > 842°\text{F} \end{cases} \qquad \text{Eq. 9.4-3}$$

Figure 9-4 presents graphically how steel Poisson's ratio varies with temperature.

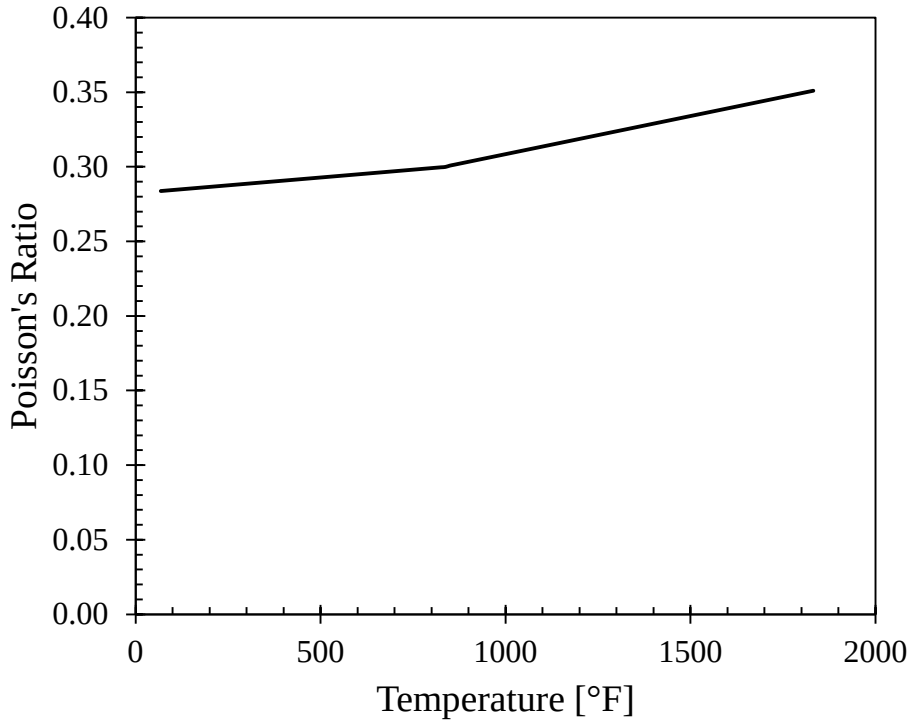

Figure 9-4 Dependence of steel Poisson's ratio vs. temperature.

According to Ancas and Gorbanescu [49], the variation of Young's modulus must be considered only up to 1832° F, because for greater temperatures, the steel has no mechanical resistance as shown in Figure 9-5. The variation of the modulus of elasticity *E* in ksi can be determined by:

$$E = \begin{cases} E_{20}\left(1 + \dfrac{5T - 160}{18000 * Log\left(\dfrac{T}{1980} - \dfrac{8}{495}\right)}\right) & for\ 68°\text{F} < T \leq 1112°\text{F} \\ -E_{20}\left(\dfrac{69T - 126408}{100T - 12830}\right) & for\ 1112°\text{F} < T \leq 1832°\text{F} \end{cases} \quad \text{Eq. 9.4-4}$$

Where E_{20} represents the modulus of elasticity at ambient temperature (68°F).

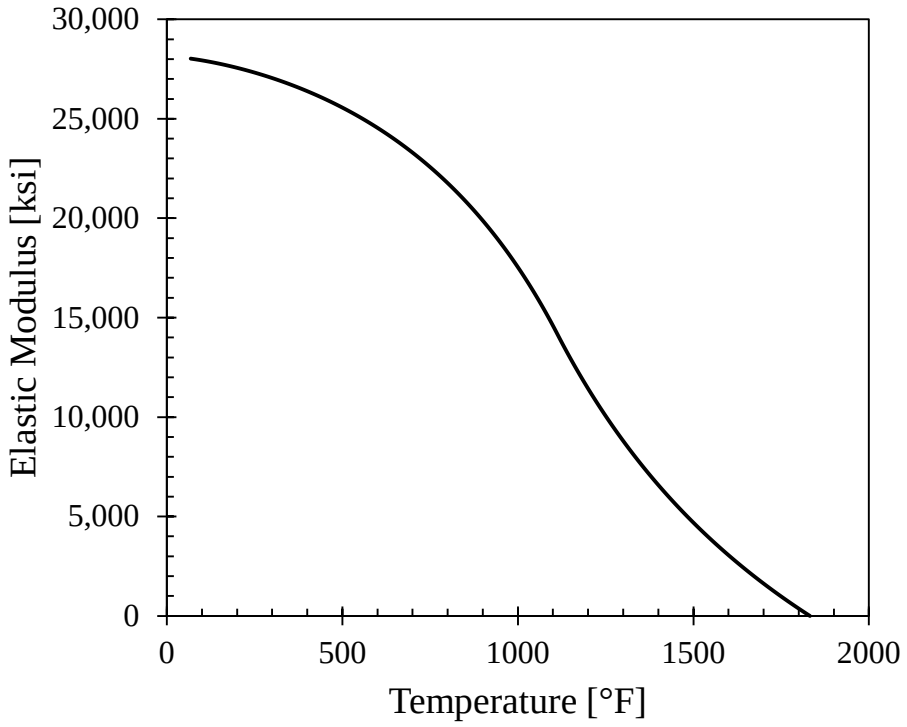

Figure 9-5 Dependence of steel Young's Modulus vs. temperature

In the above equations, the yield stress σ_y is given by the following equations:

$$\sigma_y = \begin{cases} \sigma_{y0}\left(1 + \dfrac{{}^{5}/_{9}\,(T-32)}{900 * Log\left(\dfrac{T-32}{3150}\right)}\right) & for\ 68°\text{F} < T \leq 1112°\text{F} \\ \sigma_{y0}\left(\dfrac{346 - 0.189T}{{}^{5}/_{9}\,T - 257.8}\right) & for\ 1112°\text{F} < T \leq 1832°\text{F} \end{cases} \quad \text{Eq. 9.4-5}$$

$$\sigma = \begin{cases} E\epsilon & when\ \varepsilon \leq \varepsilon_p \\ (12.5\varepsilon + 0.975)\sigma_y - \dfrac{12.5\sigma_y^2}{E} & when\ \varepsilon > \varepsilon_p \end{cases} \quad \text{Eq. 9.4-6}$$

Where σ_{y0} represents the steel yield strength at ambient temperature (68°F).

$$\varepsilon = \frac{0.975\sigma_y - 12.5\left(\sigma_y\right)^2}{E - 12.5\sigma_Y} \quad \text{Eq. 9.4-7}$$

Figure 9-6 shows how the stress strain curve for A36 steel varies with temperature.

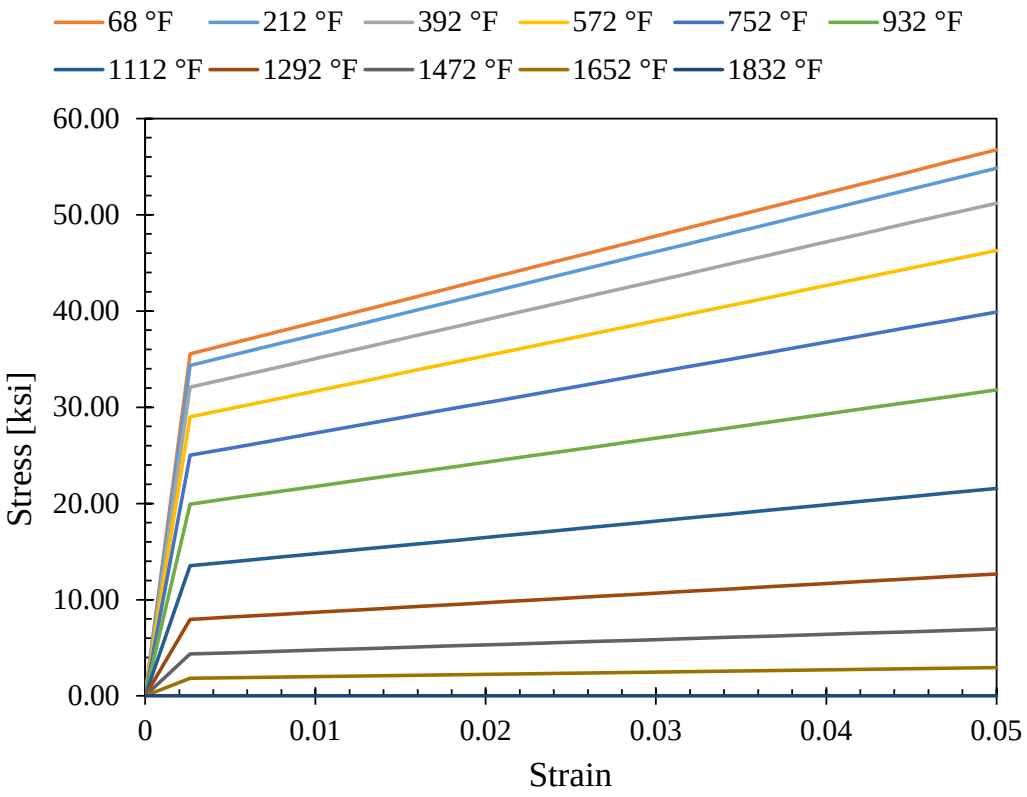

Figure 9-6 Variation of stress-strain behavior of steel with temperature.

The coefficient of thermal expansion, ε, is defined as the elongation in length occurring in a member per unit increase in temperature [50]. For the 3D finite element model of the riveted detail, the thermal expansion is required to account for the change in volume of the material.

Figure 9-7 describes the variation of linear thermal expansion as a function of temperature.

$$\varepsilon = \begin{cases} (0.00122T + 6.621) \times 10^{-6} \ ^{\circ}\mathrm{F}^{-1} & for\ T < 1832^{\circ}\mathrm{F} \\ (8.9) \times 10^{-6} \ ^{\circ}\mathrm{F}^{-1} & for\ T \geq 1832^{\circ}\mathrm{F} \end{cases} \qquad \text{Eq. 9.4-8}$$

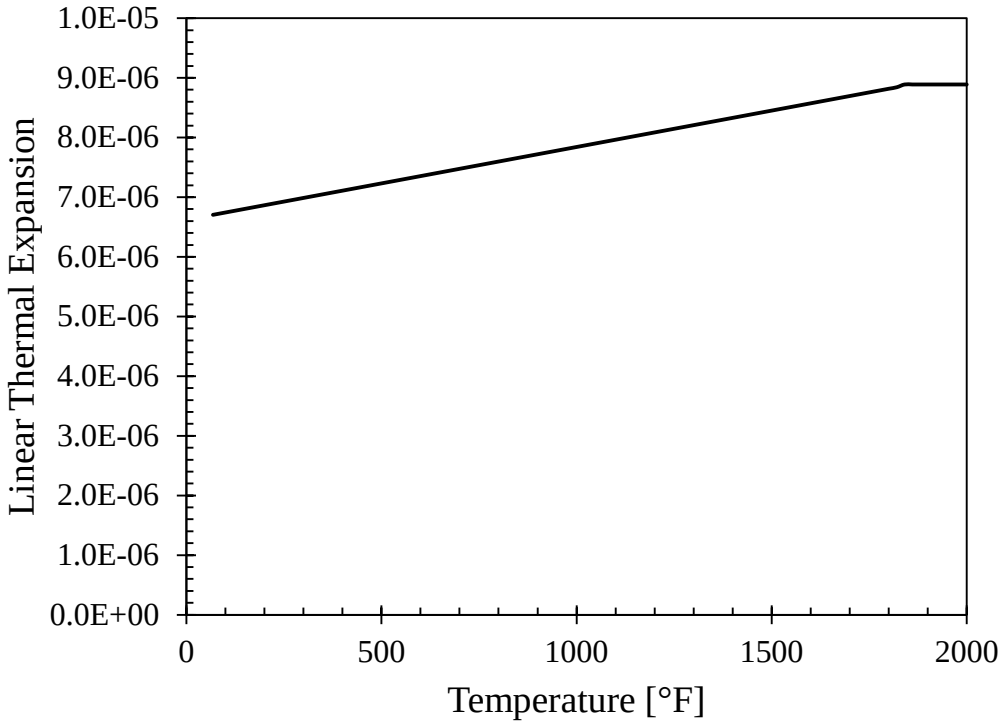

Figure 9-7 Dependence of linear thermal expansion with respect to temperature.

The standard value for the density of structural steel is 490 lb/ft^3. For most calculations and research work, density is assumed to be constant with increase of temperature. That is the case for this investigation.

Finally, the interfacial gap conductance was necessary to specify the heat transfer between surfaces; in this case, steel-air-steel interfaces. Even though a null clearance

between rivet and rivet hole was assumed, it is necessary to specify interfacial thermal conductance between contacting surfaces since they can lose contact during the analysis as needed. Table 9-2 presents the values utilized for thermal conductance in steel-air-steel-interfaces.

Table 9-2 Interfacial gap conductance.

Gap [in]	Interfacial Thermal Conductance [BTU/ft hr °F]
0	1444.47
0.0197	28.89
0.0394	14.44
0.0591	0

9.5 About the model

All components were modeled using an 8-node thermo-mechanically-coupled brick, trilinear displacement and temperature, reduced integration elements (C3D8RHT).

Figure 9-8 shows the mesh utilized on the uncracked model. The rivet consisted of approximately 17 thousand elements and each plate consists of approximately 59 thousand elements. The model requires a very refine mesh in the vicinity of the rivet hole, which is the area of the plate right under the rivet head and throughout the thickness. To study the thermal stress for various plate-thicknesses, a constant number of elements (throughout the thickness of the plate) were considered.

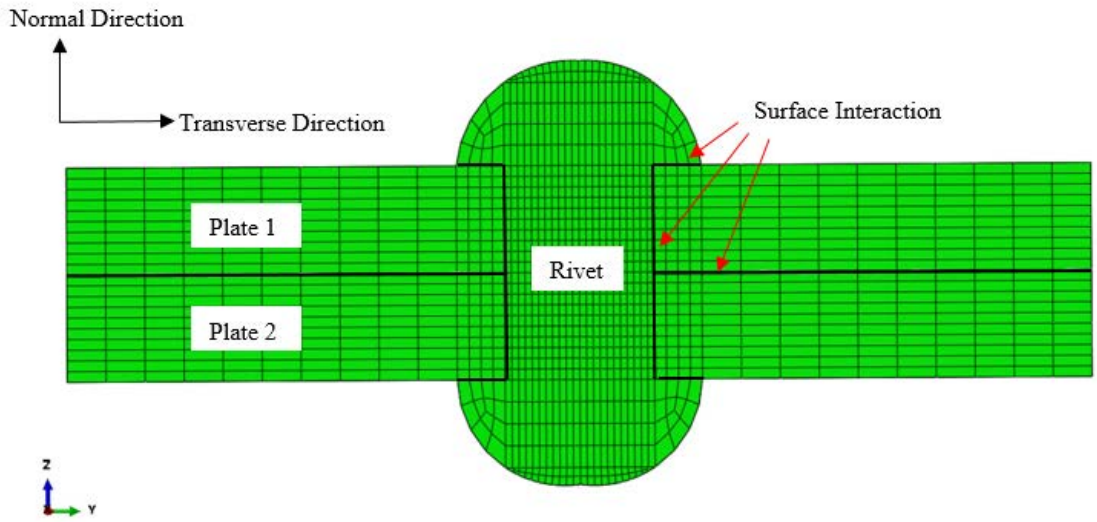

Figure 9-8 Riveted model fine mesh in critical area.

As for the cracked model, the crack was defined on ABAQUS as a seam. A seam defines an edge or a face in the model that is originally closed but can open as needed during the analysis. ABAQUS CAE places overlapping duplicate nodes along a seam when the mesh is generated. Because a seam modifies the mesh, you cannot create a seam on a dependent part instance. Therefore, the plate must be defined as an independent instance and had to be partitioned numerous times to be able to mesh properly the vicinity of the crack. Also, due to the location of the crack (at the edge of a hole) tetrahedral elements were used for the transition zone. Wedge elements were used at the crack tip and hexahedral elements around the wedge elements. Figure 9-9 and Figure 9-10 shows the mesh and the partitions used in the cracked model.

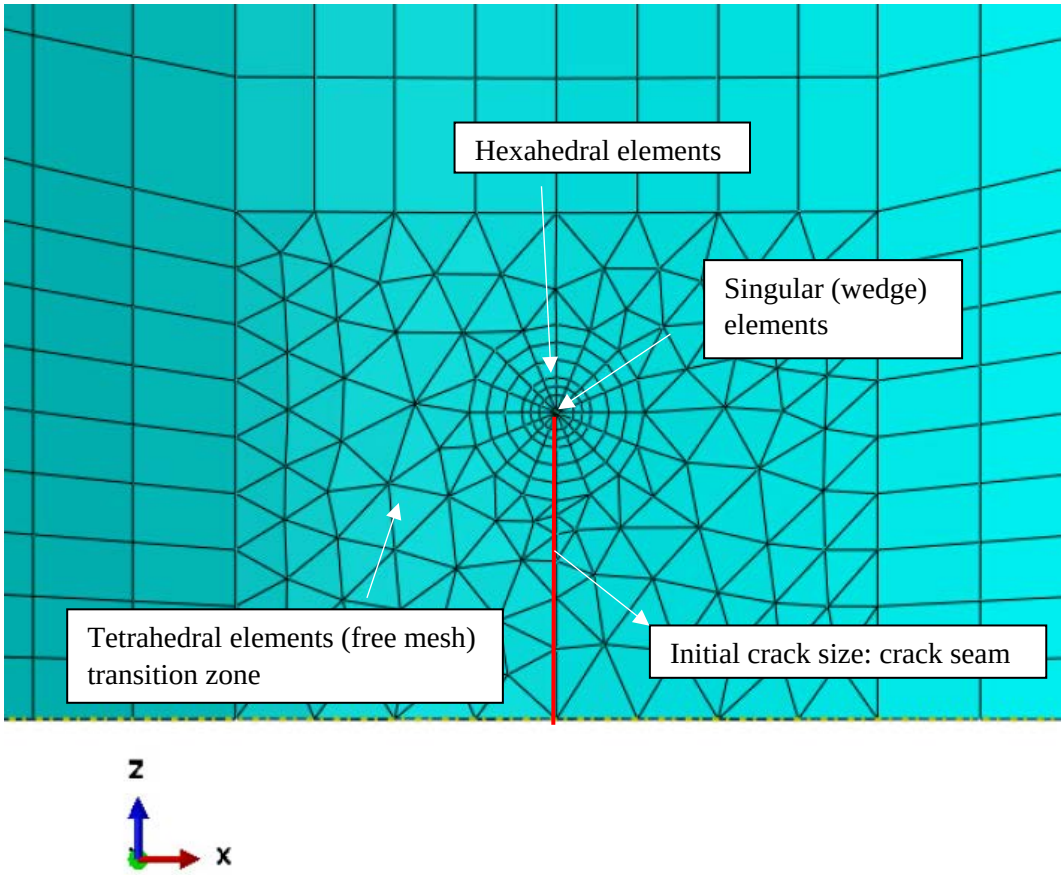

Figure 9-9 Two-dimensional view of the crack seam and element types used in the cracked model.

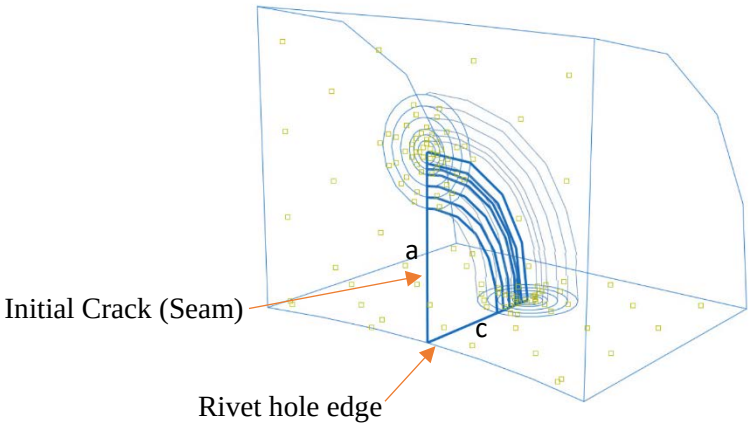

Figure 9-10 Three-dimensional view of the crack. Several partitions were created to better accommodate the mesh.

The initial temperature of the rivet was assumed to be 1868°F (1000°C) and the plates were assumed to be at ambient temperature 68°F (20°C). In order to define the initial temperature fields in ABAQUS, it was necessary to create a predefined field for the plate and for the rivet. The predefined fields state the initial condition of the plate and of the rivet.

Boundary conditions are necessary to guarantee convergence. The plates were considered to be simply supported. Moreover, a temperature boundary condition was defined to terminate the analysis when thermal equilibrium (ambient temperature) of the entire system has been reached.

All the contact surfaces have a coefficient of friction of 0.3 (tangential behavior), overclosure hard contact surface (normal behavior) and interfacial gap conductance. The master surfaces were set on the plates and the slave surfaces were set on the rivet. The *Nlgeom* option must be enabled to account for large strain plastic deformations.

9.6 Results and discussion

The complexity of the model increases significantly with the usage of contact surface interactions. Difficulty in making the analysis converge is a very common issue in contact analyses.

ABAQUS documentation suggests loading the system in small increments by reducing the increment size in the Step dialog box. After several iterations, it was found that the model converged nicely when the initial increment size was set to 0.001, with a

minimum of $1x10^{-6}$ and a maximum of 0.01. However, when the study was performed using thinner plates, these small increments alone were not sufficient to make the solution converge. To perform a parametric study of the effect of plate thickness in the residual stress field and to be unanimous between all the finite element models, the Automatic Stabilization option, within the step definition and presented in the step dialog box, was used with default values for dissipated energy fraction and maximum ratio of stabilization to strain energy, 0.002 and 0.05, respectively. If automatic stabilization is used, it is necessary to check the history output if the energy dissipated by viscous damping is less than 5% of the internal strain energy (defined as ALLSD and ALLIE, respectively, on ABAQUS). If it is less than 5%, it can be assumed that the accuracy was not significantly affected by automatic stabilization. It is important to note that not always the default value is adequate, therefore obtaining the optimal value for the damping factor is a trial and error process until a converged solution is obtained and the dissipated stabilization energy is sufficiently small.

9.6.1 Deformation

The usage of overclosure hard contact surfaces prevented the contacting surfaces from penetrating one another; it also allows them to separate and loose contact as needed. Therefore, the use of contact surfaces ensures a realistic deformed shape.

For the model to be correct, the deformation behavior should exhibit the following characteristics:

1. The rivet head will shrink in size.

2. As the rivet contracts, the plates will try to squeeze out; this will be reflected as a gap between the rivet shank and the plate.
3. As the rivet cools, the area near the rivet hole is compressed, however, far away from this area the plates will tend to separate.

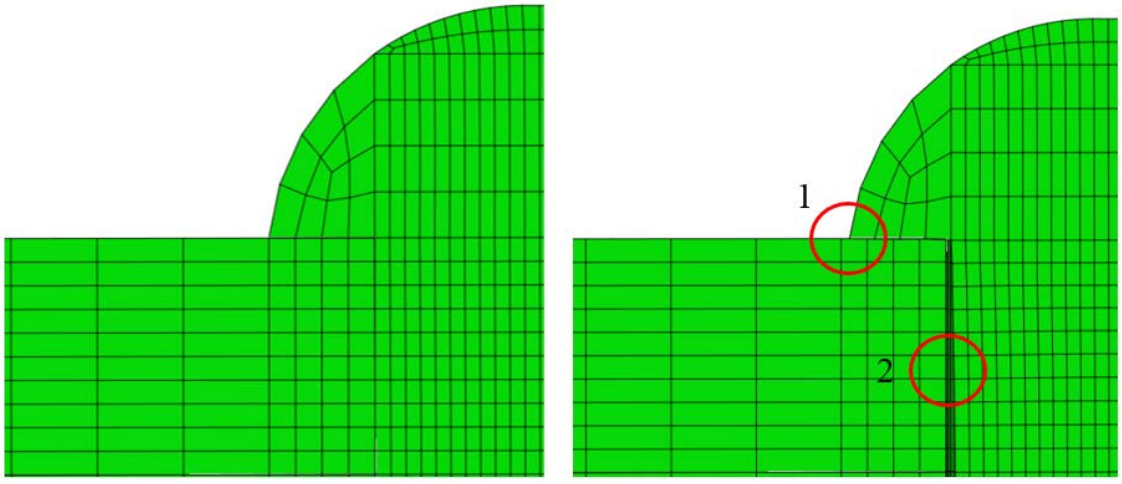

(a) Undeformed shape (b) deformed shape

Figure 9-11 (a) undeformed and (b) deformed shape. The rivet head will shrink and the plates will try to squeeze themselves out as the rivet compress.

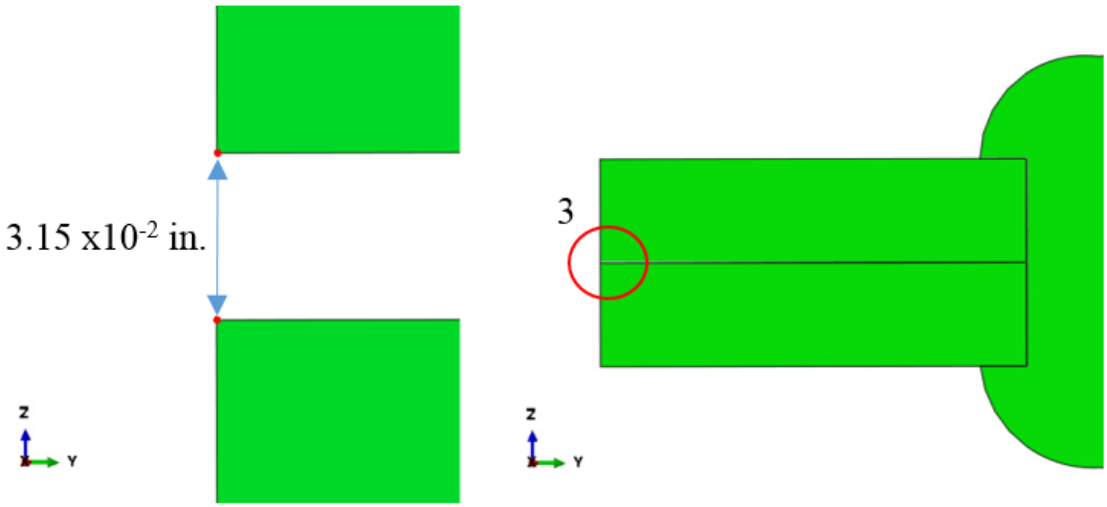

Figure 9-12 Separation of the plates far away from the rivet hole (transverse view).

Figure 9-11 shows the deformed and undeformed shape of the riveted plate seen in transverse view. Note that in the deformed shape, the rivet head has shrunk and there is a gap between the rivet shank and the plates. Figure 9-12 shows the separation of the plates in its transverse view.

9.6.2 Stresses

The stress contours were obtained for Von Mises stress criteria (Figure 9-13), clamping stress or *S33* (Figure 9-14), and finally longitudinal stress or *S11* (Figure 9-15). It is clear from Figure 9-14 that the rivet shank is in tensile stress (color red in the stress contour) and the region of plates near the rivet are in compression (color blue in the stress contour).

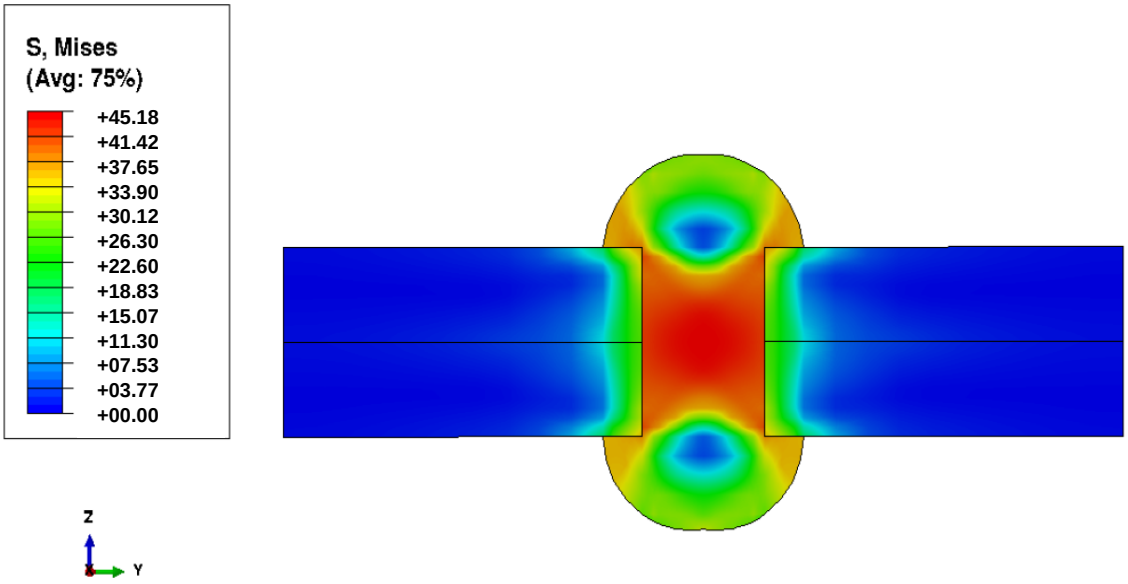

Figure 9-13 Von Misses Stress (ksi) generated around the rivet due to the temperature differential in the hot-riveting process.

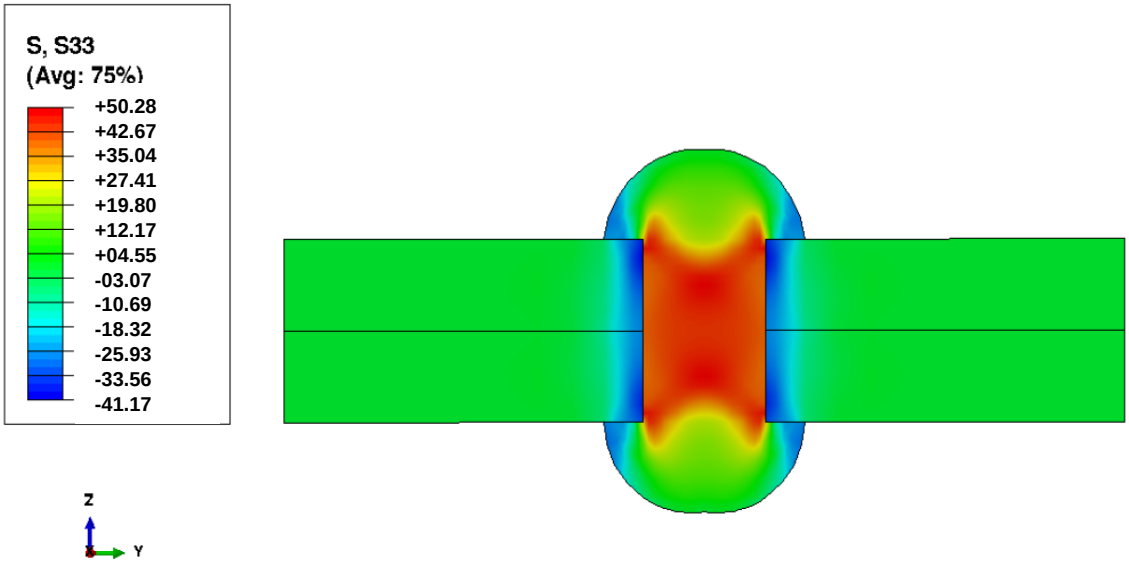

Figure 9-14 Stresses (*S33* or *z*-direction, ksi) generated around the rivet due to the temperature differential in the hot-riveting process.

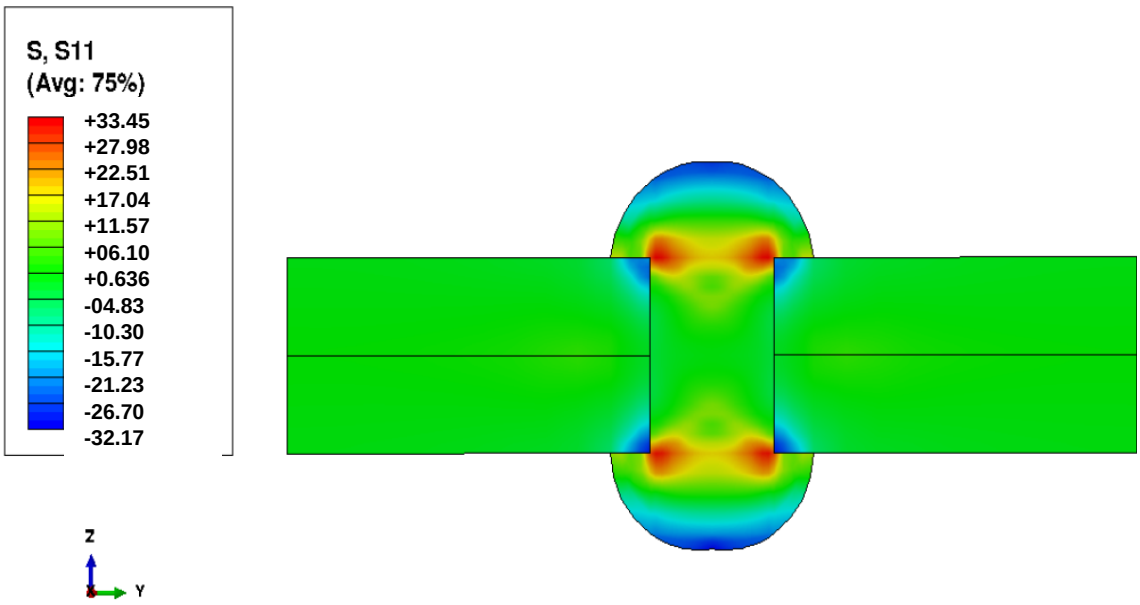

Figure 9-15 Longitudinal stresses (*S11* or *x*-direction, ksi) generated around the rivet due to the temperature differential in the hot-riveting process.

To account for the effect of clamping in the estimation of fatigue life is imperative to realize that stresses acting on the *z*-direction, called *S33* in this investigation, are not the stresses directly responsible for crack propagation. Cracking in a riveted steel component typically occurs at the edge of the hole and perpendicular to longitudinal stresses. These longitudinal stresses (*S11*) are responsible for the development of the crack, and therefore are the ones sought in this investigation. See Figure 9-16.

The hot-riveting process subjects the area right under the rivet (and throughout the thickness) to a compressive longitudinal stress (*S11*) see Figure 9-15. Even though the entire region under the rivet and at the edge of the hole is under compression, there are two possible locations where fatigue cracking may happen. The first possible location is

in the plate right under the rivet head and the second location is located between the two connecting plates (see Figure 9-17).

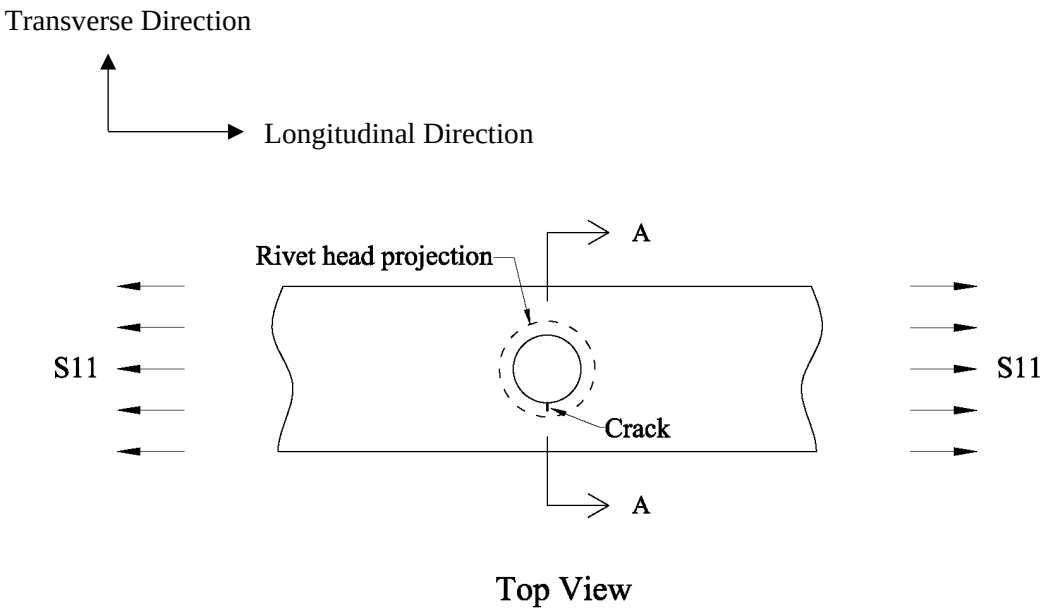

Figure 9-16 Top view of a riveted plate under longitudinal stress. Crack propagation occurs perpendicular to the stress S11.

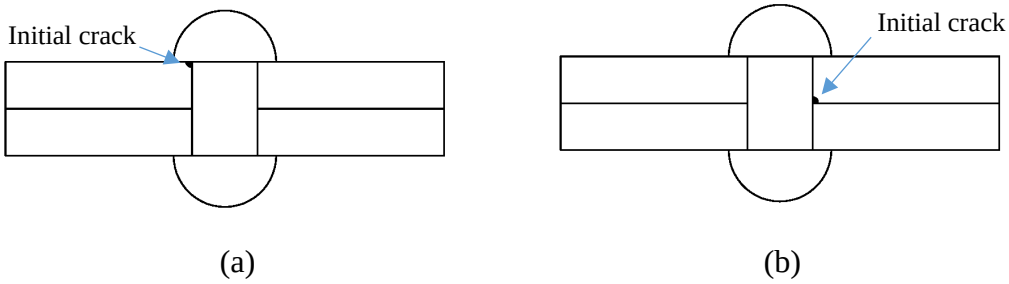

Figure 9-17 Possible locations for crack propagation in details with riveted hole.

Figure 9-19 shows that for a 5/8 in. thick plate, the beneficial effect of a localized compressive stress for the fatigue life of the component is minimum at the faying surfaces. Hence, it is more likely the crack will propagate there, Figure 9-17b. Moreover, a through-thickness crack for a 5/8 in. thick plate is rather unlikely to happen. Hence, since the rivet

hole induces a stress concentration, the crack will most likely be a quarter elliptical corner crack emanating from the hole.

This comes in accordance to the experimental analysis performed by Zhou [12]. According to Zhou, no crack grew under the rivet head, but rather, cracks initiated from other locations of the specimen. However, for the case where the initial flaw is located between plates, the crack grew and caused fracture of the plate at the net section while no new cracks initiated from anywhere else.

9.6.3 Effect of plate thickness on clamping stresses

Thicker elements generally have a lower fatigue strength than thinner elements [4]. The magnitude of the clamping stress might be dependent on the thickness of the material being fastened. In order to perform a parametric study of the effect of plate thickness in the generation of residual stresses, the finite element analysis was performed numerous times assuming different plates thicknesses. Six models were done assuming the following plates' thicknesses: 1/8 in., 1/4 in., 5/16 in., 1/2 in., 5/8 in., and 1 in.

The normal and longitudinal stresses were obtained in the following way: for each of the models, ten elements were used throughout the plate thickness. Stresses were recorded in these ten elements at the edge of the hole located at midspan. Figure 9-18 and Figure 9-19 show the normal and longitudinal stresses of the six riveted plates.

In the six cases, the plates were under compressive stress in the area underneath the rivet head and throughout the thickness. However, as the plate thickness increases, the magnitude of the stress between faying surfaces lowers significantly. From Figure 9-18,

the thicker the plate, the larger the compressive stress under the rivet head; however, the scenario changes completely between faying surfaces. The thicker the plate, the less compressive stress the plate will have between faying surfaces; moreover, for the 1-in thick plate there is no longer longitudinal compressive stress but tensile stress, see Figure 9-19. This is relevant since it will most likely dictate the possible location for future fatigue cracks. Figure 9-20 presents the resiudal stress variations thorught the contacting surfaces.

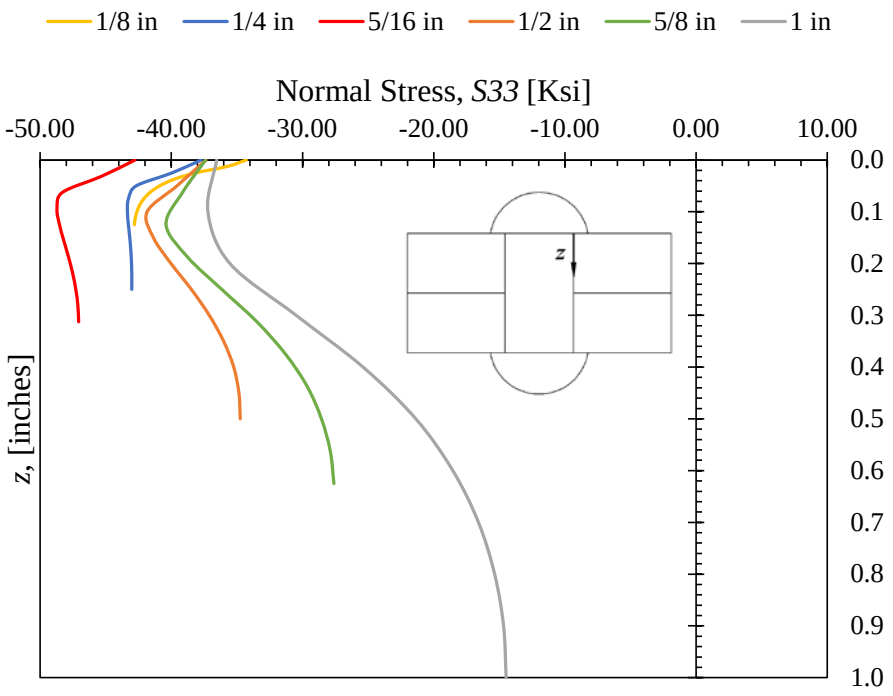

Figure 9-18 Clamping stress field variation throughout the plate thickness for different plate thicknesses.

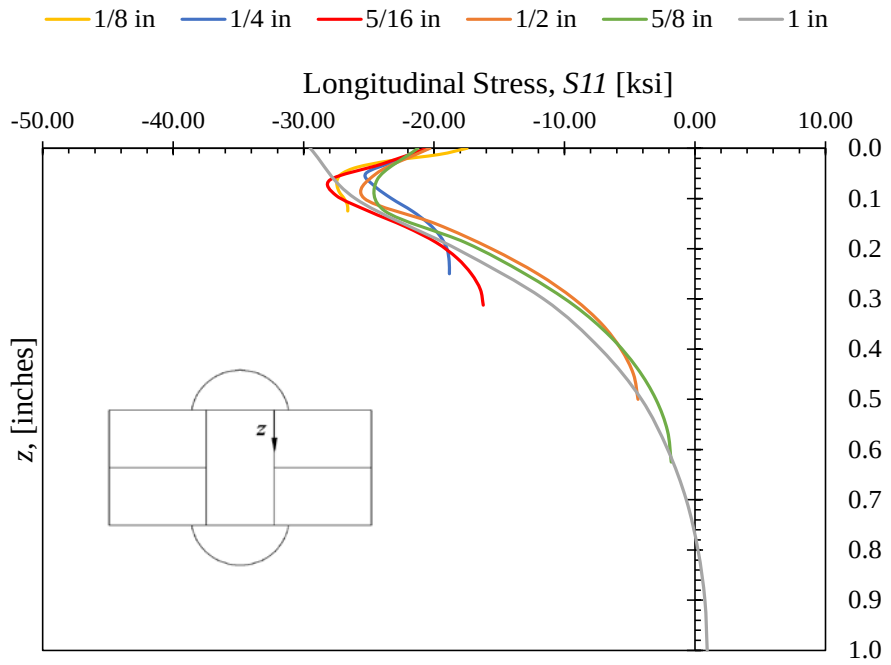

Figure 9-19 Longitudinal residual stress field variation throughout the plate thickness for different plate thicknesses.

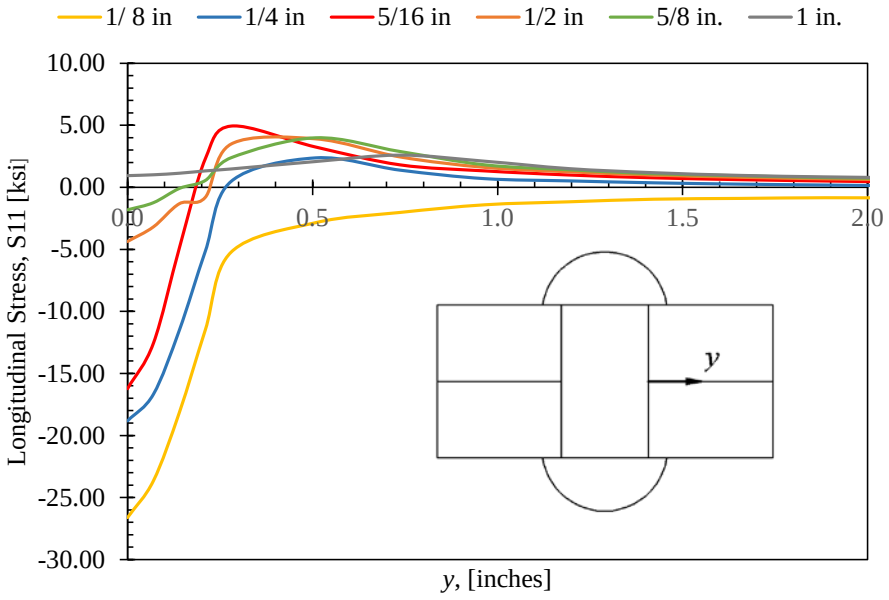

Figure 9-20 Longitudinal residual stress along the contacting surface.

9.6.4 Effect of a mechanical tensile traction (S11)

The finite element analysis was extended by subjecting the riveted plates into a mechanical tensile traction to determine how the two types of stresses (thermal and mechanical) developed. Assuming no shear transfer between plates, but instead, the component is located in a constant moment region, 8.55 ksi was applied on both plates. This tensile stress was obtained by assuming a train consisting of 3 locomotives (SD70) and 110 railcars (each weighing 315,000 lbs.), see section 7.7. Once the plates are subjected to tension, the crack will open; for an external load of 8.55 ksi, the quarter elliptical corner crack of 0.09 in. (depth and length) will exhibit an opening of 5.97 $x10^{-3}$ in., as shown in Figure 9-21. The stress contours for Von Mises also shows the stress concentrations at the crack tip, often approaching yielding stress Figure 9-22.

The solid line of Figure 9-23 represents the stress field due to thermal and mechanical stress (8.55 ksi). Crack propagation due to a longitudinal tensile stress will generate a crack perpendicular to the stress and emanating from the rivet hole, as shown in Figure 9-16. In the case of thin plates, the crack would most likely be a through thickness crack. However, if the plate is of considerable thickness, the crack could start either underneath the rivet head or, under the rivet head and between faying surfaces. Figure 9-23 describes how the clamping stress changes from compressive to tensile. Since tensile stress is responsible for crack propagation, it is likely that the crack will form between faying surfaces.

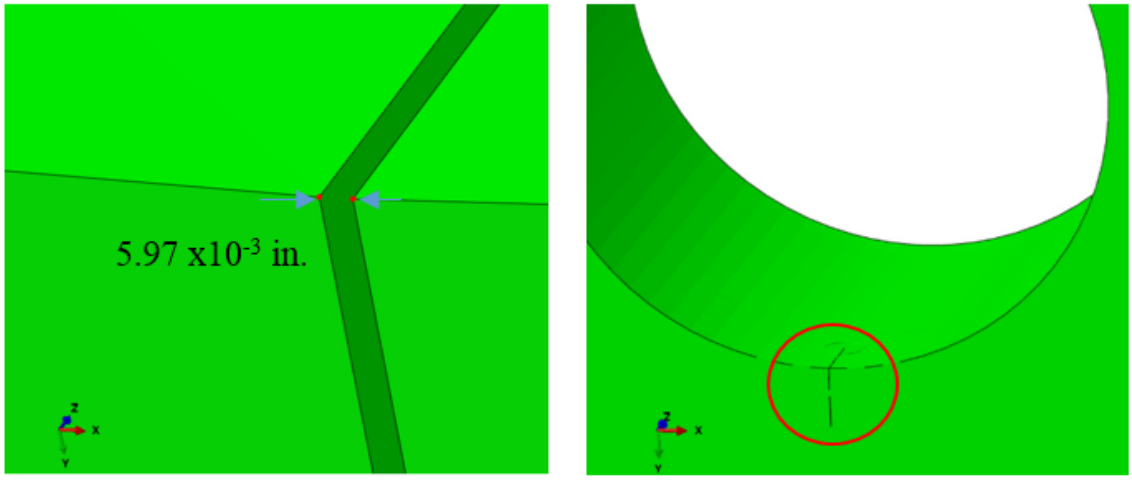

Figure 9-21 As the plates are subjected to a longitudinal tensile stress, the crack opens.

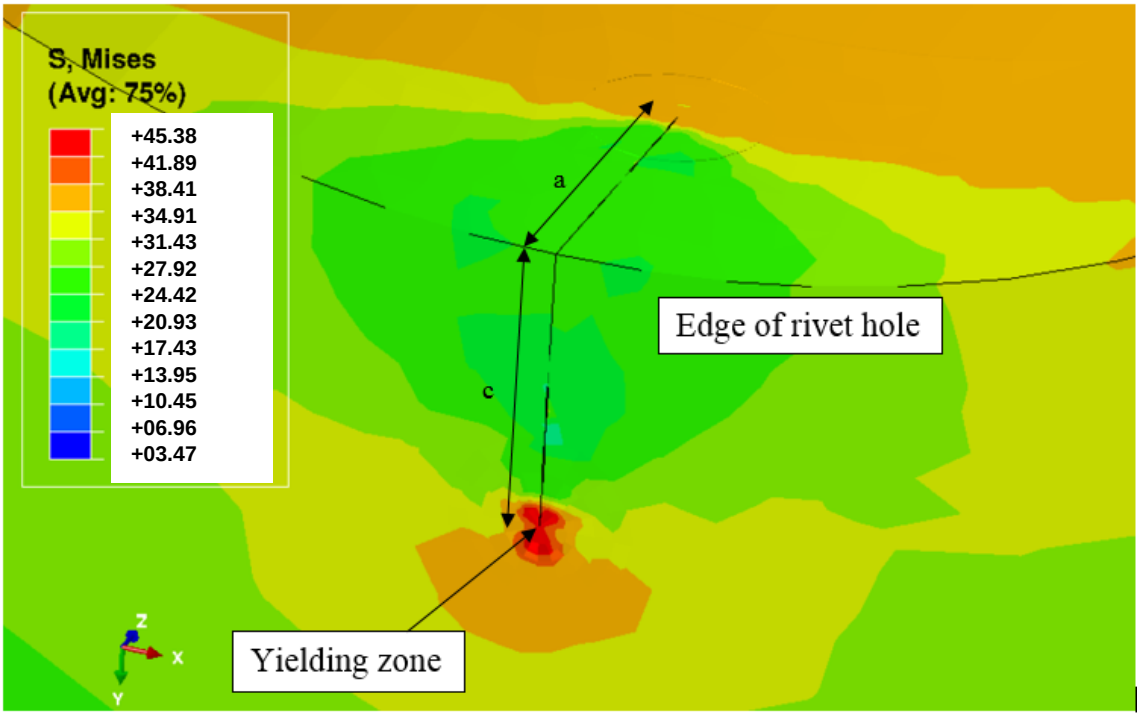

Figure 9-22 Von Mises stress (ksi) shows the yielding zone at the crack tip.

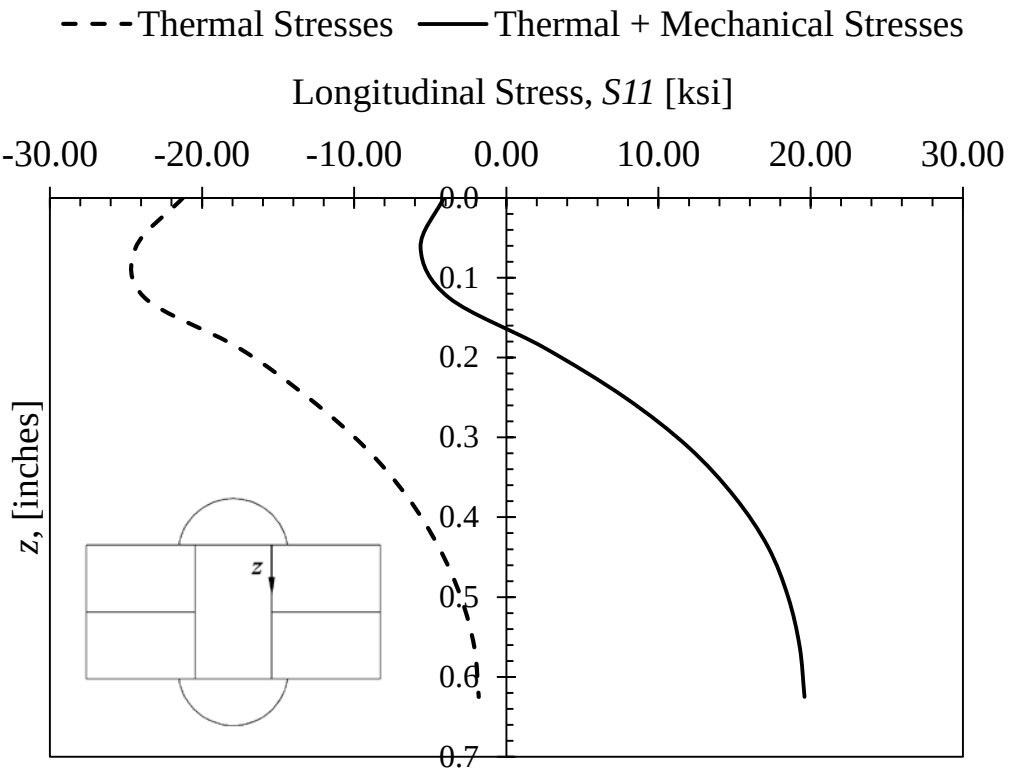

Figure 9-23 Thermal and mechanical stresses applied in the riveted model.

9.7 Residual stress redistribution

There have been many studies on the effect of residual stress on fatigue crack growth. Almost all the studies are analyzed assuming that an external applied stress superposed by the initial residual stress has an effect on fatigue crack behavior. However, it is known that the initial residual stress is released and redistributes with fatigue crack propagation. In other words, the residual stress intensity factor, $K_{residual}$, resulting from the presence of residual stress in front of crack tip, changes with crack growth [52].

Therefore, the residual stress distribution is obtained for an uncracked, and two cracked models in order to describe stress redistribution. The stress distributions along the plate thickness were obtained for the case of an unflawed plate, a plate containing a 0.10 in. crack and a third one with a 0.15 in. crack and are presented in Figure 9-24. The compressive stress accentuates at the crack tip for the cracked models. However, and similar to what Lam and Lian [53] concluded, since $K_{residual}$ is small compared with ΔK, stress redistribution does not play a major role on fatigue life. In the event the ratio of $K_{residual}$ to ΔK is large, the stress redistribution would have a more significant effect on fatigue life, and if not accounted for, it can lead to non-conservative life prediction.

Moreover, the redistribution of stress arising from the presence of a crack does not imply that the superposition principle is invalidated [25]. Finally, knowledge regarding a growing fatigue crack inside a residual stress field is limited [54].

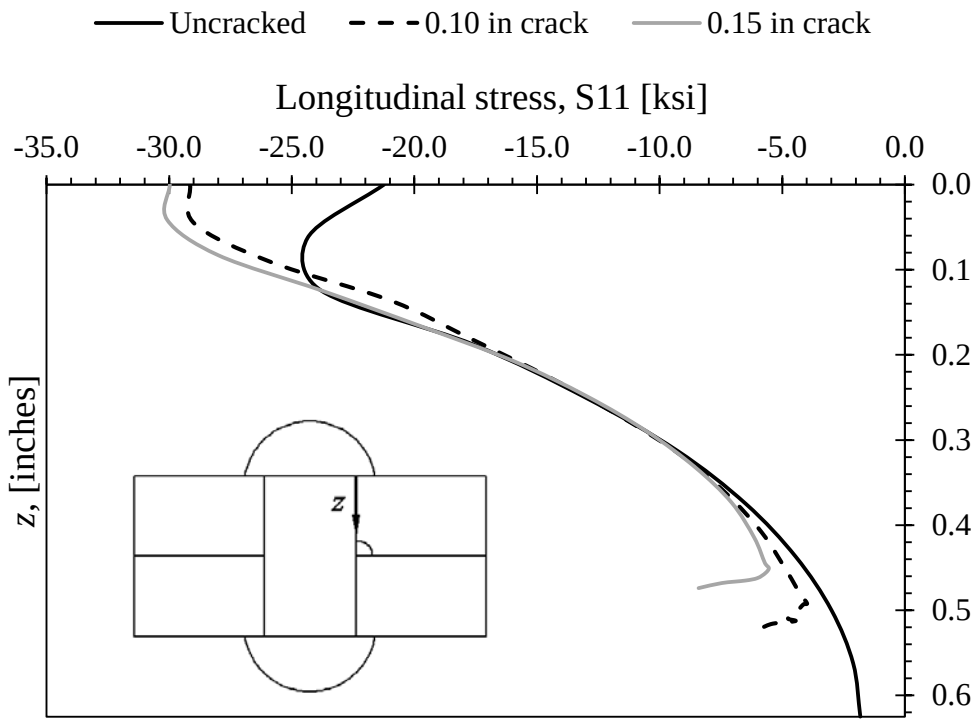

Figure 9-24 Residual stress redistribution for a 0.10 in. and 0.15 in. crack in comparison to the initial stress distribution for a 5/8-in. thick plate.

10. FATIGUE ANALYSIS USING VARIABLE AMPLITUDE LOADING AND ACCOUNTING FOR RESIDUAL STRESS

10.1 Introduction

When external loads are applied to a component with residual stresses, fatigue crack growth behavior is expected to be different from the behavior in absence of residual stresses. If the structural component presents a residual stress of the compressive type, it is expected that this localized compression will lower the probability of crack initiation and propagation, and thus it is beneficial to the fatigue life of the component. On the other hand, if localized tensile stresses are present and external loads are applied to the component, crack initiation and formation will most likely accelerate, proving to be detrimental to fatigue life [55]. Either way, accounting for residual stress in fatigue life will, most definitely, provide a more accurate estimation.

The objective of this section is to compare predictions of fatigue crack growth with and without considering residual stresses in the analysis. Utilizing the residual stresses obtained from the finite element model and explained in Chapter 9, the calculations presented in 8 will be slightly modified to account for thermal residual stress.

10.2 Superposition approach for existing residual stress

According to Nelson [27], LEFM method is the most frequently employed approach to account for the effect of an existing residual stress field on fatigue crack growth behavior. Furthermore, the most common method employed to account for

residual stresses on crack growth involves the superposition of the stress intensity factor for the initial residual stress and for the applied stress. Superposition states that the stress system due to two or more loads acting together is equal to the sum of the stresses due to each load acting separately. The residual stress field is simply added to that due to the boundary loading in order to determine the total field; provided that the body behaves in a linearly elastic fashion during the addition of boundary tractions to the residual stress field the superposition is valid [25].

Proposed by Glinka [23] and Parker [25], the superposition method is based on the principle of linear elastic fracture mechanics. Under cyclic loads, the total stress intensity factor (SIF) range and effective SIF ratio are calculated as

$$\left.\begin{aligned} \Delta K_{eff} &= K_{I_{MAX}} - K_{I_{MIN}} \\ R_{eff} &= \frac{K_{I_{MIN}} + K_{I_{RES}}}{K_{I_{MAX}} + K_{I_{RES}}} \end{aligned}\right\} K_{I_{MIN}} + K_{I_{RES}} > 0 \qquad \text{Eq. 10.2-1}$$

$$\left.\begin{aligned} \Delta K_{eff} &= K_{I_{MAX}} + K_{I_{RES}} \\ R_{eff} &= 0 \end{aligned}\right\} K_{I_{MIN}} + K_{I_{RES}} \le 0 \qquad \text{Eq. 10.2-2}$$

Equation 10.2-2 implies that the part of the fatigue cycle during which the crack is closed at its tip makes no contribution to crack growth. Therefore, under cyclic loads, only the R_{eff} changes due to the presence of residual stresses. Note that superposition is applicable only when the sum of the remote and residual stresses does not exceed yield strength of the base material.

However, Fisher et al. [4] states that often it is not possible to superimpose stresses due to residual stresses because:

1. The distribution of residual stress is different from the applied stress.
2. There is a stress concentration present. This requires that a correction factor for *K* be used on the applied loads, but not for the residual stresses.
3. There is a possibility of residual stress relaxation with crack growth. In such cases value of K_I for residual stresses should be calculated separately and then added to the K_I for the applied loads. Thus, *superposition is applied at the level of K*, the parameter that characterizes the stress field at the crack tip.

Thus, in order to account for the residual stress reduction as crack growth occurs, superposition will be applied at the *K* level. Section 10.4 describes how the superposition method was implemented in detail. The residual stress distribution was obtained through finite element model.

10.3 Stress distributions of residual stress

In order to quantify the effect of the residual stress in fatigue crack propagation, it was deemed necessary to count with the residual stress field (both magnitude and distribution in length). The finite element model of an uncracked riveted component explained in Chapter 9 was used to determine the residual stress distribution near the region where a crack is most likely to initiate and propagate.

Crack propagation in depth and in length is obtained and fitted to a high order polynomial degree. Figure 10-1 describes the longitudinal stress distribution, along the plate thickness, as a function of distance, assuming the faying surfaces is the initial starting point. Likewise, Figure 10-2 describes the longitudinal stress distribution assuming the edge of the hole is the starting point. Note that Figure 10-2 is shown until x_c reaches around 2.5 in. It can be stated that a crack larger than 2.5 in. is critical and, by that time, the structural component should be retrofitted or replaced.

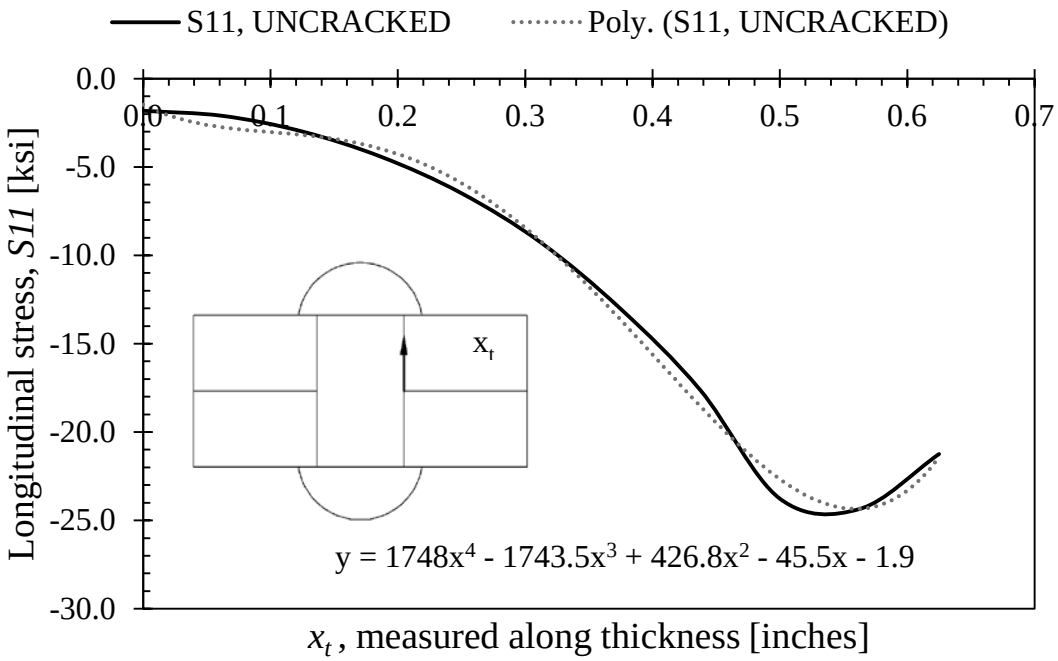

Figure 10-1 Residual stress distribution measured along the plate thickness for a 5/8-in thick plate.

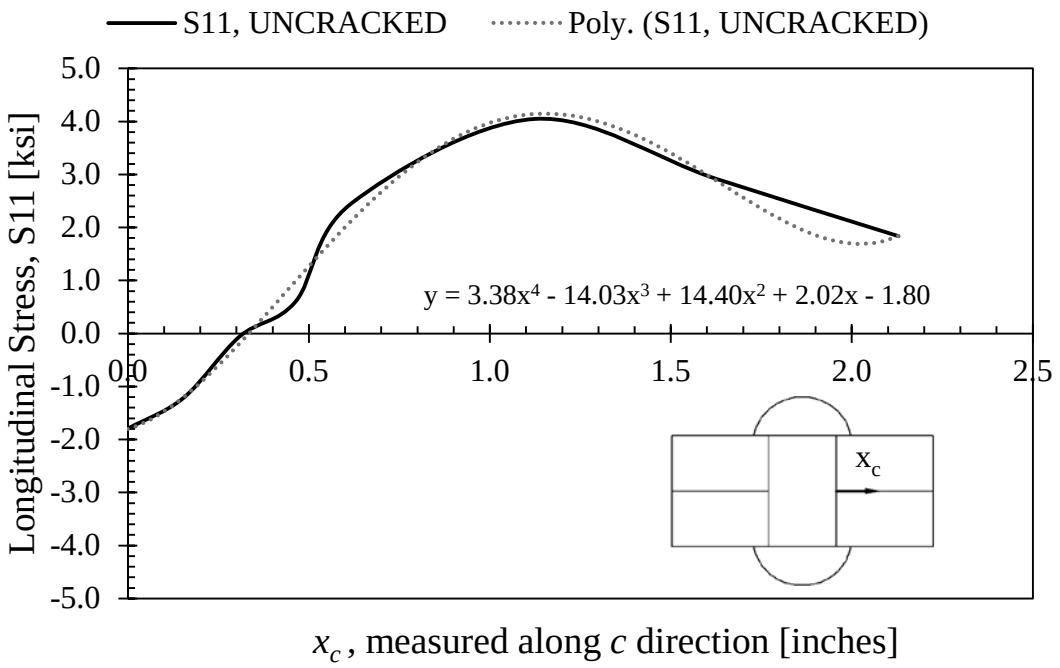

Figure 10-2 Residual stress distribution measured along the c-direction for a 5/8-in thick plate.

10.4 Algorithm

The algorithm used to evaluate the fatigue life of a riveted detail under variable amplitude loading using LEFM is the following:

For each stress range cycle part of the spectrum:

4. Assume an initial crack depth, *a*.
5. Determine K_{min}, K_{max} and K_{res}. Compute $K_{min} + K_{res}$.
   a. If $K_{min} + K_{res} > 0$, then $\Delta K = K_{I_{MAX}} - K_{I_{MIN}}$ and $R = \dfrac{K_{I_{MIN}} + K_{I_{RES}}}{K_{I_{MAX}} + K_{I_{RES}}}$
   b. If $K_{min} + K_{res} \leq 0$, then $\Delta K = K_{I_{MAX}} + K_{I_{RES}}$ and $R = 0$

6. Calculate $\Delta K_{TH} = 6.4(1-0.85R)$

    a. If $\Delta K > \Delta K_{TH}$ then

        i. Calculate crack growth using Paris-Power Law

        ii. Calculate the new crack length: $a\left(\frac{da}{dN}\right)(1)$

    b. If $\Delta K < \Delta K_{TH}$ then crack does not grow. Move on to next stress range in the spectrum.

7. Repeat the algorithm to compute crack growth in the *c*-direction.

It is important to mention that the stress intensity factor for the applied remote tension was obtained from equations 8.4-1, where the correction factors, F_{ch}, describes the effect of the remote tension at the crack tip. In other words, the correction factors, often called magnification factors, describe how the remote tension accentuates at the crack tip. On the other hand, the residual stress distributions obtained from the finite element model are the stresses around the crack zone, thus, no correction factor should be applied to this stress. Hence, and in accordance with Fisher et al. [4], superposition of the remote tension and the localized residual stress is applied at the ΔK level. Therefore, equation 8.4-1, converts to

$$K_I = (F_{ch}S_r + S_{residual})\sqrt{\frac{\pi a}{Q}} \qquad \text{Eq. 10.4-1}$$

Moreover, because the stress intensity factor equation for the applied stress and for the residual stress are different, then

$$R = \frac{S_{min} + S_{residual}}{S_{max} + S_{residual}} \neq \frac{K_{min} + K_{residual}}{K_{max} + K_{residual}} \qquad \text{Eq. 10.4-2}$$

10.5 Results and discussion

Estimation of fatigue life using linear fracture mechanics is highly susceptible to the assumed initial flaw. For this reason, the fatigue life of a riveted steel plate, with varying thickness (1/2 in., 5/8 in., and 1 in), was determined. Crack sizes were assumed large enough to force the component to have finite fatigue life for comparison purposes. Moreover, it would not be wise to compare the number of cycles for a crack to propagate through the plate thickness, if each case has different thickness. Thus, the number of cycles shown in Tables 10.1-10.3, were the ones required to reach a final crack size of 0.5 in., (equivalent to the thickness of the thinnest plate utilized in this parametric study). In some cases, crack depth reached first 0.5 in, in other cases, crack length reached it first. In other words, and only in this parametric study, failure was defined as the crack reached a size of 0.5 in. Finally, a significant improvement in fatigue life can be seen when residual stress is accounted for.

Emphasis was placed on results for $a/c > 1$ rather than $a/c < 1$ because experience indicates that naturally occurring fatigue cracks often have a/c values between 1 and 1.5 [56].

- Referring to Table 10-1, the fatigue life of the ½ in plate and the 5/8 in. plate was significantly affected by considering the thermal residual stress. For a 5/8 in. plate, the fatigue life expectancy without considering residual stresses could

be 3.8 million cycles, and by considering residual stresses the same component has enough endurance for the 80 years of service recommended by the AREMA provisions. Thus, the effect of the clamping force on the fatigue behavior of a joint is strongly dependent on the plate thickness since it will determine how the stress develops along the thickness.

- Moreover, from Table 10-1, the ratio of crack size to plate thickness (*a/t*) has a significant effect on the fatigue life. The same crack size in a thinner plate (1/2 in) presents a much lower fatigue life than the same crack size in the thickest plate (1 in).
- Referring to Table 10-2, the inclusion of residual stress affects how the crack propagates. When analyzing a quarter elliptical corner crack, the crack depth growth rate is faster that crack length growth rate. However, when residual stress is accounted for, the crack depth tip would most likely be under localized compressive stress, hindering crack propagation. On the other hand, the crack length tip would typically not encounter a localized compressive stress, and therefore its propagation will not be thwarted. This is not the case for the 1 in. plate; the thickness is large enough to develop a small tensile stress and crack propagation along the thickness is initially not hindered. In the 1-in. thick plate the crack grows in the same way as if there was no clamping stress, refer to Figure 10-3.

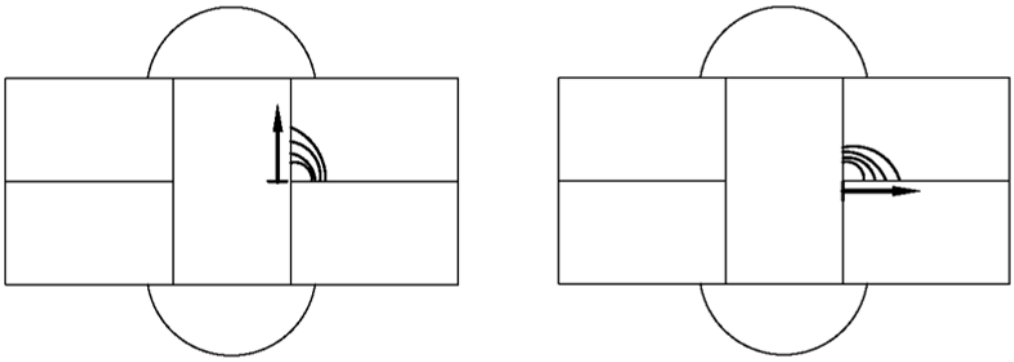

Figure 10-3 (a) crack propagation in the absence of residual stress or in thicker plates and (b) crack propagation in the presence of residual stress or in thinner plates.

- Initially, it was believed that a larger crack depth to crack length ratio will result in a lower fatigue life. However, comparing the results from Table 10-1 with Table 10-2, it can be stated that *a/c* ratio does not play a first-hand role on the fatigue life of the component. However, a more detailed study is recommended to determine the full effect of *a/c* ratio on fatigue life.

Table 10-1 Fatigue life of a riveted component with and without residual stress for different plate thicknesses, $a = c$.

	Plate thickness 1/2 in	
	No residual stress	**With residual stress**
Initial crack depth, a_O	0.09 in	0.09 in
Initial crack length, c_O	0.09 in	0.09 in
Final crack depth after N cycles, a_f	0.50 in	0.09 in
Final crack length after N cycles, c_f	0.35 in	0.09 in
Number of cycles, N	2.61E+06	> 108 millions

	Plate thickness 5/8 in	
	No residual stress	**With residual stress**
Initial crack depth, a_O	0.09 in	0.09 in
Initial crack length, c_O	0.09 in	0.09 in
Final crack depth after N cycles, a_f	0.50 in	0.09 in
Final crack length after N cycles, c_f	0.30 in	0.09 in
Number of cycles, N	3.86E+06	> 108 millions

	Plate thickness 1 in	
	No residual stress	**With residual stress**
Initial crack depth, a_O	0.09 in	0.09 in
Initial crack length, c_O	0.09 in	0.09 in
Final crack depth after N cycles, a_f	0.09 in	0.09 in
Final crack length after N cycles, c_f	0.09 in	0.09 in
Number of cycles, N	> 108 millions	> 108 millions

Table 10-2 Fatigue life of a riveted component with and without residual stress for different plate thicknesses, $a > c$.

	Plate thickness 1/2 in	
	No residual stress	**With residual stress**
Initial crack depth, a_O	0.125 in	0.125 in
Initial crack length, c_O	0.112 in	0.112 in
Final crack depth after N cycles, a_f	0.50 in	0.28 in
Final crack length after N cycles, c_f	0.35 in	0.50 in
Number of cycles, N	1.73E+06	2.97E+06

	Plate thickness 5/8 in	
	No residual stress	**With residual stress**
Initial crack depth, a_O	0.125 in	0.125 in
Initial crack length, c_O	0.112 in	0.112 in
Final crack depth after N cycles, a_f	0.50 in	0.35 in
Final crack length after N cycles, c_f	0.33 in	0.50 in
Number of cycles, N	2.03E+06	3.04E+06

	Plate thickness 1 in	
	No residual stress	**With residual stress**
Initial crack depth, a_O	0.125 in	0.125 in
Initial crack length, c_O	0.112 in	0.112 in
Final crack depth after N cycles, a_f	0.50 in	0.50 in
Final crack length after N cycles, c_f	0.30 in	0.32 in
Number of cycles, N	3.76E+06	3.07E+06

Table 10-3 Fatigue life of a riveted component with and without residual stress for different plate thicknesses, $a < c$.

	Plate thickness 1/2 in	
	No residual stress	**With residual stress**
Initial crack depth, a_O	0.112 in	0.112 in
Initial crack length, c_O	0.125 in	0.125 in
Final crack depth after N cycles, a_f	0.50 in	0.27 in
Final crack length after N cycles, c_f	0.37 in	0.50 in
Number of cycles, N	1.70E+06	2.90E+06

	Plate thickness 5/8 in	
	No residual stress	**With residual stress**
Initial crack depth, a_O	0.112 in	0.112 in
Initial crack length, c_O	0.125 in	0.125 in
Final crack depth after N cycles, a_f	0.50 in	0.35 in
Final crack length after N cycles, c_f	0.35 in	0.50 in
Number of cycles, N	1.96E+06	2.90E+06

	Plate thickness 1 in	
	No residual stress	**With residual stress**
Initial crack depth, a_O	0.112 in	0.112 in
Initial crack length, c_O	0.125 in	0.125 in
Final crack depth after N cycles, a_f	0.50 in	0.50 in
Final crack length after N cycles, c_f	0.35 in	0.33 in
Number of cycles, N	2.93E+06	2.89E+06

10.6 Comparison between fatigue life estimations using LEFM under constant amplitude loading and S-N curves

In order to compare the fatigue life estimations using S-N curves and linear elastic fracture mechanics. Palmgren-Miner's rule was used to determine the effective stress range. In this way, life estimations using LEFM are comparable to those obtained by S-N curves. This analysis was primarily done to understand how the two methods differ. It was mentioned earlier that when using S-N curves the stress range, besides the category, is the most relevant parameter. The effective stress range for Train 3, 5.02 ksi (as presented in section 7.6), was utilized. AREMA recommends obtaining rivet life estimations using either category C or D, lines blue and orange in Figure 10-4. Furthermore, life estimations using LEFM are dependent, and extremely sensitive, to the assumed initial crack size, and whether residual stresses are included or not; gray and yellow line in Figure 10-4, respectively.

In this comparison, the number of cycles to failure using the LEFM approach was assumed when either the crack length or crack depth reached 0.5 in. in length. In the case that residual stress is not accounted for, crack depth reaches 0.5 in. much earlier than the crack length. On the other hand, when accounting for residual stresses, crack length reaches 0.5 in. much earlier than the crack depth. In some cases, the crack depth stops propagating.

Estimations using LEFM show something: the moment the crack size threshold is reached, crack propagation is almost sudden. Additionally, the S-N curves do not account

for the fact that the material may present a defect or flaw that may considerable lower the fatigue life of the component.

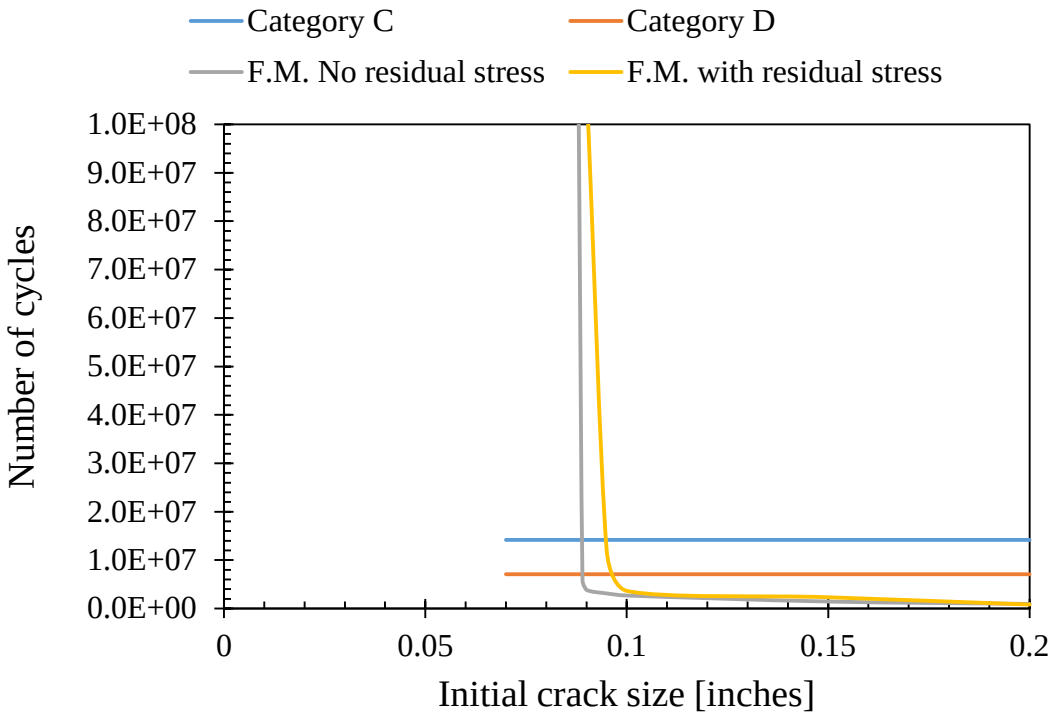

Figure 10-4 Number of cycles to failure using S-N curves and fracture mechanics (with and without residual stress).

11. CONCLUSIONS

Linear elastic fracture mechanics was used to determine the fatigue life of a riveted girder for different axle loads. The fracture mechanics approach is a reasonable methodology to obtain fatigue life of structural components. However, this approach is extremely sensitive to the assumed initial crack size. This methodology will provide acceptable estimations if the initial crack size is assumed correctly.

Initially, a LEFM was employed neglecting the effect of residual stress. This particular analysis was useful since it showed that, in the case of a quarter corner crack, the crack depth grows faster than the crack length. An increase of axle loads will most definitely decrease the fatigue life of a structural component.

A crack size threshold was determined to have a general idea what size of flaw could evolve into a fatigue crack. The applied stress range is the single most important parameter to determine if a material flaw can grow into a fatigue crack. The computation of crack size threshold proved to be of great significance to better understand fatigue crack growth, in the sense that if a material flaw is of the size of the crack size threshold, the component will most likely crack. On the other hand, if the material's flaw size is smaller than the crack size threshold, the component will most likely have infinite fatigue life.

As for the effect of overloads on the fatigue life of riveted details, one can conclude that it is more critical to have frequent overloads than having a large effective stress range. Cases where the number of overloads was frequent presented less fatigue life than those cases with less number of overloads, even when the effective stress range was larger.

A finite element model was used to estimate the clamping stresses generated in different locations by the hot riveting process. The residual thermal stresses where later used in the fracture mechanics analysis of a crack growth.

Residual thermal stress found through the finite element model were incorporated to the fatigue life estimation by means of superposition of the stress intensity factors. In most cases, the clamping stress proved to be beneficial, and hindered crack propagation. However, in the event the plate thickness is significant (approx. 1 in.) there is no longer localized compression between faying surfaces, but rather tensile stress. In this particular case, this local tensile stress will accelerate, rather than hinder, crack propagation. Finally, due to the residual stress distribution along the plate thickness, crack growth is no longer primarily throughout the thickness of the plate but rather extends and grows along the faying surfaces.

As for the use of 315,000 lbs. car in the current railroad bridges, it can be concluded that, in tight rivets can withstand the cyclic loading if there is no initial defect larger than 0.08 in. Loose rivets, large initial defects, overloads, and corrosion can definitely detriment the service life of steel riveted details. Moreover, if a micro-crack larger than 0.08 in. is located in a high stress concentration region, fatigue crack propagation will most likely happen, and in a sudden way. Retrofitting or replacing the structural member is advised.

Ultrasonic Testing is the only method that can explore subsurface material flaws and estimate their size necessary to perform a fracture mechanics analysis of the member's remaining fatigue life. Frequent inspections are highly recommended.

12. FUTURE WORK AND LIMITATIONS

In order to make this study more comprehensive and to verify and strengthen this investigation the following studies are recommended

(1) The analysis of different crack types or crack locations such as surface crack emanating from a hole.

(2) To consider the effect of multiple rivets on the development of thermal and mechanical stress distribution.

(3) To obtain the crack growth rate of a quarter elliptical corner crack emanating from a rivet hole.

(4) The evolution of the residual stress intensity factor with crack is recommended to be done, at least through a finite element approach.

(5) A further investigation on how the residual stress redistribution affects fatigue life might strengthen the assumption of utilizing the initial stress distribution.

REFERENCES

[1] GAO, "Railroad Bridges and Tunnels. Federal role in providing safety oversight and freight infrastucture investment could be better targeted.," 2007.

[2] J. F. Unsworth, "Heavy Axle Load (HAL) Effects on Fatigue Life of Steel Bridges," presented at the TRB 2003 Annual Meeting, 2003.

[3] J. F. Unsworth, *Design of Modern Steel Railway Bridges*. 2010, p. 420.

[4] J. W. Fisher, G. L. Kulak, and I. F. C. Smith, "A Fatigue Primer for Structural Engineers," N. S. B. Alliance, 1998.

[5] H. S. Reemsnyder, "Fatigue Life Extension of Riveted Connections," *Journal of the Structural Division,* vol. 101, no. 12, pp. 2591-2608, 1975.

[6] J. M. Out, J. W. Fisher, and B. T. Yen, "Fatigue strength of weathered and deteriorated riveted members, October 1984. (DOT/OST/P-34/85/016) 138p," Fritz Laboratory Reports 2282, 1984.

[7] K. A. Baker and G. L. Kulak, "Fatigue of riveted connections," *Canadian Journal of Civil Engineering,* vol. 12, pp. 184-191, 1985.

[8] J. W. Fisher, B. T. Yen, and D. Wang, "Fatigue Strength of Riveted Bridge Members," *Journal of Structural Engineering,* vol. 116, no. 11, pp. 2968-2981, 1990, Art. no. 25230.

[9] Z. Zhao, A. Haldar, and F. L. Breen Jr., "Fatigue-Reliability Evaluation of Steel Bridges," *Journal of Structural Engineering,* vol. 120, no. 5, pp. 1608-1623, 1994.

[10] J. D. DiBattista and G. L. Kulak, "Fatigue of Riveted Tension Members," University of Alberta, Edmonton, Alberta211, 1995.

[11] A. Aragón, J. M. Alegre, and F. Gutiérrez-Solana, "Effect of clamping force on the fatigue behavior of punched plates subjected to axial laoding.," *Engineering Failure Analysis,* vol. 13, pp. 271-281, 2006.

[12] Y. Zhou, "Fatigue strength evaluation of riveted bridge members," Degree of Doctor of Philosophy in Civil Engineering, Civil Engineering, Lehigh University, Bethlehem, Pennsylvania, 1994.

[13] A. De Jesus and J. Correia, "Stress intensity factors evaluation for riveted beams applying FEA with VCCT," in *5th International Conference on Bridge*

Maintenance, Safety and Management, Iabmas 2010, R. S. a. C. S. K. Dan M . Frangopol Ed. Portugal: Taylor and Francis Group, 2010, pp. 613-620.

[14] D. Otter, K. Ninnes, and L. Tunna, "Testing of a 1912-Vintage Steel Girder Span Under Heavy Axle Loads at the Facility for Accelerated Service Testing: Initial Results," presented at the Arema 2011 Annual Conference and Exposition, Minneapolis, Minnesota, 2011.

[15] L. Tunna, M. Jones, and D. Otter. (2011, August) Characterization of a Vintage Riveted Steel Deck Plate Girder Bridge Span at FAST. *Technology Digest.*

[16] D. Otter, S. M. Dick, and C. Mademann. (2013, April) FAST Steel Bridge Repairs for Effects of Corrosion and Corrugated Rail. *Technology Digest*.

[17] D. Otter, A. M. Rakoczy, and S. M. Dick. (2015, August) Steel Bridge Life Extension for Riveted Steel Girder Spans at FAST. *Technology Digest*.

[18] D. Otter, A. M. Rakoczy, and S. M. Dick. (2015) Fatigue Life and Fitness- for-Service Analysis: 32 -ft Steel Deck Plate Girder Bridge Span at FAST. *Technology Digest*.

[19] D. Otter, A. M. Rakoczy, and S. M. Dick. (2015) Fatigue Life and Fitness-for-Service Analysis: 24-foot Steel Deck Plate Girder Bridge Span at FAST. *Technology Digest*.

[20] E. A. Al-Bahkali, "Finite Element Modeling for Thermal Stresses Developed in Riveted and Rivet-Bonded Joints," *International Journal of Engineering & Technology IJET-IJENS,* vol. 11, no. 6, pp. 86-92, 2011.

[21] A. De Jesus, J. Da Silva, A. Da Silva, and A. Fernandes, "Fatigue Behavior of Riveted and Bolted Connections Made of Puddle Iron - Part II: Numerical Investigation," presented at the 21st Brazilian Congress of Mechanical Engineering, Natal, Brazil, 2011.

[22] C. Rans and P. V. Straznicky, "Riveting Process Induced Residual Stresses Around Solid Rivets in Mechanical Joints," *Journal of Aircraft,* vol. 44, no. 1, pp. 323-329, 2007.

[23] G. Glinka, "Effect of Residual Stresses on Fatigue Crack Growth in Steel Weldments Under Constant and Variable Amplitude Loads," *Fracture Mechanics, ASTM STP 677, American Society for Testing and Materials,* pp. 198-214, 1979.

[24] W. H. Cathey and J. A. F. Grandt, "Fracture Mechanics Consideration of Residual Stresses Introduced by Coldworking Fastener Holes," *Journal of Engineering Materials and Technology,* vol. 102, pp. 85-91, 1980.

[25] A. P. Parker, "Stress Intensity Factors, Crack Profiles, and Fatigue Crack Growth Rates in Residual Stress Fields," *Residual Stress in Fatigue, ASTM STP 776, American Society for Testing and Materials,* pp. 13-31, 1982.

[26] G. A. Webster and A. N. Ezeilo, "Residual Stress Distributions and their influence on fatigue lifetimes," *International Journal of Fatigue,* vol. 23, pp. S375-S383, 2001.

[27] D. V. Nelson, "Effects of Residual Stress on Fatigue Crack Propagation," in *Residual Stress in Fatigue, ASTM STP 776, American Society for Testing and Materials,* 1982, pp. 172-194.

[28] G. Servetti and X. Zhang, "Predicting fatigue crack growth rate in a welded butt joint: The role of effective R ratio in accounting for residual stress effect," *Engineering Fracture Mechanics,* vol. 76, pp. 1589-1602, 2009.

[29] M. A. Miner, "Cumulative damage in fatigue," *Journal of Applied Mechanics,* no. 67, 1945.

[30] R. I. Stephens, A. Fatemi, R. R. Stephens, and H. O. Fuchs, *Metal Fatigue in Engineering,* 2nd ed. New York: Wiley, 2001.

[31] P. B. Keating and J. W. Fisher, "Evaluation of Fatigue Tests and Design Criteria on Welded Details," in "NCHRP REPORT 286," National Cooperative Highway Research Program, Washington, D.C.286, 1986.

[32] *Manual for Railway Engineering,* 2015.

[33] P. B. Keating, "High cycle fatigue behavior of welded details under variable amplitude loading," PhD dissertation, Fritz Laboratory Report, Civil and Environmental Engineering, Lehigh University, 1987.

[34] J. M. Barsom and S. T. Rolfe, *Fracture and Fatigue Control in Structures: Applications of Fracture Mechanics,* Third ed. U.S.A.: Butterworth-Heinemann, 1999.

[35] B. C. Punmia, A. K. Jain, and A. K. Jain, *Comprehensive Design of Steel Structures*. New Delhi: Laxmi Publications LTD, 1998.

[36] B. Akesson and B. Edlund, "Fatigue Life of Riveted Railway Bridges," in *IABSE Reports*Zurich, Switzerland, 1995, pp. 1079-1084.

[37] S. M. Dick, "Legacy Train Configurations for Fatigue Life Evaluation of Steel Railway Bridges," in *Proceedings of AREMA 2016 Annual Conference, Orlando, FL. American Railway Engineering and Maintenance-of-Way Association*, September 2016: Association of American Railroads Transportation Technology Center, Inc.

[38] S. M. Dick and S. L. McCabe, "Fatigue Analysis of Steel Railway Girder Bridges."

[39] A. M. Rakoczy and D. Otter. (May 2017) Effects of short cars on bridges. *Railway Track & Structures*. 13-15.

[40] A. Skorupa, M. Skorupa, T. Machniewicz, and A. Korbel, "Fatigue crack location and fatigue life for riveted lap joints in aircraft fuselage," *International Journal of Fatigue*, vol. 58, pp. 209-217, 2014.

[41] A. Skorupa and M. Skorupa, *Riveted Lap Joints in Aircraft Fuselage*. 2012.

[42] J. C. Newman and I. S. Raju, "Stress Intensity Factor Equations for Cracks in Three-Dimensional Finite Bodies Subjected to Tension and Bending Loads," 1986.

[43] R. C. Shah, "Stress intensity factors for through and part-through cracks originating at fastener holes," presented at the Mechanics of Crack Growth ASTM STP -590, 1976.

[44] T. Siwowski, "Fatigue assessment of existing riveted truss bridges: case study," *Bulleting of the Polish Academy of Sciences, Technical Sciences*, vol. 63, no. 1, pp. 125-133, 2015.

[45] B. Akesson, *Fatigue Life of Riveted Steel Bridges*. London, United Kingdom: Taylor and Francis Ltd, 2010, p. 184.

[46] J. W. N. Fisher, A.; Keating, P.B., "Resistance of Welded Details Under Variable Amplitude Long-Life Fatigue Loading," National Cooperative Highway Research Program, Bethlehem, Pennsylvania354, 1993.

[47] A. De Jesus, H. Pinto, A. Fernandez-Canteli, E. Castillo, and J. Correia, "Fatigue Assessment of a Riveted Shear Splice Based on a Probabilistic Model," *International Journal of Fatigue*, vol. 32, pp. 453-462, 2009.

[48] B. Imam, "Fatigue analysis of riveted railway bridges," Phd Thesis, School of Engineering, University of Surrey, UK, 2006.

[49] A.-D. Ancas and D. Gorbanescu, "Theoretical Models in the study of temperature effect on steel mechanical properties," 2006.

[50] V. A. Narang, "Heat Transfer Analysis in Steel Structures," Master of Science, Civil Engineering Dept., Worcester Polytechnic Institute, 2005.

[51] *Eurocode 3: Design of steel structures,* EN 1993-1-2:2005, April 2005.

[52] Y.-B. Lee, C.-S. Chung, Y.-K. Park, and H.-K. Kim, "Effects of redistributing residual stress on the fatigue behavior of SS330 weldment," *International Journal of Fatigue,* vol. 20, no. 8, pp. 565-573, 1998.

[53] Y. C. Lam and K. S. Lian, "The effect of residual stress and its redistribution on fatigue crack growth," *Theoretical and Applied Fracture Mechanics,* vol. 12, pp. 59-66, 1989.

[54] L. Edwards, "Influence of residual stress redistribution on fatigue crack growth and damage tolerant design," *Materials Sciemce Forum,* vol. 524-524, pp. 363-372, 2006.

[55] J. F. Throop, "Fracture Mechanics Analysis of the Effects of Residual Stress on Fatigue Life," *Journal of Testing and Evaluation JTEVA,* vol. 11, no. 1, pp. 75-78, 1983.

[56] J. A. F. Grandt and T. E. Kullgren, "Stress Intensity Factors for Corner Cracked Holes Under General Loading Conditions," *Journal of Engineering Materials and Technology,* vol. 103, pp. 171-176, April 1981.